Role of Electrical Coupling via Connexin 36 Containing Gap Junctions in Sympathetic Preganglionic Neurons

by

Hossein Tavakoli

A Thesis Submitted to the Faculty of Graduate Studies of

The University of Manitoba

In partial fulfillment of the requirements of the degree of

MASTER OF SCIENCE

Department of Physiology and Pathophysiology

University of Manitoba

Winnipeg

Abstract – Gap junctions are cluster of channels on the plasma membrane formed by connexin proteins that connect cytoplasm of adjacent cells. Connexins are essential to normal development and function in neonatal and adult mammals by forming electrical synapses between cells, including neurons within the central nervous system (CNS). In the present study, we documented the distribution of connexin 36, (Cx36) in sympathetic preganglionic neurons (SPNs) in the intermediolateral column (IML), lateral funiculus, intercalatus and central autonomic area in adult and neonatal mice and rats. Additionally, we examined the functional role of Cx36 in SPNs by comparing response of Cx36 wild-type (Cx36wt) and Cx36 knockout (Cx36ko) mice to colorectal distension (CRD) as noxious stimulation. We also provided evidence for glutamatergic and GABAergic innervation of SPNs by other electrically coupled neurons in spinal cord. Our study showed that Cx36wt and Cx36ko mice respond to CRD by an increase and a decrease in BP respectively. Spinalized wildtype mice showed an increase in BP. In addition, we attempted to compare the expression of Cx36 among SPNs in intact and spinalized mice and study the organization of electrical coupling in these neurons utilizing dye coupling methods. All results taken together, this work further supports the evidence for SPN electrical coupling via Cx36 and provides more detailed understanding of its organization. It also broadens our knowledge about sympathetic activity in general.

Acknowledgment

I would like to express my deepest gratitude to my co-supervisors Drs. James I Nagy and Katinka Stecina. No part of my M.Sc. project would have been materialized without guidance and mentorship of Dr. Nagy. His immense knowledge and honest criticism were invaluable both in the realm of neuroscience and everyday life. Dr. Stecina provided a positive environment and supported me with unmeasurable amount of kindness throughout the program. Her insight into the field of neuroscience along with her enthusiasm was always encouraging during worse days.

I would like to thank all the members of my advisory committee Drs. Kristine Cowley, Brian MacNeil and Jeremy Chopek. I appreciate their availability and constructive feedback in all of our meetings. I am also thankful to our lab members Maria Setterbom and Joanne Senecal for their assistance in many stages of this research project including planning and execution of experiments.

I would also express my gratitude to my family. I would like to thank my parents for their guidance and assistance in the journey of life, without whom none of my accomplishments would have been possible. Last but not least, I would like to thank my brother, Ali, all my friends in Winnipeg and most importantly my dear fiancé, Marjan for their kindness and encouragement during my studies.

I must also recognize the financial support provided by University of Manitoba, and Faculty of Graduate Studies for this research project.

List of Figures (PART I and IV)

List of Figures (PART II)

List of Figure (PART III)

List of Tables (PART II)

List of Tables (PART III)

List of Appendices

List of Key Abbreviations

ACh – Acetylcholine

AD – Autonomic dysreflexia

AHP – After hyperpolarization

BP – Blood pressure

CA – Central autonomic

CaMKII – Ca^{+}/calmodulin-dependent kinase II

CC – Coupling coefficient

CFP – Cyan fluorescent protein

ChAT – Choline acetyltransferase

CK – Casein kinase

CNS – Central nervous system

CRD – Colorectal distension

Cx – Connexin

SCN – Suprachiasmatic nucleus

FRIL – Freeze-fracture replica immunogold labeling

HR – Heart rate

IC – Intercalatus

IML – Intermediolateral

ko – Knockout

LTP – Long term potentiation

MAPK – MAP kinase

MesV – Mesencephalic trigeminal nucleus

nNOS – Neuronal nitric oxide synthase

NPY – Neuropeptide Y

PKA – Protein kinase C

PKG – Protein kinase G

PMLD – Pelizaeus-Merzbacher–like disease

PVN – Paraventricular nucleus

RR – Respiratory rate

RVLM – Rostro ventrolateral medulla

SCI – Spinal cord injury

SLD – Short-latency depolarization

SNS – Sympathetic nervous system

SPN – Sympathetic preganglionic neuron

TRN – Thalamic reticular nucleus

UTI – Urinary tract infection

WHO – World health organization

wt – Wildtype

ZO1 – Zonula occludens-1

Table of Contents

PART I: Introduction

1.1. Gap junctions

1.1.1. Synaptic transmission: a historical perspective

The means whereby neurons communicate with each other and with peripheral organs was controversial for a long time beginning with research on neuromuscular junctions in the early 19th century and even before the term synapse was coined. Kühne and Krause, two physiologists investigating the process of signal transmission between muscle and nerve suggested that the mechanism was electrical, proposing that a "current of action" in the nerve is responsible for muscle contraction (Kandel, 2013). Later, du Bois-Reymond (Kandel, 2013) objected to the electrical transmission hypothesis and proposed chemical mediation of transmission. This disagreement about synaptic transmission modality continued but was overshadowed by more basic issues until the early 20th century. By that time, a series of studies had led to the discovery of noradrenaline and acetylcholine (ACh), where researchers Dale, Loewi and Feldberg (Dale, 1935; Loewi, 1956) were testing the potential roles of these agents in neuronal communication. For example, Feldberg and his colleges by 1936 had established a link between ACh release at the neuromuscular junction and muscle contraction (Feldberg, 1950; 1956; Kandel, 2013), providing evidence for chemical synaptic transmission. Despite this evidence, many electrophysiologists insisted on the idea that synaptic transmission was electrically mediated. They provided reasons such as the short latency required for transmission, which they thought could only be achieved by electrical synapses. As a result, a debate ensued referred to as the "soup versus spark controversy". Overtime electrophysiologists (Kuffler, Katz and Fatt) provided evidence that weakened the idea of electrical synapses as the modality of synaptic transmission (Kandel, 2013). Their studies showed that an electrical synapse could not function at any contact point between pre- and

postsynaptic cells, because such a synapse required meeting special conditions for which there was at that time no experimental support. They also discovered an irreducible delay at the neuromuscular endplate, between the action potential in the axon terminal and endplate potential, which was later termed synaptic potential. Kuffler, Fatt and Katz conducted further studies during the 1950s and 1960s, where they explained some details about chemical synapses and how they function. In particular, Kuffler's studies focused on synaptic delay and endplate potentials that ruled out electrical synapses as the form of synaptic transmission at neuromuscular junctions. It was also established that the occurrence of an action potential is related to changes in extracellular sodium, potassium and chlorine concentrations. Next, Fatt and Katz presented convincing evidence that it was ACh release from the endplate that causes the plasma membrane to be transiently permeable to sodium, potassium and chlorine ions (Fatt, 1950; Katz, 1969; Kandel, 2013). Eccles, who was another well-known neurophysiologist and a long-time strong proponent of electrical synaptic transmission, provided even more evidence against electrical synapses while studying synaptic inhibition. His investigations showed that synaptic inhibition is monophasic, causing only a hyperpolarization of motoneurons, which was contrary to what had been suggested for neuronal inhibition mediated by electrical synapses, where a diphasic activity was proposed, involving an excitatory combined with an inhibitory action. This last discovery along with other evidence convinced many electrophysiologists including Eccles himself to accept chemical transmission at synapses as the modality of neuronal communication both in the PNS and CNS (Eccles, 1976; Kandel, 2013).

A number of years later, however, Furshpan and Potter found evidence for a type of synaptic transmission that allowed even small currents to flow from pre- to postsynaptic cells with an extremely short latency in crayfish (Kandel, 2013). These were the characteristics of electrical

synapses that Kuffler had searched for but failed to find. Several years later, Bennett and his colleges elaborated on properties of the newly discovered electrical synapses and correlated those properties with occurrence of close membrane appositions that later became known as gap junctions and that were identified as the structural basis of electrical synapses. About a decade after their discovery in crayfish, the first electrical synapses were identified in the mammalian central nervous system (CNS) (Kandel, 2013).

A full half a century has now passed since the discovery of gap junctions, but the field of electrical synapses formed by these gap junctions in the mammalian CNS has witnessed a huge rise in interest only over the past twenty years. Researchers have identified a variety of connexin proteins that form gap junctions and have investigated the structure of these junctions. In the following sections, the overall structure of gap junctions and connexins expressed in the mammalian CNS will be discussed.

1.1.2. Structure of gap junctions

Gap junctions are clusters of plasma membrane channels formed by connexin proteins. Connexins create hexameric hemichannels or connexons that can produce a complete tetraspan membrane channel. These channels protrude from the plasma membranes of one cell to channels of an adjacent cell and connect head-to-head across the extracellular space, thus linking the interior of one cell to that of another (Yeager and Nicholson, 1996; Goodenough and Paul, 2009; Maeda and Tsukihara, 2011). The process of connexon docking creates a space or a gap of approximately 2 nm between the two adjacent plasma membranes; hence the name gap junction (Goodenough and Paul, 2009). Each gap junction consists of a few to thousands of channels clustered densely in a plaque (Goodenough and Paul, 2009; Evans, 2015). The approximately 1 nm diameter of a gap

junction channel has an aqueous interior, enabling ions and small molecules to pass from one cell to another. However, the aqueous interior is inaccessible from the extracellular space, which makes finding specific gap junction blockers difficult (Traub et al., 2018; Peracchia, 2019).

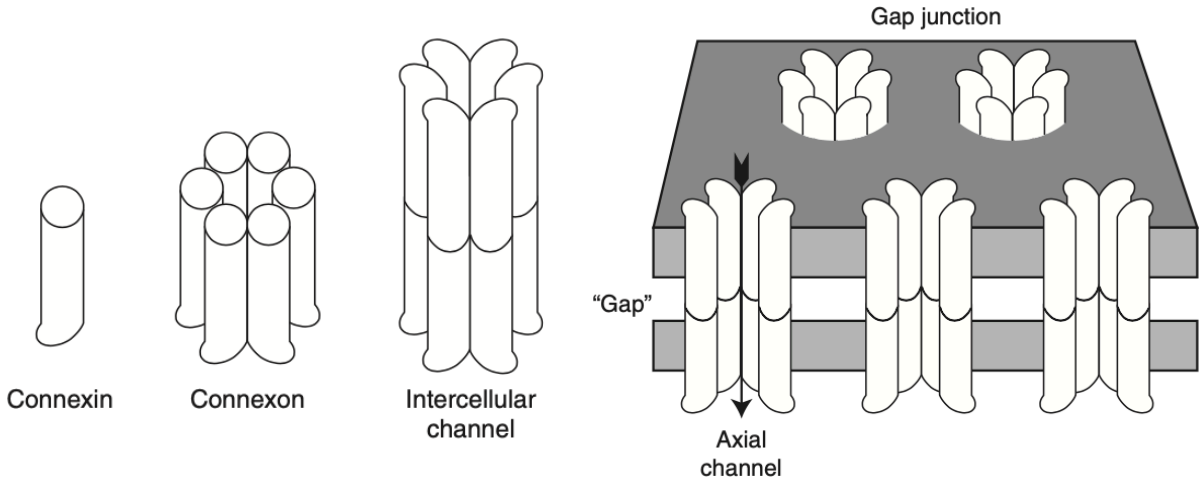

Figure 1. A diagram showing different levels of gap junction structure from connexins to gap junctional plaques (Goodenough and Paul, 2009). The arrow shows that flow at the interior of an individual channel.

To date, 20 to 21 connexin isoforms each encoded by different genes have been discovered in mammals (Goodenough and Paul, 2009; Maeda and Tsukihara, 2011). These proteins are denoted with Cx as an abbreviation for connexin and a numerical suffix which indicates their molecular weight in kDa (e.x., Cx36)(Goodenough and Paul, 2009). It was found that each connexin protein has four transmembrane alpha helices and two extracellular loops. Each of the extracellular loops have three highly conserved cysteine residues enabling the loops to form disulfide bonds that are essential for forming a functional channel (Maeda and Tsukihara, 2011). As shown by hydropathy plots, the four transmembrane sequences are hydrophobic including two that line the channel wall. On the cytoplasmic side, connexins have a short N-terminus end, in addition to a highly variable intracellular loop between the second and third transmembrane regions. They also contain a

cytoplasmic tail that is different in length and sequence from one connexin to another and is the source of variability in molecular weight among connexins (Evans, 2015). It is important to note that gap junctions consist of a greater multiprotein complex. Areas of high electron density have been observed subjacent to neuronal gap junctions that are referred to as "semi-dense cytoplasmic matrices". As an example, the scaffolding protein zonula occludens-1 (ZO1) associates with many connexins and has an essential role in the process of channel formation, which is best characterized for channels composed of Cx43 (Pereda, 2014). Many other proteins also associate with gap junctions, and these together with cytoskeletal proteins likely form the semi-dense cytoplasmic matrices.

The connexin constituents of connexons and the connexon composition of gap junctions determines the functional characteristics of gap junctional coupling. Because all isoforms of connexins, except Cx29, have the ability to oligomerize into connexons and form gap junctions, a variety of different channel types can be formed. Thus, connexons can be homomeric (formed from six identical connexin) or heteromeric (formed from different connexin isoforms) (Goodenough and Paul, 2009). For instance, Cx43 and Cx45 are both expressed in cardiac cells and form homomeric as well as heteromeric connexons that create channels with different unitary conductance, permeability and regulation properties (Martinez et al., 2002).

It is not only the connexons that can have different characteristics due to different connexin compositions. Two apposing connexons creating a complete channel can also have distinctive connexin configurations; connexons composed of identical connexins form a homotypic channel, while two apposing connexons composed of different connexins create a heterotypic channel (Goodenough and Paul, 2009). For example, Cx26, Cx30, Cx32, Cx43 and Cx47 that are among the most common connexins in the CNS, can form a variety of heterotypic gap junction channels.

Connexons composed of Cx32 can bind to those composed of Cx30 and Cx26 to create a complete gap junction channel. However, connexons formed by Cx43 can only associate with Cx47 (Rash et al., 2012). It is also the case that gap junction channels can connect two identical or different cell types, and these configurations are referred to as homologous and heterologous gap junctions, respectively (Goodenough and Paul, 2009). As an example, astrocytes can be coupled to other astrocytes by homotypic gap junctions consisting of Cx30, Cx26 and Cx43 or to oligodendrocytes by Cx30/Cx32, Cx26/Cx32 and Cx43/Cx47 heterotypic gap junctions (Nagy et al., 2004; Rash et al., 2012).

1.1.3. Connexins in the CNS

Gap junctions were first identified ultrastructurally in the mid 1960s, but the first connexins were not found until the mid 1980s. Since then, gap junctions composed of various connexins have been observed in all solid mammalian tissues (Goodenough and Paul, 2009). Interest in connexin expression in various cell types in the brain and spinal cord, and understanding their functions, began almost immediately after the discovery of the first connexins. This has been facilitated by various advances that have promoted research in the gap junction field, including development of new methods such as freeze-fracture replica immunogold labeling (FRIL), patch clamp and whole cell recording under direct cell visualization, new and more effective gap junction blockers such as mefloquine, new tracer molecules or dyes such as neurobiotin and biocytin used in dye coupling, and creation of transgenic mice with gene knockout of various connexins (Nagy et al., 2018a).

These advances have allowed identification of a variety of connexins in CNS glial cells as well as in neurons (Takeuchi et al., 2014). Astrocytes throughout the brain and spinal cord express a set

of three connexins (Cx26, Cx30, Cx43), while ependymal cells express Cx30 and Cx43 (Hussain, 2014). In addition, Cx26 has been localized in leptomeningeal projections into the cortex and most subcortical areas of the brain.(Nagy et al., 2004). Microglia express Cx43 when they undergo transformation to a reactive state (Hussain, 2014).

Oligodendrocytes in the CNS express a different set of three connexins (Cx29, Cx32, Cx47) on their cell bodies and initial segment processes, where they form heterologous gap junctions with astrocytes expressing the above noted connexins. Although Cx29 does not form gap junctions, it was localized in gray and white matter of brain and spinal cord, especially along internodal regions of myelin sheaths. Cx32 is also concentrated at nodes of Ranvier, where it can occur at processes arising from the same cell forming what are referred to as reflexive gap junctions. The reflexive gap junctions have also been detected on the inner layers of myelin surfaces (Nagy et al., 2004). Prior to the discovery of these glial connexins, it was known that astrocytes form an abundance of gap junction with oligodendrocytes, but oligodendrocytes in gray matter rarely if ever form gap junctions with each other. However, gap junctions allow communication between oligodendrocytes through astrocytes as intermediates. Because oligodendrocytes are commonly found coupled to astrocytes via different sets of connexins expressed in each cell type, the connexin combinations involved in this coupling were found to be Cx32/Cx30, Cx43/Cx47 and Cx30/Cx47 (Nagy et al., 2004). Additional CNS connexins include Cx57 that was localized in neurons in retina, and Cx45 that is also expressed in retinal neurons and was localized on stellate cells in cerebral cortex and Bergmann glial cells (Nagy and Rash, 2017; Nagy et al., 2018a). In addition, Cx30.2 was reported to occur in mouse CNS, particularly in the hippocampal neurons (Kreuzberg et al., 2008), and also in mouse retina (Pérez et al., 2010). It is noteworthy that Cx36 is the most abundant connexin expressed in neurons in different areas of the CNS such as retina, olfactory

bulb, interneurons of cerebral cortex and hippocampus where they are mostly involved in synchronization of neuronal activity (Nagy et al., 2018a). Cx36 is the focus of this thesis and will be discussed in more detail below.

1.1.4. Noncanonical functions of connexins

Aside from forming electrical synapses, gap junctions allow transfer and distribution of metabolites, acting similar to a simple channel. Gap junctions also partake in functions that are not dependent on their mediation of cell-cell communication, also known as noncanonical functions.

Gap junctions are known to regulate cell growth and differentiation, and thus are sometimes called tumor suppressors. There is evidence that tumorigenic cell lines and tumor cells have altered expression or localization of a number of connexins, such as Cx32 or Cx43. The altered connexins seem to increase the metastatic potential of cancer cells and increase tumor growth. The exact mechanism by which these connexins affect cell growth is unclear, but it includes both channel-independent and channel-dependent processes such as transfer of metabolites, including calcium ion, cAMP and inositol triphosphate (Hussain, 2014).

Aiding cell migration is another function of connexins that includes channel-dependent as well as channel-independent processes. The former requires either functional gap junctions or connexon hemichannels. For example, cell migration during embryogenesis is promoted by communication via gap junctions. Another example is wound healing, where migration of smooth muscle cells is mediated in part by increased cellular calcium concentration and cell-to-cell propagation of calcium ions occurs via functional gap junctions (Hussain, 2014). It was also shown that connexon hemichannels aid calcium wave generation by releasing ATP into the extracellular space (Hussain, 2014). Studies using transgenic mice in which carboxyl-terminal domain of Cx43 was truncated showed that this domain had a role in neuronal migration in brain even without the complete

channels or hemichannels inserted in plasma membrane. The adhesive properties of connexins, probably involving their interaction with extracellular matrix, also has a role in cell migration (Hussain, 2014). Additional studies showed that connexins are involved in single cell migrations via intracellular signaling. This process is thought to be mediated by interactions of connexin with membrane proteins such as N-Cadherin (Hussain, 2014). Gap junction-mediated adhesions also has an essential role in eye lens homeostasis, integrity and differentiation; Cx50 expressed in lens mediates cell-cell adhesion that is regulated by its second extracellular loop domain (Hu et al., 2017). Gene expression is another process affected by connexins. For example, expression of Cx32 and Cx43 was more associated with up- or downregulation of growth factor genes compared with regulation of genes for other proteins, suggesting that expression of the growth factors is in part dependent on the presence of these two connexins. (Hussain, 2014).

1.1.5. Connexins in development and disease

As noted above, connexins proteins are expressed in almost all cells of the body. As a consequence, mutations in genes coding for these proteins might be expected to result in a variety of genetic diseases and developmental abnormalities. Indeed, gap junctions formed by Cx39, Cx43 and Cx45 are essential for normal striated, smooth and heart muscle development and also their regeneration (Winterhager, 2005). In heart, eight connexins are expressed among its constituent cells, including cardiomyocytes, endothelial cells and coronary smooth muscle cells. Some of these connexins, including Cx40 and Cx45, are involved in septation processes and normal conduction of heart muscle contractions (Winterhager, 2005). The heart also has some endocrine functions in auricular and myoendocrine cells that express Cx43 and Cx45. Other organs such as kidney, heart, pancreas, pineal, thyroid, parathyroid, pituitary, adrenal gland, testis and ovary also express connexins

essential for producing and secreting hormones. In oocyte, loss of Cx37 results in premature luteinization, and loss of Cx43 in their surrounding follicles results in some forms of female infertility (Winterhager, 2005). Connexons like Cx43 and Cx32 were shown to be downregulated in many cancers such as breast cancer, but it is not exactly clear if the effect is due to junctional or nonjunctional function of the connexins (Winterhager, 2005). In the skin, gap junctions consisting of Cx43 and Cx26 are involved in development and differentiation of epidermal cells. Mutations in Cx31 and Cx30.3 cause eryjthrokeratodermia variabilis (a rare genetic disorder causing erythematous patches and thickening of the skin), and mutation in Cx26 causes palmoplantar keratodermas (a heterogenous group of disorders characterized by thickening of palm skin) alongside oculo-motor-digital dysplasia (a rare syndrome causing multitude of developmental abnormalities such as craniofacial and limbal dysmorphism) and deafness (Winterhager, 2005). Eye lens growth and homeostasis also requires gap junctions consisting of Cx43, Cx46 and Cx50 (Winterhager, 2005).

Gap junctions have an important role in CNS development, and their malfunction or absence can cause a variety of diseases. At early stages, coordination of cell differentiation and cell proliferation is in part regulated by intercellular calcium waves that are transmitted via gap junctions composed mainly of Cx43 and Cx26. Local differentiation at later stages is thought to occur partly by morphogenetic signals transmitted by gap junctions (Winterhager, 2005). These two connexins form gap junctions that promote migration of neurons along radial glial cells in the intermediate zones of the neocortex (Goodenough and Paul, 2009). A gap junction related disease in the CNS is Pelizaeus-Merzbacher–like disease (PMLD), which is characterized by nystagmus progressive spasticity and ataxia. Studies show that PMLD is associated with the mutated gene of Cx46.6 that is expressed by oligodendrocytes (Uhlenberg et al., 2004).

1.2. Connexin36

After the discovery of Cx36 in 1998, it was found that this connexin is abundantly expressed in neurons of the CNS and forms the vast majority of electrical synapses. In this section, the structure and physiology of electrical synapses formed by Cx36 are described, and major areas of the CNS in which Cx36 is expressed are listed. In addition, differences between electrical synapses and chemical synapses are considered, and role of electrical synapses during CNS development is discussed alongside their regulation under different physiological conditions.

1.2.1. Electrical synapses

As noted earlier, gap junctions allow small metabolites and ions to pass from one cell to another. However, when they connect two neurons or excitable cells, they form electrical synapses (Alcamí and Pereda, 2019). If two gap junctionally coupled neurons are in different signaling states, e.g., if an action potential occurs in one of two coupled cells creating a voltage difference across an electrical synapse, current flows through the gap junction in accordance with Ohm's law (Connors, 2009). Thus, an electrical circuit with input resistance and input capacitance as the two main parameters can represent the behavior of an electrical synapse between two excitable cells (Alcamí and Pereda, 2019). The strength of transmission via an electrical synapse depends on coupling coefficient (CC) that is defined as the voltage change in the postsynaptic cell generated by the voltage change induced in the presynaptic cell, divided by the voltage change created in the presynaptic cell. The CC is in turn dependent on input resistance and capacitance of two coupled cells (Alcamí and Pereda, 2019). A cells' input resistance is defined as the resistance against current injection and it decreases as more channels open on a cell membrane. In such state, a greater current would be required to generate the same potential compared to a current injected

into a cell with less channels open on the membrane in accordance with the Ohm's law. Input resistance is also affected by the number of cells coupled to the current-receiving cell. As the number of coupled cells increases, the resistance grows due to ions passing through gap junctions to the neighboring coupled cells. This phenomenon is called coupling resistance (Alcamí and Pereda, 2019).

Input capacitance is another variable affecting CC which is in turn influenced by membrane specific capacitance or capacitance per unit area as well as membrane size or surface area of a cell. Since neurons and their synapses represent an electrical circuit, the membrane of an excitable cell functions as a capacitor, separating electrical charges along the membrane bilayer in a process usually referred to as charging or loading. The buildup of charges across membranes takes time, which means that after current is injected into the cell, the current first charges the membrane and then starts to affect the cell's membrane potential. It is important to note that input capacitance is influenced by the number and capacitance of coupled cells as well. This means that input capacitance rises in proportion to the number of coupled cells because current needs to pass through gap junctions at each coupled cell to charge them, which affects loading. This contributes to the time needed for a current to influence a cell membrane potential (Alcamí and Pereda, 2019).

Another variable that influences the CC is the membrane time constant, which is the product of specific membrane resistance and specific membrane conductance and signifies the time when resting membrane potential reaches 63% of its total value. The time constant is usually longer in duration compared to physiological signals. However, for a gap junction to pass a signal, the signal needs to be long enough to have time to charge the cell capacitance before it flows to the coupled cell. As a result, more frequent signals that are shorter in duration are less capable of successfully

passing through gap junctions, making electrical synapses and their gap junctions low-pass filters (Alcamí and Pereda, 2019).

The CC, which is a ratio, cannot be greater than 1, since the potential change in the postsynaptic cell can never be more than what has been induced in the presynaptic cell. It is also important to note that input resistance of two coupled cells can be different, and that one determining factor for calculating CC is the resistance of the cell that receives the current, not the one in which the current originates. Consequently, signals can travel from one cell to another easier in one direction and harder in the opposite direction if the leakiness of two coupled cells are different. This condition makes the CC asymmetrical (Connors, 2009). Another feature of gap junction is that they transmit each phase of action potentials with different efficacy. Each action potential is composed of two main phases, a brief depolarizing phase and often a longer after hyperpolarization (AHP). Interestingly, AHPs are transmitted more effectively to the coupled cell and are more pronounced, whereas the depolarization is attenuated in comparison. This means that the CC is different for these two phases. As a consequence, frequent action potential in a contradicting way can result in the coupled cell being less excitable and more hyperpolarized (Connors, 2009; Alcamí and Pereda, 2019).

1.2.2. Cx36 expression in CNS

Studies have shown that Cx36 is expressed in many areas of the CNS and partakes in various essential functions (Nagy et al., 2018a). In retina, Cx36 forms either homotypic or heterotypic gap junctions in cone cells, AII amacrine cells and ganglion cells, where it contributes to enhancement of visual reception. For example, homotypic Cx36-containing junctions in the cone receptors, decrease the noise during phototransduction, which consequently improves the signal to noise

ratio. Heterotypic Cx36-containing gap junctions on the other hand, couple cones to rods. They provide an alternative pathway for scotopic signals transmitting via rod receptors, when the primary pathway is saturated. In addition, there are evidence to suggest that the alternative pathway utilizing gap junctions targets a different group of ganglion cells downstream than those targeted by the primary route (Stewart and Béla, 2009). Cx36 is also involved in forming electrical synapses in olfactory bulb mitral cells. These gap junctions are essential for rapid synchronization of spikes. They form mixed glutamatergic/electrical synapses which contribute to high-order information coding in olfactory bulb (Christie et al., 2005; Rash et al., 2005). In cerebral cortex, a number of GABAergic interneuron subtypes form Cx36-containing gap junctions that contribute to the generation of synchronous interneuron activity (Blatow et al., 2003; Hestrin and Galarreta, 2005; Ma et al., 2011; Takeuchi et al., 2014). Synchronization of inhibitory interneurons via Cx36 also occurs in hippocampus where those interneurons govern high frequency γ-oscillations of pyramidal cells (Fukuda and Kosaka, 2000; Hormuzdi et al., 2001; Maier et al., 2002; Buhl et al., 2003; Traub et al., 2018). It has been shown that Cx36 knockout (ko) mice have slower theta oscillations compared to wild-type mice, which impacts on hippocampal interneurons which are crucial in normal spatial coding and short-term spatial memory (Allen et al., 2011). In the thalamic reticular nucleus (TRN) Cx36-containing gap junctions are involved in synchronization of burst firing and contribute to the inhibitory input to the thalamic relay cells. They also support spindle frequency rhythms of small neuronal clusters in the TRN (Landisman et al., 2002; Long et al., 2004). In the suprachiasmatic nucleus (SCN), neuron spiking activity is synchronized by gap junctions formed by Cx36. Studies show that Cx36ko mice have impaired circadian rhythms and a delay in onset of activity during transition to constant darkness, suggesting that gap junctions are essential in normal circadian behavior (Long et al., 2005; Rash et al., 2007). The inferior olive is

another CNS site where electrical synapses formed by Cx36 produce subthreshold network oscillations, resulting in synchronous firing of Purkinje cells, which is essential for temporal precision of movement and is impaired in mice with reduced junctional coupling or with Cx36ko (Sasaki et al., 1989; Dimitris et al., 2004; Leznik and Llinás, 2005; Blenkinsop and Lang, 2006; Placantonakis et al., 2006; Hoge et al., 2011; De Gruijl et al., 2014). Electrical synapses formed by Cx36 contribute to synchronous activity of the inspiratory phase of respiration and modulate respiratory frequency by coupling neurons in respiratory nuclei of brainstem such as neurons in PreBötzinger complex (Rekling et al., 2000; Bou-Flores and Berger, 2001; Solomon, 2003; Solomon et al., 2003). Electrical coupling is also involved in normal auditory functions, including maintenance of appropriate threshold in auditory brainstem which is elevated in Cx36 null mice (Blakley et al., 2015). In spinal cord, electrical synapses formed by Cx36 contribute to the phenomenon of primary afferent presynaptic inhibition (Bautista et al., 2012). Additionally, gap junctions couple sexually dimorphic motoneurons in dorsomedial and dorsolateral nucleus (Bautista et al., 2014b).

1.2.3. Electrical vs chemical synapses

Electrical and chemical synaptic transmission have similarities and differences in the way they function. Presynaptic neurons forming chemical synapses need to be depolarized to threshold for action potentials to occur in order to pass signals to a postsynaptic neuron. As a consequence, signal transmission in these synapses is an all-or-none event (Alcamí and Pereda, 2019). However, electrical synapses can transmit any level of depolarization to their coupled cells as long as the signal incidence is low in frequency (Alcamí and Pereda, 2019). In addition, chemical synaptic transmission is episodic due to the all-or-none nature of action potentials, while electrical synaptic

transmission can be continuous (Alcamí and Pereda, 2019). When an action potential reaches a chemical synapse, an influx of calcium ion is needed in order to release the neurotransmitter into the synaptic cleft where it affects the postsynaptic cell. But electrical synapses do not depend on calcium because the pre- and postsynaptic neurons are directly connected via gap junction channels (Alcamí and Pereda, 2019). Further, a chemical synapse is functionally unidirectional during information processing in neuronal circuit. In contrast, electrical synapses are bidirectional with respect to flow of ions and passage of signals, thereby making the definition of pre- and postsynaptic neuron arbitrary (Alcamí and Pereda, 2019). These characteristics has been used in some electrophysiological studies to detect electrical synapses or differentiate them from chemical synapses.

1.2.4. Electrical synapses during development

Electrical synapses are expressed in the mammalian nervous system since the early stages of life, during development and thereafter. Studies indicate that gap junctions are essential in many processes from the prenatal phase. At this early stage, gap junctions provide neuroblasts with routes to coordinate metabolic processes rather than electrical communication. Furthermore, they have an essential role in synchronization of calcium waves and their propagation in the brain which are needed for neuronal proliferation and differentiation (Bruzzone and Dermietzel, 2006). In postnatal stage, despite that fact that gap junctions continue to perform as mediators of metabolic substrates they start to mediate neuronal communications by acting as electrical synapses in different CNS areas. In retina, for example, electrical coupling has been observed among ganglion cells and amacrine cells (Penn et al., 1994), where they generate spontaneous depolarizations and modulate the firing pattern of individual ganglion cells leading to their correlated activity

(Blankenship et al., 2011). Suprachiasmatic nucleus (SCN), is another brain area where electrical synapses are important in modulation of synchronous activity during development (Wang et al., 2014). Electrical synapses have also been identified in neonatal thalamus. In early postnatal mice, thalamic ventrobasal nucleus neurons communicate primarily via electrical synapses (Lee et al., 2010). It has been demonstrated that they have an essential role in the development of thalamic inhibitory networks by coupling reticular neurons (Zolnik and Connors, 2016). Electrical synapses formed of several connexin isoforms have also been localized in developing cerebral cortex especially during the first weeks (Bittman et al., 2002). These synapses cause synchronization of neural oscillations which recent findings suggest is related to cortical circuit development (Uhlhaas et al., 2010). Spinal cord is another CNS area that expresses electrical synapses in developmental phases starting from the embryonic stage. For instance, studies have demonstrated expression of gap junctions in neonatal rat in motoneurons of lumbar segments (Chang et al., 1999). It has been suggested that electrical coupling ensures spread of subthreshold oscillations among specific collections of motoneurons (Tresch and Kiehn, 2000; Vinay et al., 2000). It is noteworthy that despite the decrease in gap junction expression or their disappearance in some areas of adult mammalian CNS, electrical synapses remain an integral part of the nervous system well after development and into adulthood (Nagy et al., 2018a) as it was discussed in earlier.

1.2.5. Regulation and plasticity of electrical synapses

Gap junctions are not static, but rather can change their synaptic strength or CC according to physiological activities in their environment. Gap junctions are regulated at two main levels; unitary conductance of each channel and number of channels assembled and inserted into the plasma membrane (Goodenough and Paul, 2009). Fast regulatory mechanisms of unitary

conductance include voltage-gating, phosphorylation, pH change, and actions of neurotransmitters and neuromodulators on electrical synapses. Connexins can respond to voltage potential changes and close or open their gap junction channels based on voltage across two coupled cells. However, they are different in their sensitivity to voltage changes; thus, heterotypic gap junctions composed of different connexons can display rectification across the channel(Goodenough and Paul, 2009). In this situation, one connexon could respond by rapidly closing due to the voltage change, while the other stays open. The phenomenon can result in either channel closure in response to postsynaptic potential or channel opening in response to presynaptic potential. This type of voltage-dependent channel regulation is observed in dendro-dendritic heterotypic (Cx45/Cx43) gap junctions in the CNS (Goodenough and Paul, 2009). Conductance across a gap junction can also change depending on connexin phosphorylation state. This occurs through the actions of serine/threonine kinases and tyrosine kinases such as protein kinase C (PKC), MAP kinase (MAPK), cAMP-dependent protein kinase, casein kinase (CK), p34cdc2, protein kinase G (PKG) and Ca^{+}/calmodulin-dependent kinase II (CaMKII). Conductance at Cx36-containing gap junction channels is well known to be regulated by Cx36 phosphorylation. This occurs in retina when photoreceptors coupled via Cx36-containing gap junctions adapt to dark and light visual fields. For example, in a bright environment, dopamine D4 receptors inhibit adenylyl cyclase in response to dopamine release and lower protein kinase A (PKA) activity, which in turn reduces connexin phosphorylation and uncouples cells in retina. Conversely, activating adenosine receptors results in an increase in coupling (Goodenough and Paul, 2009; Li et al., 2013). Another transmitter noradrenaline modulates gap junctions in GABAergic networks of the hippocampus. Application of noradrenaline onto stratum lacunosum-molecular interneurons *in vitro* caused a decrease in electrical coupling, suggesting that this process prevents hypersynchronous activity (Zsiros and

Maccaferri, 2008). Application of histamine onto vasopressin neurons in supraoptic nucleus caused an increase in electrical coupling (Zsiros and Maccaferri, 2008). Serotonin (5-HT) has shown to uncouple neurons in somatosensory cortex of neonatal rats, suggesting a role of 5-HT in modulation of gap junctions (Rörig and Sutor, 1996). Acetylcholine reduces electrical coupling in the CA1 area of the hippocampus, as shown by decreased dye coupling, spikelet frequency and spikelet amplitude after application of carbachol, a cholinergic agonist (Velazquez et al., 1997). Nitric oxide released from corticostriatal fibers increased gap junctional coupling in the striatum (O'Donnell and Grace, 1996). Gap junctional conductance can also be influenced by changes in pH. All connexin isoforms decrease their conductance in response to intercellular acidification except Cx36 (Račkauskas et al., 2010). Cx36-containing gap junctions increase their conductance when intracellular concentration of magnesium is high and decrease it when it is low. However, intracellular alkalization results in junctional conductance decrease independent of magnesium concentration (Rimkute et al., 2018).

Electrical coupling can also be modified by change in connexin production and gap junction formation. Connexins have a high turnover with a half-life of approximately 1 to 5 hrs, which is many times faster than other membrane proteins (Goodenough and Paul, 2009; Pereda, 2014; Evans, 2015). The turnover occurs by adding connexon subunits to the edges of gap junction plaques. Gap junction assembly is usually associated with a number of phosphorylation steps including phosphorylation of residues for intracellular connexin transport (Goodenough and Paul, 2009). Studies show that different connexins use different intracellular trafficking routes. For example, Cx26 is inserted into the plasma membrane post-translationally while Cx43 and Cx32 use the conventional secretory pathway (Evans, 2015). In addition, interaction with binding proteins such as CIP85, ZO-1 and tubulin can also influence the assembly process by inhibiting

connexin synthesis or its dysregulation. For instance, Cx43 binding to ZO-1 regulates accretion of connexons in the membrane (Goodenough and Paul, 2009). Degradation also contributes to turnover, which occurs by the removal of connexon subunits from the center of plaques. A large portion of a gap junction can also be removed by internalization which results in a huge double-membraned intracellular vesicle. Similar to the production pathway, phosphorylation plays an important role in connexin degradation by either blocking or enhancing the degradation in proteasome or lysosome. For example, serine phosphorylation in Cx45.6, which is the counterpart of Cx50 in the chick leads to its degradation (Goodenough and Paul, 2009).

As noted above, there is evidence that electrical synapses are dynamic and change in an activity-dependent manner (Bennett, 1997; Pereda et al., 2013). Activity-dependent modification of electrical synapses occurs at excitatory mixed synapses and those formed by GABAergic inhibitory neurons. Studies on glutamatergic mixed synapses on goldfish Mauthner cells showed that gap junctional conductance can change based on level of activity and can result in short-term potentiation (LTP) and long-term potentiation (LTP). For instance, gap junctions formed of Cx36 in AII amacrine cells of retina cause LTP by high frequency presynaptic activity. These activity-dependent potentiations chiefly regulated by CaMKII and PKA (Pereda et al., 2013). In the dorsal area of the thalamus, TRN neurons that serve as relay neurons for thalamocortical inhibition and are coupled by Cx36-containing gap junctions can also change their coupling state depending on their level of activity. Further. coordinated burst firings of pairs of coupled neurons in TRN has shown to induce long-term depression (LTD) in these neurons. The above described production mechanisms governing production and deregulation of gap junctions including phosphorylation, were suggested to contribute to the occurrence of LTD (Haas et al., 2011).

1.3. Sympathetic nervous system

The sympathetic nervous system (SNS) is a subdivision of the autonomic nervous system and has central and peripheral components (Martin and David, 2012). In the time of external stress and threats, the SNS is engaged to increase cardiac output and peripheral vasoconstriction to augment overall blood pressure in the body. This occurs in order to direct the blood flow toward skeletal muscles, heart muscle and the brain that face increased physiological need .(Diamond and Cribbet, 2013). Sensory information related to autonomic functions in peripheral tissues reaches the spinal cord via dorsal roots and cranial sensory ganglia. The received information is processed in coordinated areas of the brain including the hypothalamus in what is called the central autonomic network (Kandel, 2013). Autonomic information reaching the nucleus of solitary tract is transmitted via ascending projections to higher brain centers such as forebrain and via descending projections to brainstem and spinal cord. The descending projections control the activity of sympathetic preganglionic neurons (SPNs) in the spinal cord that are located in the thoracic and upper lumbar segments in lateral horns(Kandel, 2013; Deuchars and Lall, 2015). SPNs innervate sympathetic postganglionic neurons whose cell bodies are mostly located in sympathetic ganglia. SPNs are the final neurons in the CNS from which sympathetic outflow occurs (Deuchars and Lall, 2015). SPNs send their axons through the ventral roots to synapse onto postganglionic neurons that are located in paravertebral sympathetic ganglia in the sympathetic chain or in prevertebral sympathetic ganglia. All paravertebral ganglia except the stellate ganglion and superior cervical ganglia are located bilateral to the spinal cord with generally one ganglion per segment, while prevertebral ganglia are located outside the chain and closer to the end organ (Kandel, 2013). Sympathetic postganglionic neurons synapse onto their end organs such as heart, blood vessels, bronchial airways, pilomotor muscles, salivary and sweat glands (Kandel, 2013). Chromaffin cells

in adrenal medulla are an exception since they receive their input directly through SPN axons without a postganglionic neuron as an intermediate (Appel and Elde, 1988).

1.3.1. Neurotransmitters of the sympathetic nervous system

All SPNs release ACh onto sympathetic postganglionic neurons in ganglia. Sympathetic postganglionic neurons can have more than one type of cholinergic receptor, including nicotinic as well as muscarinic ACh receptors that produce fast and slow excitatory postsynaptic potentials, respectively. Excitation of postganglionic neurons results in release of noradrenaline from these cells, which in turn can result in a variety of physiological responses based on the type of adrenergic receptors with which noradrenaline interacts. Interaction with α_1 receptor results in vasoconstriction and smooth muscle contraction in urethra, gastrointestinal tract and iris. Interaction with α_2 receptors located on the presynaptic cell results mostly in presynaptic inhibition and reduction of norepinephrine release. Interaction with β_1 receptor located on heart muscles increases heart rate and strength of contraction. Interaction with β_2 receptor causes smooth muscle relaxation in airways as well as glycogenolysis in liver. Furthermore, binding β_3 receptor can stimulate lipolysis in fat cells and reduce bladder contraction (Kandel, 2013). Both sympathetic preganglionic and postganglionic neurons can release more than one transmitter at a time along with their main neurotransmitters ACh and norepinephrine (Kandel, 2013). For example, ATP is released from sympathetic postganglionic neurons along with norepinephrine and causes vasocontraction when bound to P_2X receptors and vasodilation when bound to P_2Y receptors (Pablo Huidobro-Toro and Verónica Donoso, 2004). Another example is neuropeptide Y (NPY) that can also be released along with norepinephrine from sympathetic postganglionic neurons and has two types of receptors, NPY_1 and NPY_2. The former is located postjunctionally and potentiates

vasoconstriction or facilitates vasomotor responses in a variety of vessels when bound to NPY. In contrast, NPY_2 is located prejunctionally and generally reduces the release of other SPN neurotransmitters (Pablo Huidobro-Toro and Verónica Donoso, 2004).

1.3.2. Sympathetic preganglionic neurons

SPNs receive inputs from supraspinal centers and from interneurons on which primary afferents converge in the spinal cord. Studies have shown that severing connection to SPNs from supraspinal centers by spinalization causes a reduction in their activity. Severing the dorsal roots reduces SPN activity in a similar way. The dorsal root activity is identified by the shorter latency response to stimulation compared to spinalization (Deuchars and Lall, 2015). Considering neurochemical profile of SPNs, a number of markers can be used in combination with other methods such as retrograde tracing to label these neurons for anatomical studies. For example, since all SPNs are cholinergic, one marker is choline acetyltransferase (ChAT) enzyme that produces acetylcholine (Deuchars and Lall, 2015). Additionally, most SPNs especially in more lateral regions of the IML express neuronal nitric oxide synthase (nNOS), which is an indication of nitric oxide production (Deuchars and Lall, 2015). However, there is a degree of variability in nNOS expression in SPN projections to the adrenal gland and postganglionic neurons (Anderson et al., 1993; Hinrichs and Llewellyn-Smith, 2009). Consequently, caution is required in interpreting data derived from nNOS labeling. SPNs are located mostly in thoracic and upper lumbar segments of the spinal cord and include four major nuclei that are organized bilaterally (Deuchars and Lall, 2015). The majority of SPNs are in the intermediolateral cell column (IML) that is located laterally in gray matter bordering the lateral funiculus white matter. They cluster in groups that have different shapes and distances from each other which changes based on their spinal cord segments (Deuchars and Lall,

2015). SPN dendrites can extend rostrocaudally for hundreds of micrometers through the clusters (Dembowsky et al., 1985) and can also extend mediolaterally forming a complex network of neuronal processes (Pyner and Coote, 1994, 1995). Lateral to the IML in the white matter, a group of SPNs are located in the lateral funiculus (Deuchars and Lall, 2015), where they form mostly mediolaterally oriented dendritic processes (Petras and Cummings, 1972; Barber et al., 1984). Additional SPN groups are located in the intercalated nucleus (IC) medial to the IML, and the central autonomic area (CA) near the central canal (Deuchars and Lall, 2015). These four nuclei and their processes form a ladder-like structure when examined in horizontal spinal cord sections (Hosoya et al., 1991; Llewellyn-Smith, 2009b).

SPNs innervate many organs throughout the body. Despite many studies conducted on SPN projections, the exact pathway with which each SPN or SPN group reaches its target is not clear. It is known that SPNs project via the ventral root from the segment in which they are located (Kuo et al., 1980; Rubin and Purves, 1980). It is also known that each SPN innervates many (about 200 in humans and 15 in rats) postganglionic neurons (Deuchars and Lall, 2015). Bilateral organs such as adrenal gland receive ipsilateral sympathetic input that generally arise from the thoracic segments of spinal cord (Appel and Elde, 1988; Deuchars and Lall, 2015), although some contralateral projections have been identified in lumbar segments (Deuchars and Lall, 2015). Aside from segmental projections, retrograde double-labeling studies illustrated that different organs might receive input from one SPN population but not the exact same neurons, implying SPN specific functionality. Furthermore, similar studies have provided evidence for differential projections of SPNs based on their mediolateral and rostrocaudal location (Deuchars and Lall, 2015). Overall, it can be concluded that there is some degree of topographical organization in

SPNs. However, it is not possible to identify the function of an individual or a group of SPNs based solely on their spinal cord location.

1.3.3. Electrophysiological and anatomical evidence of electrical coupling in SPNs

A series of studies conducted in the 1990s provided the first evidence for electrical coupling between SPNs. Logan and his colleges embarked on these studies based on their observation of spontaneous membrane potential oscillations in a population of SPNs. These oscillations (i.e. spikelet) were characterized as having a fast depolarization and a slower hyperpolarization. Previously, spikelets had been observed in neurons of other CNS areas such as locus coeruleus, where they were later shown to be the product of electrical coupling (Logan et al., 1996a). As a result, Logan and his colleges predicted that electrical coupling of SPNs gives rise to their spontaneous membrane potential oscillations similar to those in locus coeruleus neurons. They used rat spinal cord slices *in vitro* combined with whole-cell recording techniques to test for SPN electrical coupling and showed that about 26% of SPNs oscillate spontaneously. They established the presence of electrical coupling based on criteria used by researchers in the electrical synapse field. According to this criteria, a short-latency depolarization (SLD) evoked by antidromic stimulation of axons is electrotonic in origin if at least three of the following is true for these depolarizations: Shorter latency compared to monosynaptic chemical potentials, insensitivity to calcium removal from the medium, insensitivity to membrane potential change, graded response to increased stimulus intensity, resistance to high frequency stimulation and resistance to collision with action potentials from the soma (Logan et al., 1996a). Using voltage-clamp recordings from oscillating SPNs, they showed that these oscillations are present independent of the membrane potential. In addition, they showed that frequency of spikelets can be changed in response to

injecting a current through the recording electrode, while many neurotransmitter antagonists did not affect the oscillations (Logan et al., 1996a). These findings indicated that SPN spikelets do not have a postsynaptic origin resulting from neurotransmitter release. To test the latency, Logan and his colleges adopted protocols similar to those used to demonstrate electrical synaptic interactions between neonatal spinal motoneurons. They stimulated SPNs antidromically via ventral roots to induce an action potential in one SPN and recorded the response in the other SPN that was presumably coupled to the stimulated cell. They applied lidocaine to the recorded cell to prevent spike firing in response to the action potential in the neighboring neuron. A biphasic remnant was revealed at the same latency as the antidromic stimulation which kept occurring after each ventral root stimulation (with 20 Hz frequency) even after 3 hrs of lidocaine application. These biphasic remnants were insensitive to membrane hyperpolarizations and produced graded response with increasing intensity of ventral root stimulations. Moreover, the recorded oscillations did not disappear in a low-calcium, high-magnesium medium (Logan et al., 1996a). These characteristics fulfilled the SLD criteria which was taken to indicate SPN electrical coupling. The same research group investigated the properties of electrical synapses between SPNs in more detail a few years later. They showed that current injection into either of a pair of two presumably coupled SPNs results in generation of a spikelet in the other. The bidirectionality of signal transmission was further evidence that electrical synapses were involved (Nolan et al., 1999). They also observed that upon increasing the frequency of stimulations in one cell, the coupled cell showed a dramatic attenuation in response to higher frequency components, while slower events such as AHPs were affected the least, which was consistent with low-pass filtering behavior of electrical synapse (Nolan et al., 1999). Furthermore, they recorded action potential firing and subthreshold membrane oscillations from pairs of SPNs simultaneously, which showed synchronous activity in the

recorded pairs. The same synchronization was observed when they injected positive current in one cell and recorded from the other (Nolan et al., 1999). This was another indication of electrical synapses between SPNs, because a hallmark of these synapses is that they confer synchronization of neuronal activity, as has been shown in many CNS site, In addition to physiological evidence, Logan and his colleges showed one case of biocytin tracer transfer between SPNs in the IML, which has not been repeated since (Logan et al., 1996b). About a decade later, immunohistochemical labelling showed Cx36 puncta (small dots of immunolabelling) associated with SPNs in IML in rats (Marina et al., 2008). A few years later, Lall and colleges co-labeled SPNs with antibodies against ChAT and antibody against cyan fluorescent protein as a reporter for Cx36 expression in transgenic mice (Lall et al., 2017). These studies illustrated that Cx36 is expressed in SPNs from which it can be inferred that this connexin is responsible for SPN electrical coupling.

1.4. Autonomic dysreflexia

Spinal cord injury (SCI) influences many individuals around the world. According to the world health organization (WHO), between 250,000 to 500,000 suffer a SCI each year (WHO, 2013). In Canada, it is estimated that over 85,556 people live with SCI including 51% traumatic SCI and 49% non-traumatic SCI (Noonan et al., 2012). Although the life expectancy for people with SCI has improved significantly from 1950 to 1980, with slower improvements since 2010, estimates show that it still ranges between 18% to 88% compared with general population (Savic et al., 2017). One of the leading causes of death in these individuals is cardiovascular diseases that occurs secondary to the spinal injury (Savic et al., 2017; Chopra et al., 2018; Eldahan and Rabchevsky, 2018). In general, 92% of people with chronic cervical or thoracic SCI experience sudden outbursts

of blood pressure (BP) increase in response to innocuous and noxious stimuli. This condition is referred to as autonomic dysreflexia (AD) (Hou and Rabchevsky, 2014; Lee and Joo, 2017). Usually, patients report experiencing AD symptoms and episodes between one month to one year after the injury. An AD episode is an increase in systolic blood pressure of 25 mm Hg which becomes more severe and more frequent if the injury is more complete. In addition, AD patients experience different degree of cardiovascular dysfunction depending on the spinal level of injury. Normally, sensory afferent impulses are generated due to cutaneous or visceral stimulations such as bladder and rectum distension, pressure ulcers, fractures, urinary tract infections (UTIs), and sexual intercourse. These stimuli lead to an increase in sympathetic activity as a reflex. The increase in sympathetic outflow results in vasoconstriction in lower part of the body and BP rise. The rise in BP is detected in the carotid sinus in the heart which leads to vagal stimulation and parasympathetic outflow. This is accompanied by the inhibition of the sympathetic nervous system via the spinal cord that restores the blood pressure balance. In people with SCI, communication between supraspinal centers regulating the sympathetic response and sympathetic neurons downstream in spinal cord is heavily disrupted. As a consequence, inhibition of sympathetic outflow does not occur which leads to generalized vasoconstriction and systemic hypertension. Concurrently, the parasympathetic nervous system continues to function undisturbed and causes bradycardia and vasodilation above the injury level. Patients with AD experience severe headaches, visual disturbance, nasal stiffness, anxiety, nausea as well as diaphoresis, flushing, and piloerection above the injury level, and dry and pale skin below the injury level. Other complications such as pulmonary edema, left ventricle dysfunction, retinal detachment, intercranial hemorrhage, seizures or death can result from hypertension. A range of cardiac problems can also develop due to AD such as tachycardia, arrhythmias and atrial fibrillation,

However, bradycardia, is the most common form of cardiac issue that can lead to cardiac arrest in more severe cases (Rabchevsky, 2006; Wan and Krassioukov, 2014; 2020).

A number of treatments including non-pharmacological and pharmacological are available for AD. In individuals with milder AD symptoms, hypertension is usually alleviated after removal of the stimulus that caused the hypertension. Postural maneuver can also be beneficial by lowering arterial BP through redistribution of blood in the lower extremities of the body (Eldahan and Rabchevsky, 2018). In more severe cases a variety of drugs including nitrates, nifedipine, prazosin and botulinum toxin can be employed to manage AD symptoms such as hypertension, all of which are more or less involved in inducing smooth muscle relaxation and vasodilation (Eldahan and Rabchevsky, 2018). It is important to note that all of these treatments are helpful in managing the symptoms and increase the overall quality of life for AD patients.

A variety of mechanisms have been suggested to contribute to development of AD. These mechanisms include loss of supraspinal input to SPNs, synaptic reorganization of SPNs, primary afferent sprouting of nociceptors, plasticity of ascending lumbosacral propriospinal fibers all in the spinal cord and adrenergic hypersensitivity in the periphery (Eldahan and Rabchevsky, 2018). Because SPNs are electrically coupled via Cx36-containing gap junctions (Logan et al., 1996a; Logan et al., 1996b; Nolan et al., 1999; Marina et al., 2008), the impact of SCI on Cx36 levels should be considered which has been examined, and reported using western blotting. These studies show that Cx36 expression decreases one week after transection and increases back to the normal levels in two weeks (Yates et al., 2008). In another study, using Cx36 wild-type and Cx36ko mice, animals with Cx36 ablation showed higher variance in heart rate (HR) and blood pressure (BP), and attenuated response to noxious stimulation (Lall et al., 2017). Another study has shown different BP response after application of noxious stimulation to Cx36 wild-type and Cx36ko mice

under isoflurane anesthesia (Coleman, 2019). Considering the evidence, a candidate for AD development might be potential differences in Cx36 expression before and after SCI.

1.5. Functional consideration of electrical coupling in SPNs

As it was presented earlier, there is a bulk of evidence indicating that SPNs are electrically coupled via Cx36-containing gap junctions (Logan et al., 1996a; Logan et al., 1996b; Nolan et al., 1999; Marina et al., 2008; Lall et al., 2017). However, the mere existence of gap junctions in mammalian SPNs raises more questions for future research than it provides answers. Numerous studies have provided evidence for functional roles of gap junctions acting as electrical synapses in different CNS areas including retina, olfactory bulb, hippocampus, cerebral cortex, suprachiasmatic nucleus, thalamic reticular nucleus, inferior olive and respiratory nuclei (Sasaki et al., 1989; Rekling et al., 2000; Landisman et al., 2002; Christie et al., 2005; Fukuda et al., 2006; Rash et al., 2007; Stewart and Béla, 2009; Allen et al., 2011; Ma et al., 2011; Bautista et al., 2014b; Blakley et al., 2015). Thus, it would be reasonable to believe that electrical synapses have a similarly important function in SPNs. A few studies have provided evidence of potential role of SPN electrical coupling particularly in heart rate and blood pressure regulation (Lall et al., 2017; Coleman, 2019). But their exact functional relevance is yet to be discovered in future studies. It is noteworthy that electrical coupling changes in some conditions such as peripheral nerve injury (Chang et al., 2000). Therefore, comparing the behavior of SPNs after SCI with their behavior in normal conditions and in Cx36ko animals would be another step to determine the exact function of electrical coupling in these neurons. It is also noteworthy that SPNs innervate many different organs mostly through postganglionic neurons which results in increase or decrease in sympathetic activity at the end organ. In some cases this can be problematic if the changes were physiologically

at odds and happened simultaneously (Jänig, 1996; Morrison, 2001). For example, exposure to warm temperature increases sympathetic sudomotor activity while inhibiting cutaneous vasoconstrictor fibers (Morrison, 2001). Obviously, coupling such SPNs that induce opposite (Excitation vs inhibition) effects downstream is not physiologically favorable. One explanation for such phenomenon is electrical coupling only in SPNs that have the same physiological affect after exposure to a stimulus. In other words, SPNs that respond by increasing activity to a certain stimulus should not fire at the same time as those that have to be inhibited. Gap junctions have shown to be highly modulated and plastic as well (Bennett, 1997; Pereda et al., 2013; Alcamí and Pereda, 2019), that enables them to open and close based on the signals they receive. Consequently, it is important to ask: which SPN groups are coupled? And, is the SPN coupling up- or downregulated during different sympathetic responses. An extensive and thorough documentation of Cx36 expression in SPNs brings us another step closer to answering these questions. SPN activity is also influenced by inputs from interneurons in the spinal cord and various groups of supraspinal neurons in central autonomic centers of the brain, adding to the complexity (Deuchars and Lall, 2015). In the brain, the rostro ventrolateral medulla (RVLM), A5 noradrenergic cell group of pontine region, raphe nuclei, the lateral hypothalamus, and the paraventricular nucleus (PVN) of hypothalamus to a higher extent and Barrington's nucleus, Kolliker-Fuse nucleus, the nucleus subcoeruleus, the arcuate nucleus, and the infralimbic cortex to a lesser extent provide input to SPNs. Apparently, retrograde tracing studies indicate that SPNs generate different outputs depending on the level of contribution from each of the autonomic supraspinal centers (Deuchars and Lall, 2015). Interneurons located in lamina V, VII and X (Deuchars and Lall, 2015), that receive sensory and supraspinal input, in turn, affect SPN activity. Interestingly, double retrograde labeling from different organs has rarely resulted in double labeled interneurons suggesting their

functional specificity (Deuchars and Lall, 2015). These observations make it difficult to predict the coupling status of SPNs and further emphasizes the significance of a comprehensive documentation of Cx36 expression in these neurons.

1.6. Overall objectives

Considering the lack of detailed anatomical data regarding Cx36 presence and distribution in SPNs, it would be beneficial to investigate the extent of Cx36 expression in rat and mouse models using immunohistochemistry. Moreover, evidence suggest differential HR and BP responses to noxious stimuli in Cx36ko and Cx36wt mice *in vivo* making it useful to examine these parameters in SCI mice to better understand the behavior of autonomic circuits after incidence of SCI and in conditions such as AD. In our study we aim to: 1) document the distribution of Cx36 among the four nuclei of SPNs, using immunofluorescence labelling for Cx36 ,and ChAT, nNOS and peripherin labelling for SPNs in adult and developing rat and mouse and 2) to examine the potential contribution of Cx36 on HR and BP regulation in response to noxious stimuli. We hypothesise that Cx36 is widely expressed in SPNs. We also hypothesise that spinalized mice have an increased HR and BP response to noxious stimuli compared to the intact Cx36wt mice.

PART II: Manuscript 1

Interrelationships between spinal sympathetic preganglionic neurons, autonomic systems and electrical synapses formed by connexin36-containing gap junctions

J.I. Nagy, H. Tavakoli, J. M. M Senecal, and K. Stecina*

Department of Physiology and Pathophysiology, Max Rady College of Medicine, Rady Faculty of Health Sciences, University of Manitoba, Winnipeg, Canada

Running title: Sympathetic preganglionic neurons and connexin36

No. of pages: 34
No. of figures: 6
No. of Tables: 1
No. of words: Abstract, 247; Introduction, 718; Discussion, 1552

*Address for correspondence:
Dr. James I. Nagy
Department of Physiology and Pathophysiology
Max Rady College of Medicine
Rady Faculty of Health Sciences
University of Manitoba
745 Bannatyne Ave, Winnipeg, Manitoba
Canada R3E 0J9
Email: James.Nagy@umanitoba.ca
Tel. (204) 789-3767
Fax (204) 789-3934

Highlights

- Connexin36 is highly expressed by sympathetic preganglionic neurons (SPNs)
- Connnexin36 is detected along the entire length of the spinal thoracic intermediolateral cell column
- SPNs are innervated by glutamatergic neurons that express Cx36
- SPNs receive GABAergic terminal contacts from neurons that express Cx36

Abstract – Spinal sympathetic preganglionic neurons (SPNs) are among the many neuronal populations in the mammalian central nervous system (CNS) where there is evidence for electrical coupling between cell pairs linked by gap junctions composed of connexin36 (Cx36). Understanding the organization of this coupling in relation to autonomic functions of spinal sympathetic systems requires knowledge of how these junctions are deployed among SPNs. Here, we document the distribution of immunofluorescence labelling for Cx36 among SPNs identified by immunolabelling of their various markers, including choline acetyltransferase, nitric oxide and peripherin in adult and developing mouse and rat. In adult animals, labelling of Cx36 was exclusively punctate and dense concentrations of Cx36-puncta were distributed along the entire length of the spinal thoracic intermediolateral cell column (IML). These puncta were also seen in association with SPN dendritic processes in the lateral funiculus, the intercalated and central autonomic areas and those within and extending medially from the IML. All labelling for Cx36 was absent from spinal cords of Cx36 knockout mice. High densities of Cx36-puncta were already evident among clusters of SPNs in the IML of mouse and rat at postnatal days 10-12. In Cx36-eGFP mice, eGFP reporter was absent in SPNs, thus representing false negative detection, but was associated with glutamatergic and GABAergic terminals localized along SPN dendrites. These results indicate widespread Cx36 expression in SPNs, further supporting evidence of electrical coupling between these cells, and suggest that SPNs may be innervated by a set of neurons that themselves may be electrically coupled.

Keywords: spinal autonomic neurons, gap junctions, electrical synapses, electrical coupling, immunofluorescence

Introduction

It is now widely recognized that electrical synapses formed by gap junctions between neurons (Bennett, 1997) are common in the mammalian central nervous system (CNS) (Connors et al., 2004; Connors, 2009; Pereda et al., 2013; Pereda, 2014). In brain, such synapses are found between both excitatory neurons and between inhibitory neurons, and they occur at a variety of subcellular locations to produce soma-somatic, soma-dendritic and proximal or distal dendro-dendritic synapses (Nagy et al., 2018). They also occur at nerve terminal contacts with post-synaptic neuronal somata or dendrites to create morphologically mixed chemical/electrical synapses (Nagy et al., 2019). Among the family of twenty connexins, more than half of which are expressed in cells of the CNS, the vast majority of electrical synapses are formed by gap junctions composed of connexin36 (Cx36) which is widely expressed in neurons of developing and adult CNS (Condorelli et al., 2000; Rash et al., 2000, 2001; Nagy et al., 2018). The Cx36-containing gap junctions that form electrical synapses are themselves complex entities, being composed of a variety of structural and regulatory proteins that have multiple interactions with Cx36 and with each other (Li et al., 2004, 2012; Lynn et al., 2012; Nagy and Lynn, 2018). This structural complexity together with associated intracellular signalling processes almost certainly contributes to the highly dynamic nature of electrical synapses, which can display plasticity in their strength of synaptic transmission (Hass et al., 2011, 2016; Pereda, 2014; O'Brien, 2014). Electrical synapses confer a variety of subtle, but critical properties to pairs of coupled neurons and to the activities of coupled neuronal networks (Curti, O'Brien, 2016; Alcami and Pereda, 2019). Among these is synchronization of subthreshold membrane potentials among coupled cells, which promotes synchronation of action potentials in a coupled population of neurons, resulting in synchronous network activity (Hormuzdi et al., 2004; Connors, 2009; Alcami and Pereda, 2019; Pereda, 2014; Pereda et al., 2013).

In contrast to major advances in understanding of electrically coupled systems in brain, studies of the functional contributions of electrical synapses to neuronal network activities in the spinal cord have been less extensive, though there is evidence for such synapses among various spinal neurons. These include coupling of motoneurons to each other during development (Fulton et al., 1980) and in sexually dimorphic motor nuclei in mature animals (Bautista and Nagy, 2014), and their formation of morphologically mixed synapses with primary afferent terminals (Rash et al., 1996; Bautista et al., 2014a). There is also evidence for electrical coupling between spinal interneurons, including a set of those that mediate presynaptic inhibition (Bautista et al., 2012) and another set related to locomotor rhythm generation (Hinckley and Ziskind-Conhaim, 2006; Wilson et al., 2007). These findings are

consistent with wide-spread immunofluorescence labelling of Cx36 in numerous areas of rat and mouse spinal cord (Bautista and Nagy, 2014; Bautista et al., 2012, 2014a,b), much of which has not yet been attributed to any particular neuronal type, but which likely forms the gap junctional basis for the electrical coupling observed.

Among electrically coupled classes of neurons in spinal cord, perhaps the most studied so far is coupling between sympathetic preganglionic neurons (SPNs). Early electrophysiological evidence satisfying criteria for neuronal electrical coupling, together with biocytin-tracer transfer, between SPNs was provided in several reports (Logan et al., 1996a,b; Nolan et al., 1999; van den Top, 2003; Pierce et al., 2010; Deuchars, 2015). In addition, putative Cx36 immunoreactivity has been detected largely intracellularly in SPNs of adult rat spinal thoracic segments 6-8, albeit with an anti-Cx36 antibody of uncertain specificity (Marina et al., 2008). More recently, transgenic mice with cyan fluorescent protein (CFP) reporter for Cx36 expression were shown to display CFP in a high percentage of SPNs in the intermediolateral cell column (IML) of the lateral horn, and Cx36 knockout (ko) mice showed deficits in heart rate and blood pressure regulation, which in part may be attributed to ablation of Cx36 in SPNs (Lall et al., 2017). Similar deficiencies in SPN related activities were seen after application of the gap junction blocker mefloquine in a working heart brain stem preparation (Lall et al., 2012). In order to aid interpretation of these and future physiological studies related to the contribution of SPN electrical coupling to the functional activities of spinal sympathetic systems, we examined immunofluorescence labelling of Cx36 associated with SPNs throughout the thoracic and upper lumbar segments using an anti-Cx36 antibody with proven specificity of Cx36 detection.

EXPERIMENTAL PROCEDURES

Animals and antibodies

Animals were obtained from the Central Animal Care Services at the University of Manitoba and used according to approved protocols by the Central Animal Care Committee of University of Manitoba, with minimization of stress and the numbers of animals used. Tissues from some animals were taken for use in other studies, thereby contributing to reduction of the total number of rats and mice used by laboratory personnel in various unrelated studies. Animals used in this study included: a total of ten adult male wild-type C57 BL/6-129SvEv mice greater than six weeks of age and weighing 25 to 30 g, and three similar aged C57 BL/6-129SvEv transgenic male Cx36 null mice, colonies of which were established at the University of Manitoba through generous provision of wild-type and Cx36 null breeding pairs (Deans

et al., 2001) from Dr. David Paul (Harvard); transgenic adult male (n = 9) and female (n = 9) mice in which Cx36 expression is normal and bacterial artificial chromosome provides eGFP expression driven by the Cx36 promoter, designated Cx36-eGFP mice. No differences in results were seen in male *vs.* female mice. The Cx36-eGFP mice were taken from a colony established at the University of Manitoba starting with breeding pairs obtained from UC Davis Mutant Mouse Regional Resource Center (Davis, CA, USA; see also http://www.gensat.org/index.html); four Cx36-eGFP mice at neonatal ages of 12-15 days; four adult male Sprague-Dawley rats at two months of age and weighing 200 to 275 g; and three male Sprague-Dawley rats at postnatal age 10. Both rats and mice were used because data from early literature related to the present work were often derived from rat tissues, and more recent similarly related studies involved the use of mice.

Immunofluorescence studies were conducted with the list of monoclonal and polyclonal primary antibodies given in Table 1, with the host species in which they were generated, antibody catalog designations, the commercial sources and the concentration or the dilution at which they were used during incubation with tissue sections. Western blotting and/or immunohistochemical labelling validation of antibody specificity for target proteins was provided by the commercial supplier. The monoclonal anti-Cx36 antibody (ThermoFisher, Rockford, Il, USA; formerly Life Technologies Corporation, and originally Invitrogen/Zymed Laboratories) used was previously characterized for specificity of Cx36 detection in various regions of rodent brain and confirmed using Cx36 null mice (Li et al., 2004; Rash et al., 2007a,b; Curti et al., 2012). Secondary antibodies included Cy3-conjugated donkey anti-mouse, anti-rabbit and anti-goat IgG diluted 1:600 (Jackson ImmunoResearch Laboratories, West Grove, PA, USA), AlexaFlour 488-conjugated donkey anti-mouse, anti-rabbit, anti-goat and anti-guinea pig IgG diluted 1:600 (Molecular Probes, Eugene, OR, USA), and Cy5-conjugated donkey anti-mouse, anti-rabbit and anti-chicken IgG diluted 1:500 (Jackson ImmunoResearch Laboratories). All primary and secondary antibodies were diluted in 50 mM Tris-HCl, pH 7.4, containing 1.5% sodium chloride (TBS) and 0.3% Triton X-100 (TBSTr), which additionally contained 10% normal donkey serum depending on the secondary antibodies used.

Table 1 here

Tissue preparation

Rats and mice were deeply anaesthetized and euthanized with an overdose of equithesin (3 ml/kg), placed on a bed of ice, and perfused transcardially with cold (4 ºC) 50 mM sodium phosphate buffer (pH

7.4), containing 0.1% sodium nitrite, 0.9% NaCl and 1 unit/ml heparin, using a total volume of 3 ml for mice and 25 ml for rats. This was followed by perfusion with cold (4 °C) fixative consisting of 0.16 mM sodium phosphate buffer (pH 7.4), 0.2% picric acid, and either 1%, 2% or 4% formaldehyde which was prepared by diluting a stock 20% solution of formaldehyde that had been stored as provided by the manufacturer in sealed ampules (Electron Microscopy Sciences, Hatfield, PA, USA). Mice were perfused with a fixative volume of 40 ml, and rats with a volume of 100 to 150 ml. Following perfusion with fixative, animals were perfused with a cold (4 °C) solution consisting of 10% sucrose in 25 mM sodium phosphate buffer (pH 7.4) to clear vasculature of fixative and to prevent overfixation. Brains were removed and stored at 4 °C for 24-48 h in cryoprotectant containing 25 mM sodium phosphate buffer (pH 7.4), 10% sucrose and 0.04% sodium azide. Alternately, for some animals perfused with 4% formaldehyde/picric acid fixative, brains were removed, post-fixed for 2 hrs in the same fixative and then transferred to cryoprotectant. For weak tissue fixation conditions (1% or 2% fixative), brains were taken for sectioning no longer than a few days after cryoprotection. Stronger fixations allowed longer times in cryoprotectant. Tissues were quickly frozen using dry-ice and sectioned at a thickness of 15 μm using a cryostat. Consecutive horizontal sections of the entire rostral and caudal half of thoracic and upper lumbar spinal cords were separately collected, or consecutive transverse sections of selected thoracic levels were collected. Sections were collected on gelatinized glass slides and then stored at -35 °C for up to several months before use.

Immunofluorescence procedures

The various antibodies listed in Table 1 produced optimal immunofluorescence labelling at different fixation strengths: labelling of Cx36 was optimal with 1% formaldehyde fixative and weak with 2%; labelling of peripherin was adequate using 1% fixative but best using 4% fixative with no post-fix; labelling of nNOS was robust with weak and strong fixation; labelling of ChAT was unacceptable with 1% or 2% fixative and only adequate with 4% fixation; labelling of eGFP was very poor, barely adequate and optimal with 1%, 2% and 4% fixation, respectively. Labelling of vglut1, vglut2 and eGFP was very poor with at 1% fixation, barely adequate at 2% and optimal at 4% fixation; labelling of synaptophysin was only examined at 4% fixation with which it was robust. Sections were processed for immunofluorescence staining as we previously described (Li et al., 2008; Curti et al., 2012; Nagy et al., 2013). Slide-mounted sections were removed from storage, air-dried at room temperature under a fan for 10 min, and then rehydrated in TBSTr for 20 min. For double and triple immunofluorescence,

sections were incubated simultaneously with two or three primary antibodies for 24 h at 4 °C, then washed for 1 h in TBSTr and incubated with appropriate secondary antibodies for 1.5 h at room temperature. The sections were then washed in TBSTr for 20 min, and then in TBS for 30 min. All sections were coversliped with the antifade medium Fluoromount-G (SouthernBiotech, Birmingham, AB, USA) and stored at -20 ºC prior to examination by fluorescence microscopy. Control procedures, involving omission of one of the primary antibodies with inclusion of the secondary antibodies used for double or triple labelling, indicated absence of inappropriate cross-reactions between primary and secondary antibodies for all of the combinations used in this study.

Immunofluorescence was examined either on a wide-field Zeiss Imager Z2 microscope or a Zeiss 710 laser scanning confocal microscope using ZEN image capture and analysis software (Carl Zeiss Canada, Toronto, Ontario, Canada). Data from wide-field and confocal microscopes were collected either as single scan images or z-stack images with multiple scans capturing a thickness of 2 to 4 µm of tissue at z scanning intervals of typically 0.4 to 0.6 µm using 10x and 20x objective lenses for wide-field images and a 40x objective lens for confocal images. Images were processed using Zeiss ZEN Black and Zeiss ZEN Blue software, and final images were assembled using CorelDraw Graphics (Corel Corp., Ottawa, Canada) and Adobe Photoshop CS software (Adobe Systems, San Jose, CA, USA). Images with Cy5 immunolabelling were pseudocoloured either blue or green depending on best quality for presentation. Unless otherwise indicated, images depict fields photographed from horizontal sections.

RESULTS

Association of Cx36 with SPN in adult mouse

Our analysis of the distribution and cellular localization of immunofluorescence labelling for Cx36 in relation to sites harbouring SPNs in thoracic and upper lumbar regions of spinal cord required selection of appropriate markers for SPNs. Typically, a well-characterized marker would be immunolabelling for ChAT in the cholinergic SPNs. However, various antibodies we have used for immunofluorescence detection of Cx36 in the CNS, including the one used here, produce optimal Cx36 detection only in tissues subject to weak (1 or 2%) formaldehyde fixation with no post-fix, while we have often found sufficient labelling for ChAT in spinal cholinergic neurons only after strong (4%) fixation together with a post-fixation. The alternate markers chosen were peripherin and nNOS, immunolabelling of which is compatible with labelling of Cx36 using weaker tissue fixation. Peripherin is an intermediate filament protein highly expressed in neurons of the peripheral nervous system, but is also found in central

neurons, including SPNs, that have projections to peripheral structures (Parysek and Goldman, 1988; Clarke et al., 2010; Zhao and Liem, 2016). Similarly, nNOS is expressed in the majority of SPNs (Reuss and Reuss, 2001; Hinrichs and Llewellyn-Smith, 2009) and is robustly detected by immunofluorescence under a wide variety of fixation conditions. Here, we confirmed the utility of these markers for immunofluorescence labelling of SPNs by showing that neurons in the IML immunopositive$^{(+)}$ for ChAT are uniformly peripherin^{+} (Fig. 1A) and that peripherin^{+} SPNs are nNOS^{+} in most regions of the IML (Fig. 1B).

Figure 1 here

Immunofluorescence labelling for Cx36 in mouse spinal cord horizontal sections simultaneously labelled for either nNOS or peripherin was examined along the entire rostrocaudal length of the IML at thoracic and upper lumbar levels. In sections through the centre of the IML in the dorsoventral plane, nNOS^{+} neuronal somata and long dendritic processes of SPNs were seen running rostrocaudally often in continuity along the length of the IML, as shown in a low magnification photomontage (Fig. 2A1). Intermittent bundles of nNOS^{+} dendrites were emitted from the IML and traversed medially reaching close to the central canal, similar to the organization of ChAT^{+} SPNs described in rat (Barber et al., 1984). Immunofluorescence labelling of Cx36 was distributed at various densities in all regions of spinal cord gray matter. Immunolabelling was most concentrated in intermittently occurring patches that straddle the central canal area in what we previously described as PACx domains (Fig. 2A2), in which nerve terminals of primary afferents form mixed (chemical/electrical) synapses on clusters of neuronal somata in each patch (Bautista et al., 2014a). Immunolabelling of Cx36 was distributed continuously at moderate density along the IML and sparsely in intermediate gray matter regions medial to the IML (Fig. 2A2), where in both of these areas Cx36^{+} elements often following the course of nNOS^{+} neuronal somata and their dendrites (Fig. 2A1). Curiously, nNOS^{+} SPN dendrites extending medially invariably avoided the PACx domains to continue their medial trajectories between these domains. The association patterns of Cx36 with SPNs was similar whether SPNs were labelled with nNOS or peripherin.

A higher magnification of immunolabelling for Cx36 among peripherin^{+} SPNs and peripherin^{+} primary afferents in a PACx domain is shown in Fig. 2B. As in all other areas of the CNS we have examined, labelling of Cx36 had an exclusively punctate (*i.e.,* Cx36-puncta) appearance in these and other spinal cord regions. The punctate nature of labelling for Cx36 is less evident in the low magnification images showing a large area of the spinal cord in Fig. 2A. This was due to the requirement for image intensification, and hence saturation of labelling in the PACx domains, to allow visualization

of Cx36-puncta in the IML, which were more diminutive. We previously noted that Cx36-puncta detected *in vivo* reflect the localization of ultrastructurally-defined Cx36-containning gap junctions, thus allowing these immunofluorescent puncta to serve as a marker for electrical synapses formed by these junctions (Li et al., 2004; Kamasawa et al., 2006; Curti et al., 2012; Bautista and Nagy, 2014; Bautista et al., 2014a; Rubio and Nagy; 2015; Nagy et al., 2018, 2019). Others have also correlated localization of punctate immunofluorescence labelling of Cx36 to ultrastructurally detected neuronal gap junctions *in vivo* (Fukuda, 2009; Shigematsu et al., 2019). For reasons yet to be determined, intracellular labelling with our anti-Cx36 antibodies remains largely undetectable at least in neurons *in vivo*. Specificity of Cx36 detection by the antibody against Cx36 used here has been reported in a number of CNS regions (Li et al., 2012; Rash et al., 2007a,b; Curti et al., 2012), and is further evident with respect to detection of Cx36-puncta associated with SPNs, as shown by the absence of these puncta in spinal cord sections of Cx36 knockout mice (Fig. 2C, showing a field in the IML similar to that in a section from wild-type mouse in Fig. 2B). Intracellular background fluorescence in SPNs was of equal intensity in spinal cord sections from wild-type *vs.* Cx36 knockout mice.

Figure 2 here

Details of immunolabelling for Cx36 in association with SPNs is shown in Fig. 3. Within the thoracic spinal sympathetic system, Cx36-puncta were seen localized to each of its previously described four cell groups (Barber et al., 1984), including the principal intermediolateral nucleus (IMLp) consisting of intermittent clusters of SPNs in the lateral horn IML, the central autonomic cell column (CA) dorsal to the central canal, the intercalated nucleus (IC) located between IMLp and CA, and the funicular intermediolateral neurons (IMLf) in white matter lateral to the IMLp. Although not examined quantitatively, no major differences were evident in the density or distribution of Cx36-puncta associated with these cell groups at different thoracic spinal levels. The appearance of Cx36-puncta associated with SPNs in the IMLp is shown in Fig. 3A in a section labelled for ChAT, though albeit poorly in weakly fixed tissue as required for optimal labelling of Cx36. Sparse Cx36-puncta were seen around SPN neuronal somata and were more frequently localized to their $ChAT^+$ processes. Some Cx36-puncta localized to the surface of these somata appeared in their central regions in this maximum intensity projection of z-stack images, where localization of puncta in the z plane is confounded. Cx36-puncta were somewhat more concentrated among bundles of tightly packed rostrocaudally running dendrites in the IML or those that were slightly dispersed, allowing localization of these puncta to individual dendrites, as shown in an image double labelled for Cx36 and nNOS (Fig. 3B).

In regions of the IML displaying rostrocaudal fluctuations in the density of $nNOS^+$ SPN dendrites, the distribution of high densities of Cx36-puncta were very closely confined to areas occupied by these dendrites, with adjacent regions containing very few puncta (Fig. 3C), indicating selectively with which Cx36-puncta were restricted to regions of SPN elements. This is also evident among medial dendritic projections of SPNs, where Cx36-puncta were concentrated on these processes (Fig. 3D; higher magnification of the boxed area in Fig. 2A1). Other sympathetic cell groups also displayed a similar association of Cx36-puncta with SPN processes. In the IMLf, separate bundles of SPN dendrites penetrating into the lateral funiculus were accompanied by multiple Cx36-puncta along the length of individual processes, which increased in density at point of their convergence (Fig. 3E). Cx36-punta were also evident but considerably more sparse along SPN dendritic processes in the IC (Fig. 3F) and CA (Fig. 3G). It would be expected that Cx36-puncta as a marker of electrical synapses would be encountered at points of intersection between neuronal elements engaged in electrical coupling. Examples of this are not uncommon (Curti et al., 2012; Bautista and Nagy, 2014; Nagy and Rash, 2017) and instances of such localization were also evident in the present work, but the frequent co-alignment and close apposition of multiple SPN dendritic processes often prevented identification of specific dendrites harboring Cx36-puncta at their appositions.

Figure 3 here

Association of Cx36 with SPNs in adult rat and during development

Early electrophysiological studies providing evidence of gap junction-mediated electrical coupling between SPNs *in vitro* were conducted using rat thoracic spinal cord, and specifically spinal cord slices from animals between the ages of 7 to 22 days old (Logan et al., 1996a,b; Nolan et al., 1999). Slices of CNS tissues are often prepared from young animals for *ex vivo* analyses of neuronal and network electrical activities because slices at earlier stages of development remain more viable *vs.* those from adults. We therefore examined Cx36 association with SPNs in rat, both in adult and at earlier ages, as well as in mouse at younger ages. As in adult mouse, immunolabelling for Cx36 in adult rat was distributed throughout the thoracic IML in the lateral horn (Fig. 4A) as well as in the other SPN groups (not shown) described above in mouse. No major qualitative differences were observed in labelling patterns of Cx36 in relation to SPNs in adult rat *vs.* mouse. Labelling was again exclusively punctate, and Cx36-puncta were often localized along SPN dendritic processes (Fig. 4B).

Figure 4 here

As in other CNS regions (Pereda, 2014), electrical coupling between spinal neurons may be more prevalent during development, as suggested by the generally higher levels Cx36-puncta seen in the spinal cord at younger ages (Bautista et al., 2012; Bautista and Nagy, 2014). Not surprisingly, therefore, rich collections of Cx36-puncta were already evident among SPNs in rat spinal cord at postnatal day 10, as shown in IMLp neuronal clusters labelled for both ChAT and peripherin (Fig. 4C1). Although labelling for SPN markers along dendrites was poor at this age, some Cx36-puncta could be seen along the initial dendritic segments of SPNs (Fig. 4D) and, as in adults' cord, very few if any Cx36-puncta were localized to SPN neuronal somata.

Localization of eGFP in Cx36-eGFP mice

We next examined eGFP expression in spinal SPNs of transgenic Cx36-eGFP mice (Fig. 5), in which Cx36 expression is normal and bacterial artificial chromosome provides eGFP expression driven by the Cx36 promoter. We previously reported the localization of $eGFP^+$ neurons in several areas of the nervous system in these mice (Bautista and Nagy, 2014; Nagy and Rash, 2017; Nagy et al., 2018), and noted various technical considerations involving the use of this mouse strain (Rubio and Nagy, 2015). One of those was the occurrence of false-negative eGFP expression in neurons known to be electrically coupled and known to express Cx36. Here, we unfortunately found that SPNs represent another example of such a false-negative result, as shown by the absence of immunolabelling for eGFP in $peripherin^+$ SPN somata of the IML Fig. (5A,B), despite the presence of many $eGFP^+$ neurons distributed in other spinal cord regions (not shown), which served as a positive control for eGFP detection in neuronal somata. Among several hundred SPNs visualized by their markers (nNOS or peripherin), only a few SPNs were seen faintly labelled for eGFP (Fig. 5C). However, the entire length of the IML and the various SPN cell groups were invested with $eGFP^+$ elements (Fig. 5A-C) that appeared to be nerve terminals or varicose axons (Fig. 5D). These elements were not labelled for the SPN marker peripherin (Fig. 5E) but were closely associated or in contact with $peripherin^+$ SPN dendrites (Fig. 5E,F).

Figure 5 here

Double immunolabelling for eGFP and the nerve terminal marker synaptophysin in thoracic spinal cord sections showed that the vast majority of $eGFP^+$ elements in the IML were also $synaptophysin^+$, confirming that these elements were synaptic boutons (Figs 6A,B). We therefore sought to determine the transmitter identity of these boutons. They were not $ChAT^+$ (not shown), as might be

expected given the paucity of cholinergic terminals in the IML (Barber et al., 1984; Markham and Vaughn, 1990) and the lack of SPN recurrent axon collateral innervation of the IML area (Dembowsky et al., 1985; Shen and Dun, 1990). Nor were they labelled for the glutamatergic terminal marker vglut1 (not shown), which was expected given the near absence of vglut1$^+$ terminals in the IML (Fig. 6C). Double labelling for eGFP and the GABAergic terminal marker GAD showed that a small percentage of the eGFP$^+$ boutons were also GAD$^+$ (Fig. 6D). Double labelling for eGFP and the glutamatergic terminal marker vglut2 revealed that some of eGFP$^+$ boutons were also vglut2$^+$ (Fig. 6E,F). The exact numbers could not be obtained but the estimates, derived from counts of all eGFP$^+$ boutons *vs.* double labelled (eGFP$^+$/GAD$^+$ or eGFP$^+$/vglut2$^+$) boutons in single scan confocal images were similar to those shown in Fig. 6D and 6F. These results suggest that Cx36-expressing SPNs in the IML receive a minor innervation from inhibitory GABAergic neurons and a major innervation from excitatory glutamatergic neurons that themselves express Cx36 and are electrically coupled.

Figure 6 here

DISCUSSION

The present result provides clarification of the distribution and relative density of immunofluorescent Cx36-puncta in spinal sympathetic nuclei and the association of these puncta with SPNs. We show Cx36-puncta localized to SPN dendritic processes in each of the spinal sympathetic nuclear subdivisions, and this localization was evident at all thoracic and upper lumber levels in adult mouse and rat. Further, Cx36-puncta were already present in abundance among SPNs at early ages, consistent with reports of electrically coupled SPNs in young animals (Logan et al., 1996a,b; Nolan et al., 1999; van den Top, 2003). The concentrations and expanse of Cx36-puncta in adult animals paralleled very closely the density and distribution of SPN somata and dendrites, which was iterated along the entire length of the IML. The absence of any detectable qualitative heterogeneity or mismatch between the density of Cx36-puncta and that of immunolabelled SPN elements along the rostrocaudal axis of the IML suggests a uniformity of Cx36 expression in SPN. This is consistent with a report where CFP reporter for Cx36 expression was found in the vast majority (94%) of ChAT$^+$ SPNs (Lall et al., 2017), suggesting that all or nearly all SPNs at least in the IML have gap junction formation capability. In this context and as noted in the Results section, it bares repetition that evidence from studies of numerous brain regions has indicated that immunofluorescent Cx36-puncta represent the localization of Cx36-containing gap junctions and hence electrical synapses (Li et al., 2004; Kamasawa et al., 2006 Fukuda, 2009; Curti et

al., 2012; Bautista and Nagy, 2014; Bautista et al., 2014a; Rubio and Nagy; 2015; Nagy et al., 2018, 2019; Shigematsu et al., 2019), and this is almost certainly true for Cx36-puncta associated with SPNs. With respect to the subcellular localization of these puncta, our results differ somewhat from those of Marina et al. (2008), who reported immunofluorescence labelling of Cx36 associated with SPNs and motoneurons, with detectability of what they referred to as minuscule Cx36-puncta by visualization only at high 63x objective lens magnification. Further, they reported intracellular punctate labelling within these two neuronal populations, and absence of cell surface labelling around both SPN and motoneuronal somata. In contrast, Cx36-puncta observed in the present work were evident at wide-field 10x objective magnification, occasional puncta were seen at SPN somatic surfaces, where intracellular labelling was minimal or absent. Further, we have previously reported an abundance of Cx36-puncta associated with the surfaces of motoneuronal somata and their initial dendrites, and an absence of intracellular immunolabelling of Cx36 in motoneurons (Bautista and Nagy, 2014; Bautista et al., 2014a,b). Differences in our results likely arise from the different anti-Cx36 antibodies used. Ours has been well-characterized (Li et al., 2012; Rash et al., 2007a,b; Curti et al., 2012; Lynn et al., 2018), including by demonstration of absence of Cx36 detection among SPNs in Cx36 ko mice (present data), whereas there remains some confusion surrounding the origin of that used by Marina et al. (2008); the specificity of their antibody was said to have been confirmed by western blotting, but the reference they cited for where this was done presented no western blots and used an anti-Cx36 antibody generated against a different sequence (Bittman et al., 2002) than the Cx36 sequence used for generation of antibody used by Marina et al. (2008).

Organization of SPN coupling

Understanding the organization of neuronal coupling in the spinal SPN system represents a major challenge. In many other systems where the localization of Cx36-containing electrical synapses has been studied, the deployment Cx36-puncta among apposing neuronal somata and/or dendrites is readily amenable to analysis as afforded by visualization of distinct cellular architectural features in combination with appropriate cell markers, thus allowing these puncta to serve as indicators for the identification of coupling partners and for the extent of coupling (Fukuda, 2009; Vervaeke et al., 2010; Nagy, 2012; Bautista and Nagy, 2014; Shigematsu et al., 2019). This approach to discerning coupling relationships among SPNs was precluded for most regions of the IML due to the tight bundling of their rostrocaudally oriented dendrites (Markham et al., 1991; Hosoya et al., 1991; Ezerman and Forehand, 1996), the intermingling of these with SPN somata and the inability to follow medially directed dendrites back to

their somata. The alternative approach involving dye coupling can reveal large networks of coupled neurons, but has so far had limited applicability among SPNs, with single cell injections of biocytin resulting in frequent absence of dye transfer or its transfer to only a few neurons (Logan et al., 1996a,b), which is not peculiar to SPNs, but has been encountered in other systems that are known to be well coupled by electrical synapses (Galarreta and Hestrin, 2001). Dye-transfer of SPNs injected with lucifer yellow has also been reported (Shen and Dun, 1990), but Cx36-containing gap junctions are known to be poorly permeable to this dye (Hormuzdi et al., 2004; Lee et al., 2014). It appears that individual SPNs may have at least several coupling partners and evidence for coupling was found in 26-28% of SPNs in both rat and mouse (Logan et al., 1996a,b; Lall et al., 2017). The remaining three-quarters of SPNs may not form gap junctions despite having capability to do so as noted above, or their junctional channels may have undergone either artifactual closure during spinal cord slice preparation or may normally be closed, but subject to regulation from closed to open states. The latter possibility is plausible given the now recognized highly dynamic nature of electrical synapses and their regulation by a plethora of neurotransmitter and neuromodulatory agents (O'Brien, 2014; Pereda, 2014; Pereda et al., 2013). Further, there is evidence in other systems that electrical synapses between neurons clearly linked by Cx36-containing gap junctions can exit in a silent or uncoupled state (Curti et al., 2012).

SPN coupling partners

If all SPNs do in fact form gap junctions, as suggested by the high percentage of those containing CFP reporter for Cx36 expression (Lall et la., 2017), then the question becomes whether they do so indiscriminately with each other or if there is selectivity in the choice of coupling partners. There is evidence for selectivity of coupling in other systems, e.g., among GABAergic cortical neurons where coupling occurs only between neuronal classes with similar electrophysiological properties (Galarreta and Hestrin, 2001), among GABAergic thalamic reticular nucleus neurons where coupling occurs preferentially between cells that are functionally and anatomically related (Lee et al., 2014), and among hypothalamic magnocellular neurons where coupling occurs only between cells containing similar peptide hormones (Cobbett et al., 1985). Because one hallmark function of electrical synapses is to promote synchronous neuronal activity, this function applied to SPNs would appear to require selectivity of coupling in distinct SPN populations that increase *vs.* those that concomitantly decrease their activities under specific physiological conditions, *i.e.,* selective coupling among SPNs with non-reciprocal actions in peripheral tissues and lack of coupling or regulated coupling among those with reciprocal actions (Cabot, 1996). Requirement of selectivity of coupling is especially true because the extensive dendrites

and somata of SPNs with reciprocal *vs.* non-reciprocal functions in different target tissues are highly intermingled along the IML (Cabot, 1996; Janig, 1996; Deuchars and Lall, 2015). The organization patterns and selectivity of coupling between SPNs could ideally be studied using retrograde transsynaptic transport of pseudorabies virus injected into different peripheral tissues to label SPNs followed by examination of dye-coupling patterns among labelled cells once a dye is developed that is readily permeable across gap junctions formed by SPNs.

Innervation of SPNs by coupled neurons

Our findings of $eGFP^+$ boutons in the IML of Cx36-eGFP mice that were immunopositive for either GAD or vglut2 raise the possibility that electrically coupled SPNs receive innervation from a set of inhibitory GABAergic neurons as well as another set of excitatory glutamatergic neurons that express Cx36 and may themselves be electrically coupled. The origin of these boutons is uncertain given the many inputs to SPNs from supraspinal sources and from spinal interneurons (Morrison, 2001; Llewellyn-Smith, 2009; Deuchars, 2011; Deuchars and Lall, 2015). However, $eGFP^+$ neurons are distributed in many regions of the spinal cord in Cx36-eGFP mice, with particularly dense concentrations of those around the central canal. Thus, one possible source of the GABAergic $eGFP^+$ terminals in the IML includes interneurons located dorsal to the central canal in lamina X, which have been reported to provide monosynaptic inhibitory input to SPNs (Deuchars et al., 2005; Deuchars, 2015). The $eGFP^+/vglut2^+$ terminals may have a similar origin from interneurons located in the central canal area. Within this area, a group of interneurons identified by their expression of the transcription factor Hb9 were shown to be $vglut2^+$ and were found to be electrically coupled not to each other, but to a set of non-Hb9 neurons that also were dye-coupled (Wilson et al., 2005, 2007). Although Hb9 neurons have been implicated in the control of rhythmic locomotor activity, it has been suggested that some of these neurons are well positioned to also influence rhythmic sympathetic activity, perhaps through projections to both sympathetic and somatic motor systems (Deuchars, 2007). The possibility of electrical coupling between interneurons antecedent to SPNs could further aid synchronous sympathetic output and may represent yet another site at which global genetic ablation of Cx36 in mice could compromise normal physiological functions of this output that have been reported in these mice (Lall et al., 2017).

Acknowledgements

This work was supported by grants from the Canadian Institutes of Health Research and the Canadian Natural Sciences and Engineering Research Council to K.S and J.I.N. These funding sources had no involvement in the design or any other facet of this report. We thank B. McLean for excellent technical assistance.

Conflict of interest

The authors have no conflict of interest to declare.

Author contributions

All of the authors contributed to collection and analyses of the immunofluorescence data and participated in writing the manuscript.

Data statement

The raw data will not be deposited in a public repository due to the complexity of its assembly, but it can be obtained upon request to the corresponding author.

Abbreviations

CA, central autonomic cell column; ChAT, choline acetyltransferase; CNS, central nervous system; CFP, cyan fluorescent protein; Cx36, connexin36; GAD, glutamic acid decarboxylase; eGFP, enhanced green fluorescent protein; IML, intermediolateral cell column; IMLp, principal intermediolateral nucleus; IMLf, funicular intermediolateral neurons; IC, intercalated nucleus; ko, knockout; nNOS, nitric oxide synthase; SPN(s), sympathetic preganglionic neurons; TBS, 50 mM Tris-HCl containing 1.5% sodium chloride; TBST, 50 mM Tris-HCl containing 1.5% sodium chloride and 0.3% Triton X-100; vglut1 and vglut2, vesicular glutamic acid transporter 1 and 2.

REFERENCES CITED IN PART II

Alcami P, Pereda AE (2019) Beyond plasticity: the dynamic impact of electrical synapses on neural circuits. Nat Rev Neurosci 20:253-271.

Barber RP, Phelps PE, Hourser CR, Crawford GD, Salvaterra PM, Vaughn JE (1984) The morphology and distribution of neurons containing choline acetyltransferase in the adult rat spinal cord: an immunocytochemical study. J Comp Neurol 229:329-346.

Bautista W, Nagy JI, Dai Y, McCrea DA (2012) Requirement of neuronal connexin36 in pathways mediating presynaptic inhibition of primary afferents in functionally mature mouse spinal cord. J Physiol 590:3821-39.

Bautista W, Nagy JI (2014) Connexin36 in gap junctions forming electrical synapses between motoneurons in sexually dimorphic motor nuclei in spinal cord of rat and mouse. Eur J Neurosci 39:771-787.

Bautista W, McCrea DA, Nagy JI (2014a) Connexin36 identified at morphologically mixed chemical/electrical synapses on trigeminal motoneurons and at primary afferent terminals on spinal cord neurons in adult mouse and rat. Neuroscience 263:159-180.

Bautista W, Rash JE, Vanderpool KG, Yasumura T, Nagy JI (2014b) Re-evaluation of connexins associated with motoneurons in rodent spinal cord, sexually dimorphic motor nuclei and trigeminal motor nucleus. Eur J Neurosci 39:757-770.

Bennett MVL (1997) Gap junctions as electrical synapses. J Neurocytol 26:349-366.

Bittman K, Becker DL, Cicirata F, Parnavelas JG (2002) Connexin expression in homotypic and heterotypic cell coupling in the developing cerebral cortex. J Comp Neurol 443:201-212.

Cabot JB (1996) Some principles of the spinal organization of the sympathetic preganglionic outflow. Prog Brain Res 107:29-42.

Clarke WT, Edwards B, McCullagh KJ, Kemp MW, Moorwood C, Sherman, DL, Burgess M, Davies KE (2010) Syncoilin modulates peripherin filament networks and is necessary for large-calibre motor neurons. J Cell Sci 123:2543-52.

Cobbett P, Smithson KG, Hatton GI (1985) Dye-coupled magnocellular peptidergic neurons of the rat paraventricular nucleus show homotypic immunoreactivity. Neuroscience 16:885-895.

Condorelli DF, Belluardo, N, Trovato-Salinaro A, Mudo, G (2000) Expression of Cx36 in mammalian neurons. Brain Res Rev 32:72-85.

Connors BW, Long MA (2004) Electrical synapses in the mammalian brain. Annu Rev Neurosci 27:393-418.

Connors, B.W. (2009) Electrical signaling with neuronal gap junctions. In: A.Harris, D.Locke (Eds.), Connexins: A Guide, Humana Press/Springer, pp. 143-164.

Curti S, Hoge G, Nagy JI, and Pereda AE (2012) Synergy between electrical coupling and membrane properties promotes strong synchronization of neurons of the mesencephalic trigeminal nucleus. J. Neurosci 32:4341-4359.

Curti S, O'Brien J (2016) Characteristics and plasticity of electrical synaptic transmission. BMC Cell Biol Suppl 1, 24:60-70, S

Deans MR, Gibson JR, Sellitto C, Connors BW, Paul DL (2001) Synchronous activity of inhibitory networks in neocortex requires electrical synapses containing connexin36. Neuron 31:477–485.

Dembowsky K, Czachurski J, Seller H (1985) Morphology of sympathetic preganglionic neurons in the thoracic spinal cord of the cat: an intracellular horseradish peroxidase study. J Comp Neurol 238:453-465.

Deuchars SA, Milligan CJ, Stornetta RL, Deuchars J (2005) GABAergic neurons in the central region of the spinal cord: a novel substrate for sympathetic inhibition. J Neurosci 25:1063-1070.

Deuchars SA (2011) Spinal interneurons in the control of autonomic function. In: Central Regulation of Autonomic Functions, ed. Llewellyn-Smith IJ & Verberne AJ, pp 140-160, Oxford University Press, NY.

Deuchars SA (2015) How sympathetic are your spinal cord circuits? Exp Physiol 100:366-372.
Deuchars SA and Lall (2015) Sympathetic preganglionic neurons: properties and inputs. Comp Physiol 5:829-869.

Ezerman EB, Forehand CJ (1996) Development and segmental organization of rostrocaudal dendrites of rat sympathetic preganglionic neurons. J Auto Nerv Syst 57:29-35.

Fukuda J (2009) Network architecture of gap junction-coupled neuronal linkage in the striatum. J Neurosci 29:1235-1243.

Fulton BP, Miledi R, Takahashi (1980) Electrical synapses between motoneurons in the spinal cord of the newborn rat. Proc R Soc London Ser B 206:115-120.

Galarreta M, Shaul Hestrin S (2001) Electrical synapses between GABA-releasing interneurons. Nat Rev Neurosci 2:425-433.

Haas JS, Zavala B, Landisman CE (2011) Activity-dependent long-term depression of electrical synapses. Science 334:389-393.

Haas JS, Greenwald CM, Pereda AE (2016) Activity-dependent plasticity of electrical synapses: increasing evidence for its presence and functional roles in the mammalian brain. BMC Cell Biol Suppl 1:14, 24:51-57.

Hinckley CA, Ziskind-Conhaim L (2006) Electrical coupling between locomotor-related excitatory interneurons in the mammalian spinal cord. J Neurosci 26:8477-8483.

Hinrichs JM, Llewellyn-Smith IJ (2009) Variability in the occurrence of nitric oxide synthase immunoreactivity in different populations of rat sympathetic preganglionic neurons. J Comp Neurol 514:492-506.

Hormuzdi SG, Filippov MA., Mitropoulon G, Monyer H, Bruzzone R (2004) Electrical synapses: a dynamic signaling system that shapes the activity of neuronal networks. Biochem Biophys Acta 1662: 113-137.

Hosoya Y, Okado N, Sugiura Y, Kohno K (1991) Coincidence of ladder-like patterns in distributions of monoaminergic terminals and sympathetic preganglionic neurons in rat spinal cord. Exp Brain Res 86:224-228.

Janig W (1996) Spinal cord reflex organization of sympathetic systems. Prog Brain Res 107:43-77.

Kamasawa N, Furman CS, Davidson KGV, Sampson JA, Magnie AR, Gebhardt BR, Kamasawa M, Yasumura T, Zumbrunnen JR, Pickard GE, Nagy JI, Rash JE (2006) Abundance and ultrastructural diversity of neuronal gap junctions in the OFF and ON sublaminae of the inner plexiform layer of rat and mouse retina. Neuroscience 142:1093-1117.

Lall VK, Dutschmann M, Deuchars J, Deuchars SA (2012) The anti-malarial drug mefloquine disrupts central autonomic and respiratory control in the working heart brainstem preparation of the rat. J Biomed Sci 19:103-114.

Lall VK, Bruce G, Voytenko L, Drinkhill M, Wellershaus K, Willecke K, Deuchars J, Deuchars SA (2017) Physiologic regulation of heart rate and blood pressure involves connexin36-containing gap junctions. FASEB J 31:3966-3977.

Lee SC, Patrick, SL, Richardson KA, Connors BW (2014) Two functionally distinct networks of gap junction-coupled inhibitory neurons in the thalamic reticular nucleus. J Neurosci 34:13170-13182.

Li X, Lynn BD, Nagy JI (2012) The effector and scaffolding proteins AF6 and MUPP1 interact with connexin36 and localize at gap junctions that form electrical synapses in rodent brain. Eur J Neurosci 35:166-181.

Llewellyn-Smith IJ (2009) Anatomy of synaptic circuits controlling the activity of sympathetic preganglionic neurons. J Chem Anat 38:231-239.

Logan SD, Spanswick D, Pickering AE, Gibson IC, Nolan MF, Cammack C (1996a) Gap junction coupling and the regulation of excitability in sympathetic preganglionic neurons. J Auto Nerv Syst 58:202-206.

Logan SD, Pickering AE, Gibson IC, Nolan MF, Spanswick D (1996b) Electrotonic coupling between rat sympathetic preganglionic neurons in vitro. J Physiol 495:491-502

Lynn BD, Li X, Nagy JI (2012) Under construction: Building the macromolecular superstructure and signaling components of an electrical synapse. J Membr Biol 245:303-317.

Lynn BD, Li X, Hormuzdi SG, Griffiths, EK, McGlade CJ, Nagy JI (2018) E3 ubiquitin ligases LNX1 and LNX2 localize at neuronal gap junctions formed by connexin36 in rodent brain and molecularly interact with connexin36. Eur J Neurosi. 48:3062-3081.

Marina N, Becker DL, Gilbey MP (2008) Immunohistochemical detection of connexin36 in sympathetic preganglionic and somatic motoneurons in the adult rat. Auton Neurosci 139:15-23.

Markham JA, Vaughn JE (1990) Ultrastructural analysis of choline acetyltransferase-immunoreactive sympathetic preganglionic neurons and their dendritic bundles in rat thoracic spinal cord. Synapse 5:299-312.

Markham JA, Phelps PE, Vaughn JE (1991) Development of rostocaudal dendritic bundles in rat thoracic spinal cord: analysis of cholinergic sympathetic preganglionic neurons. Dev Brain Res 61:229-236.

Morrison SF (2001) Differential control of sympathetic outflow. Am J Physiol 281:R683-R698.

Nagy JI (2012) Evidence for connexin36 localization at hippocampal mossy fiber terminals suggesting mixed chemical/electrical transmission by granule cells. Brain Res 1487:107-122.

Nagy JI, Rash JE (2017) Cx36, Cx43 and Cx45 in mouse and rat cerebellar cortex: species-specific expression, compensation in Cx36 null mice and co-localization in neurons vs. glia. Eur J Neurosci 46:1790-1804.

Nagy JI, Lynn BD (2018) Structural and intermolecular associations between connexin36 and protein components of the adherens junction-neuronal gap junction complex. Neuroscience 384:241-261.

Nagy JI, Lynn BD, Senecal JMM, Stecina K (2018) Connexin36 expression in primary afferent neurons in relation to the axon reflex and modality coding of somatic sensation. Neuroscience 383:216-234.

Nagy JI, Pereda AE, Rash JE (2018) Electrical synapses in mammalian CNS: Past eras, present focus and future directions. Biochim Biophys Acta 1860:102-123.

Nagy JI, Pereda AE, Rash JE (2019) On the occurrence and enigmatic functions of mixed (chemical plus electrical) synapses in the mammalian CNS. Neurosci Lett 695:53-64.

Nolan MF, Logan SD, Spanswick D (1999) Electrophysiological properties of electrical synpases between rat sympathetic preganglionic neurons in vitro. J Physiol 519:753-764.

O'Brien J (2014) The ever-changing electrical synapse. Curr Opin Neurobiol 29:64-72.

Parysek LM, Goldman RD (1988) Distribution of a novel 57 kDa intermediate filament (IF) protein in the nervous system. J Neurosci 8:555-563.

Pereda AE, Curti S, Hoge G, Cachope R, Flores CE, Rash JE (2013) Gap junction-mediated electrical transmission: Regulatory mechanisms and plasticity. Biochim Biophys Acta 1828:134-146.

Pereda AE (2014) Electrical synapses and their functional interactions with chemical synapses. Nat Rev Neurosci 15:250-263.

Pierce ML, Deuchars J, Deuchars SA (2010) Spontaneous rhythmogenic capabilities of sympathetic neuronal assemblies in the rat spinal cord slice. Neuroscience 170:827-838.

Rash JE, Dillman RK, Bilhartz BL, Duffy HS, Whalen LR, Yasumura T (1996) Mixed synapses discovered and mapped throughout mammalian spinal cord. Proc Natl Acad Sci 93:4235-4239.

Rash JE, Staines WA, Yasumura T, Pate, D, Hudson CS, Stelmack GL, Nagy J. (2000) Immunogold evidence that neuronal gap junctions in adult rat brain and spinal cord contain connexin36 (Cx36) but not Cx32 or Cx43. Proc Natl Acad Sci 97:7573-7578.

Rash JE, Yasumura T, Dudek FE, Nagy JI (2001) Cell-specific expression of connexins, and evidence for restricted gap junctional coupling between glial cells and between neurons. J Neurosci 21:1983-2000.

Rash JE, Olson CO, Pouliot WA, Davidson KGV, Yasumura T, Furman CS, Royer S, Kamasawa N, Nagy JI, Dudek FE (2007a) Connexin36, miniature neuronal gap junctions, and limited electrotonic coupling in rodent suprachiasmatic nucleus (SCN). Neuroscience 149:350-371.

Rash JE, Olson CO, Davidson KGV, Yasumura T, Kamasawa N, Nagy JI (2007b) Identification of connexin36 in gap junctions between neurons in rodent locus coeruleus. Neuroscience 147:938-956.

Reuss MH, Reuss S (2001) Nitric oxide synathase neurons in the rodent spinal cord: distribution, relation to substance P fibers and effects of dorsal rhizotomy. J Chem Neuroanat 21:181-196.

Rubio ME, Nagy JI (2015) Connexin36 expression in major centers of the auditory system in the CNS of mouse and rat: evidence for neurons forming purely electrical synapses and morphologically mixed synapses. Neuroscience. 303:604-629.

Shen E, Dun NJ (1990) Neonate rat sympathetic neurons intracellulary labelled with lucifer yellow in thin spinal cord slices. J Auto Nerv Syst 29:247-254.

Shigematsu N, Nishi A, Fukuda T (2019) Gap junctions interconnect different subtypes of parvalbumin-positive interneurons in barrels and septa with connectivity unique to each subtype. Cereb Cortex 29:1414-1429.

van den Top M, Nolan MF, Lee K, Richardson PJ, Buijs RM, Davies CD, Spanswick D (2003) Orexins induce increased excitability and synchronisation of rat sympathetic preganglionic neurones *J Physiol* 549:809–821.

Vervaeke K, Lőrincz A, Gleeson P, Farinella M, Nusser Z, Silver RA (2010) Rapid desynchronization of an electrically coupled interneuron network with sparse excitatory synaptic input. Neuron 12:435-451.

Wilson JM, Cowan AI, Brownstone RM (2007) Heterogeneous electrotonic coupling and synchronization of rhythmic bursting activity in mouse Hb9 interneurons. J Neurophysiol 98:2370-2381.

Wilson JM, Hartley R, Maxwell DJ, Todd AJ, Lieberam I, Kaltschmidt JA, Yoshida Y, Jessell TM, Brownstone RM (2005) Conditional rhythmicity of ventral spinal interneurons defined by expression of the Hb9 homeodomain protein. J Neurosci 25:5710-5719.

Zhao, J, Liem RK (2016) a-Internexin and peripherin: expression, assembly, functions and roles in disease. Meth Enzymol 568:477-507.

Table 1. Primary antibodies used for immunofluorescence labelling, with type, species in which they were produced, designated catalogue number by supplier, dilution employed in this study and commercial source.

Antibody	Type	Species	Designation	Dilution	Source*
Cx36	monoclonal	mouse	39-4200	2-4 µg/ml	ThermoFisher
peripherin	polyclonal	chicken	AB9282	2 µg/ml	EMD Millipore
nNOS	polyclonal	rabbit	C7D7	2 µg/ml	Cell Signalling
ChAT	polyclonal	goat	AB144	1:100	EMD Millipore
eGFP	monoclonal	rabbit	G10362	2 µg/ml	ThermoFisher
synaptophysin	polyclonal	guinea pig	101 004	1:500	Synaptic Systems
GAD	polyclonal	rabbit	ADI-MSA-225-E	1:250	Enzo Life Sciences
vglut1	polyclonal	guinea pig	AB5905	1:500	EMD Millipore
vglut2	polyclonal	guinea pig	135 404	1:500	Synaptic Systems

*Addresses of commercial sources are as follows: ThermoFisher, Rockford IL, USA; EMD Millipore, Temecula CA, USA; Cell Signalling, Davers MA, USA; Synaptic Systems, Gottingen, Germany; Enzo Life Sciences, Farmingdale NY, USA.

Figure legends

Fig. 1. ChAT, peripherin and nNOS localization in SPNs of the IML in a horizontal spinal cord section at midthoracic level of adult mouse, indicating the utility of peripherin and nNOS as markers of SPNs. (A) The same field showing immunofluorescence labelling for ChAT (A1) and peripherin (A2), with total co-localization of labelling in SPNs of the IML (arrows), as shown in overlay (A3). (B) The same field showing immunolabelling for nNOS (B1) and peripherin (B2), with co-localization of labelling in SPNs (arrows), as shown in overlay (B3).

Fig. 2. Association of Cx36 with SPNs in a horizontal midthoracic spinal cord section of adult mouse. (A) Low magnification showing a 1.2 mm length of spinal cord with overlay of immunofluorescence labelling for nNOS and Cx36 (A1) and, in the same field, labelling of Cx36 alone (A2). $nNOS^+$ neuronal somata located in the IML have dendrites heavily distributed along the length of the IML (A1, large arrow) and intermittently emit dendritic processes medially (A1, small arrows). Cx36-puncta are distributed along the IML (A2, large arrow) and are highly concentrated within PACx domains adjacent to the central canal (A1, A2, arrowheads). Medially directed bundles of SPN dendrites occupy regions between the PACx domains (A1, asterisks). Overlap of red and green fluorophores is seen as yellow. (B) Magnification of clusters of SPNs in the IML (arrows) and a portion of a PACx domain (arrowhead) labelled for Cx36 and peripherin (B1) and, in the same field, labelling of Cx36 alone (B2), showing the punctate appearance of Cx36 labelling (arrows). (C) A similar field as in B, but from a Cx36 ko mouse, showing $peripherin^+$ SPNs in IML (C1, arrows) and a total absence of labelling for Cx36 (C2).

Fig. 3. Immunofluorescence localization of Cx36-puncta at SPN somata and their processes in horizontal spinal thoracic sections of adult mouse. (A) Overlay of labelling for Cx36 and ChAT, showing $ChAT^+$ neuronal somata (arrowheads) in the IML and Cx36-puncta associated with $ChAT^+$ processes. (B) Overlay of immunolabelling for Cx36 and nNOS, showing Cx36-puncta intermingled among $nNOS^+$ SPN dendrites (arrows) in the IML. (C) Two patches of SPN neuronal somata and their dendritic processes (arrows) immunolabelled for Cx36 and nNOS (C1, overlay; C2, in the same field Cx36 alone), showing overlap in distribution of Cx36-puncta and $nNOS^+$ elements. (D) Magnification of the boxed area in Fig. 2 A1 with labelling of Cx36 among clusters of $nNOS^+$ SPN neurons (arrows) (D1, overlay;

D2, Cx36 channel alone), showing Cx36-puncta concentrated along their medially directed dendrites (arrowheads). (E) Overlay image of labelling for Cx36 and peripherin in the IML (arrow) and lateral funiculus (LF), showing Cx36-puncta localized to peripherin$^+$ SPN dendritic projections into the LF (arrowheads), with a concentration of puncta at a confluence of two dendritic bundles (box, magnified in inset). (F,G) Overlay of labelling for Cx36 and peripherin, showing peripherin$^+$ SPN neurons in the IC (F) and CA (G) spinal regions with Cx36-puncta associated with their dendrites (F,G, arrows) and somata (G, arrowhead).

Fig. 4. Immunofluorescence labelling of Cx36 in the IML of adult rat and neonatal rat and mouse. (A) Immunolabelling of Cx36 in IML of adult rat with overlay of labelling for peripherin (A1) and, in the same field, labelling for Cx36 in the red channel alone (A2), showing Cx36-puncta (A2, arrows) highly concentrated among peripherin$^+$ SPN somata and processes (A1, arrows), and peripherin$^+$ dendrites projecting medially (A1, arrowhead). (C) Magnification of the boxed area in A1, showing Cx36-puncta localized to peripherin$^+$ dendrites (arrows). (C,D) Low magnification of labelling for Cx36, ChAT and peripherin in the IML of PD10 rat (C), with boxed area in C magnified in D, showing overlay of labelling for Cx36/ChAT (D1), Cx36/peripherin and Cx36/ChAT/peripherin (D3). All ChAT$^+$ neurons are peripherin$^+$ and Cx36-puncta are highly concentrated among these neurons. (E) Neonatal mouse

Fig. 5. Immunofluorescence labelling of eGFP and peripherin in the IML in horizontal midthoracic sections of Cx36-eGFP adult mouse. (A,B) Images showing distribution of eGFP$^+$ processes (green) among a dense cluster of peripherin$^+$ SPNs in the IML (A, arrows), and among a bundle of peripherin$^+$ SPN dendrites (B, arrows) penetrating into the lateral funiculus (LF, arrowhead). (C) Images of labelling for eGFP and peripherin in overlay (C1) and, in the same field, labelling of eGFP alone (C2), showing peripherin$^+$ SPN neuronal somata and their dendrites largely devoid of labelling for eGFP, and only weak eGFP labelling in a few peripherin$^+$ neurons (C2, arrows). (D) Image showing varicose appearance of and eGFP$^+$ process in the IML (D1, arrow) and lack eGFP/peripherin co-localization (D2). (E,F) Labelling for eGFP (E1) and, in the same field, peripherin (E2), showing association and close apposition of eGFP$^+$ processes or eGFP-puncta to peripherin$^+$ dendrites, as seen in overlay (E3, arrows). (F) Magnification of the boxed area in E, showing eGFP association with peripherin$^+$ processes (arrows).

Fig. 6. Nerve terminal and transmitter identification of $eGFP^+$ processes in the IML of Cx36-eGFP adult mice. (A) Immunofluorescence labelling of eGFP (A1) and, in the same field, synaptophysin (A2), showing that most $eGFP^+$ elements are $synaptophysin^+$, as seen in overlay (A3, arrows). (B) Magnification of the boxed area in A. (C) Immunolabelling of vglut1 and overlay of the same field with labelling of peripherin in SPNs, showing near absence of $vglut1^+$ terminals in the IML (C1, asterisks). (D) Immunolabelling of GAD (D1) and overlay of the same field with labelling of eGFP (D2), showing GAD/eGFP co-localization in a proportion of $eGFP^+$terminals (arrows). (E1-3) The same field with immunolabelling of vglut2, eGFP and peripherin, where $vglut2^+$ terminals (E1) are highly concentrated among $eGFP^+$ terminals (E2) in areas of $peripherin^+$ SPNs of the IML (E3), and showing a high degree of eGFP/vglut2 co-localization, as seen in image overlay (E3, arrows). (F) Magnification of the boxed area in E showing eGFP/vglut2 co-localization (arrows).

Figure 1.

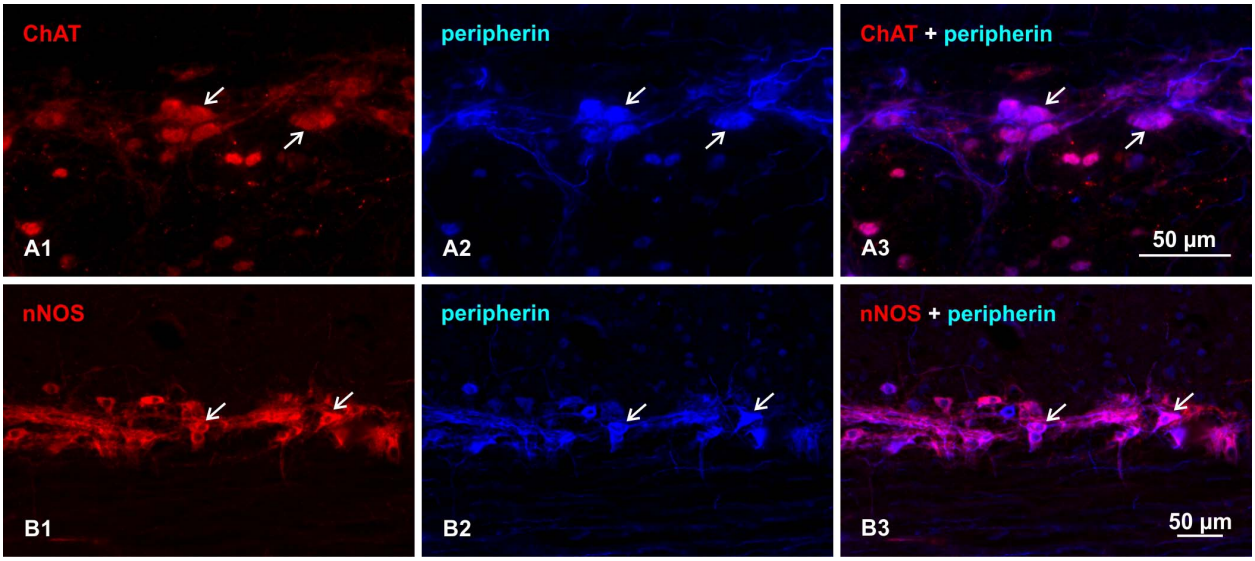
ChAT
peripherin
ChAT + peripherin
A1
A2
A3
50 µm
nNOS
peripherin
nNOS + peripherin
B1
B2
B3
50 µm

Figure 2.

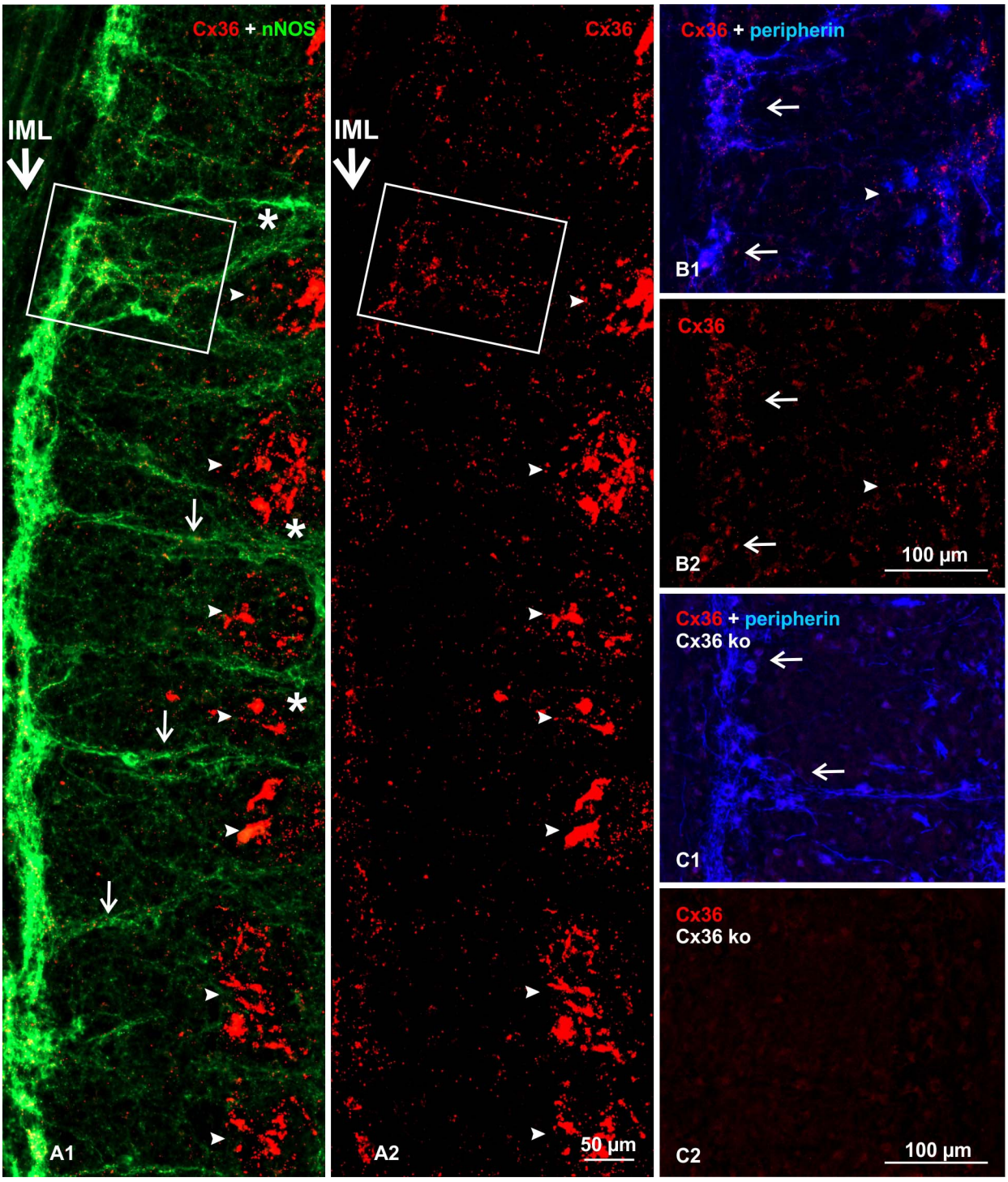
Cx36 + nNOS
IML
A1
Cx36
IML
A2
50 µm
Cx36 + peripherin
B1
Cx36
B2
100 µm
Cx36 + peripherin
Cx36 ko
C1
Cx36
Cx36 ko
C2
100 µm

Figure 3.

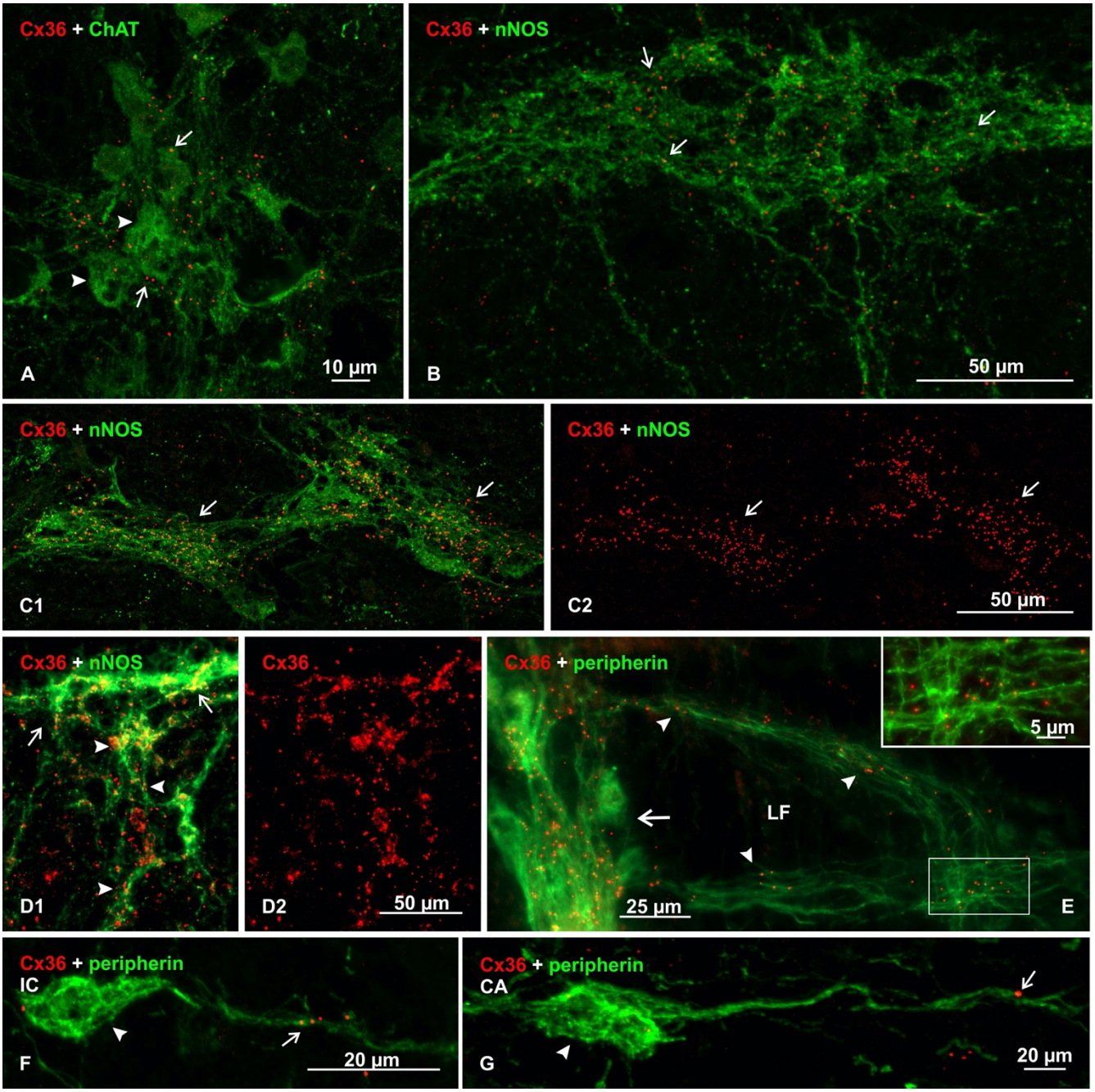
Cx36 + ChAT
A
10 µm
Cx36 + nNOS
B
50 µm
Cx36 + nNOS
C1
Cx36 + nNOS
C2
50 µm
Cx36 + nNOS
D1
Cx36
D2
50 µm
Cx36 + peripherin
5 µm
LF
25 µm
E
Cx36 + peripherin
IC
F
20 µm
Cx36 + peripherin
CA
G
20 µm

Figure 4.

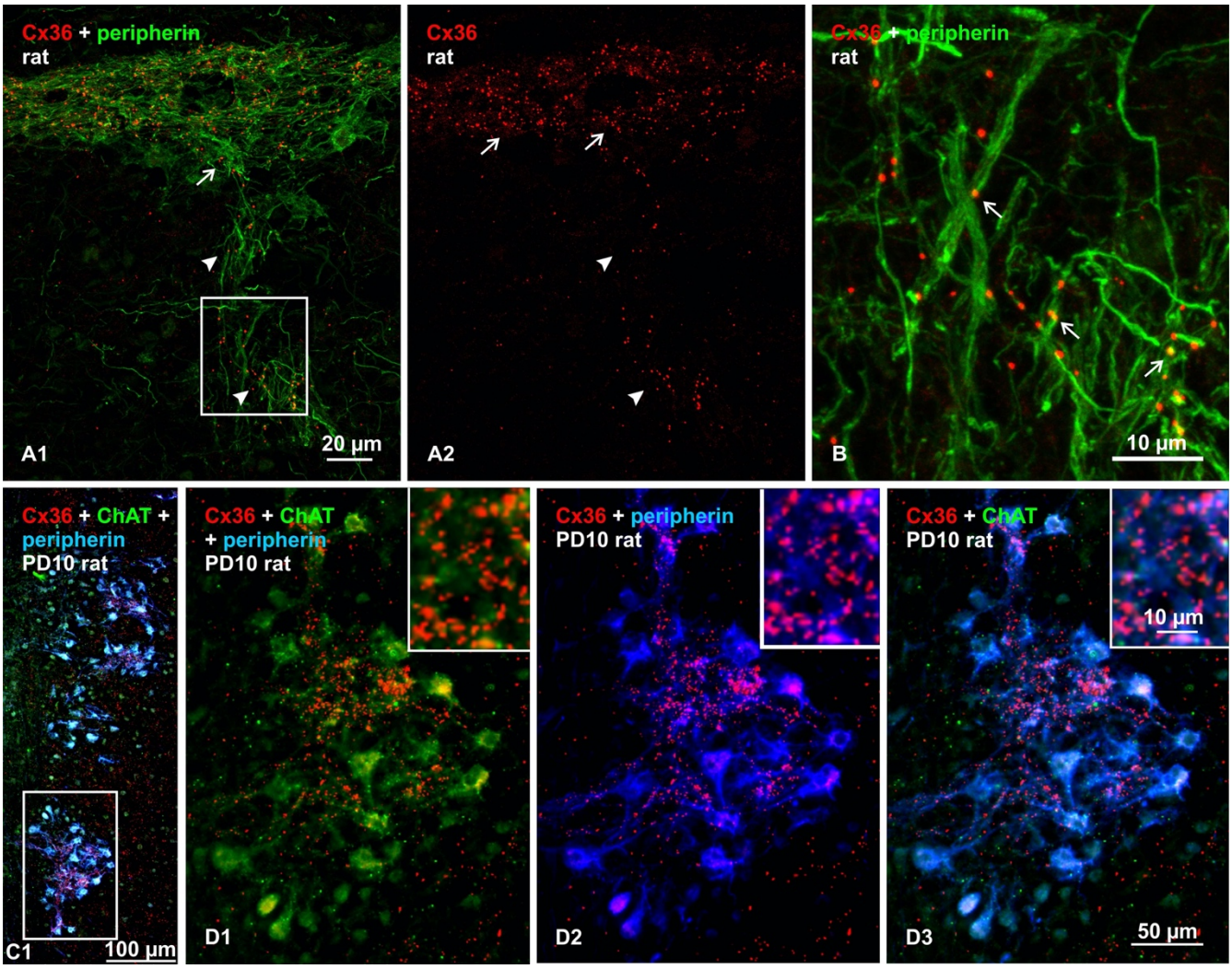
Cx36 + peripherin
rat
A1
20 µm
Cx36
rat
A2
Cx36 + peripherin
rat
B
10 µm
Cx36 + ChAT +
peripherin
PD10 rat
C1
100 µm
Cx36 + ChAT
+ peripherin
PD10 rat
D1
Cx36 + peripherin
PD10 rat
D2
Cx36 + ChAT
PD10 rat
10 µm
D3
50 µm

Figure 5.

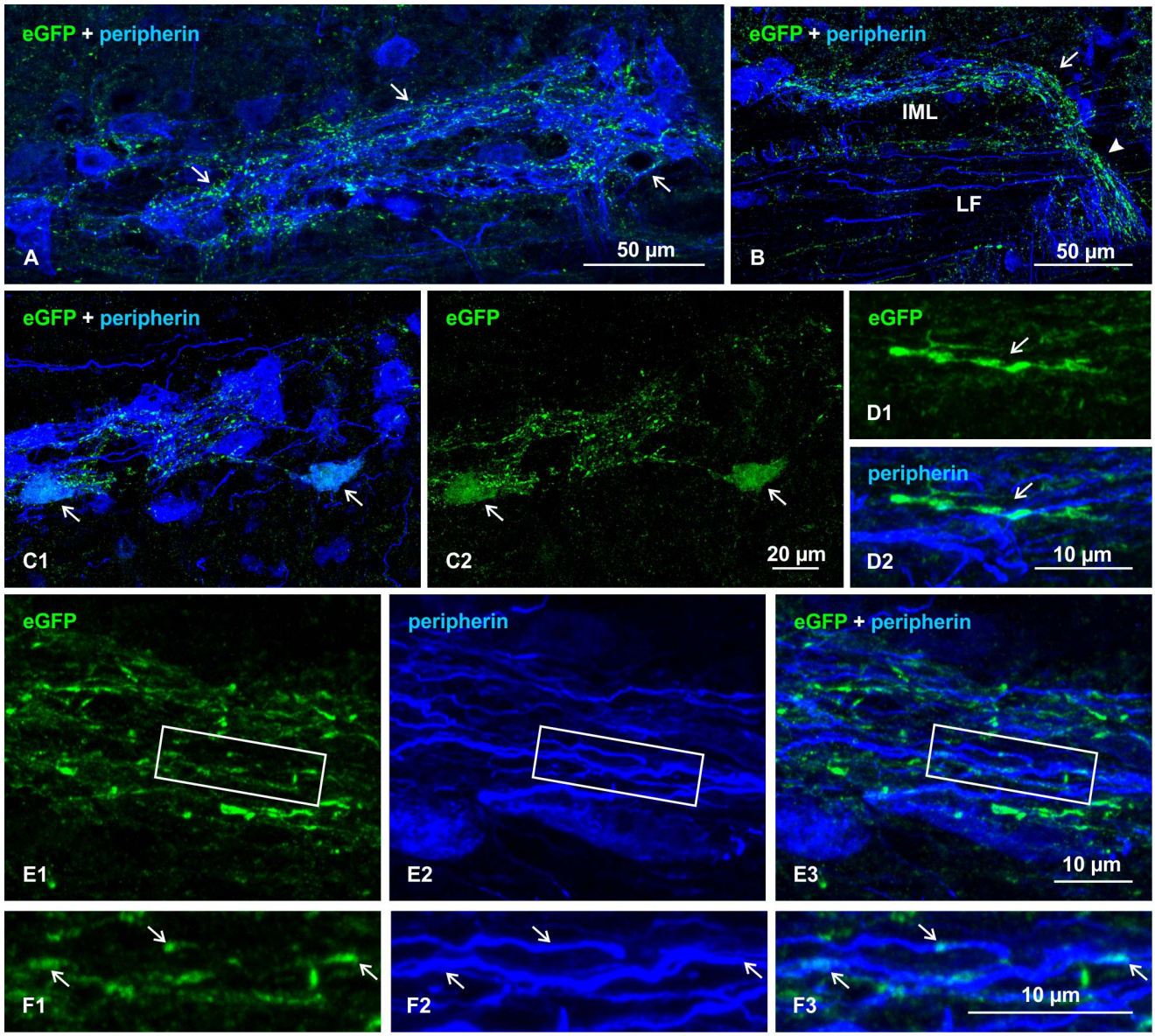
eGFP + peripherin
A
50 µm
eGFP + peripherin
IML
LF
B
50 µm
eGFP + peripherin
C1
eGFP
C2
20 µm
eGFP
D1
peripherin
D2
10 µm
eGFP
E1
peripherin
E2
eGFP + peripherin
E3
10 µm
F1
F2
F3
10 µm

Figure 6.

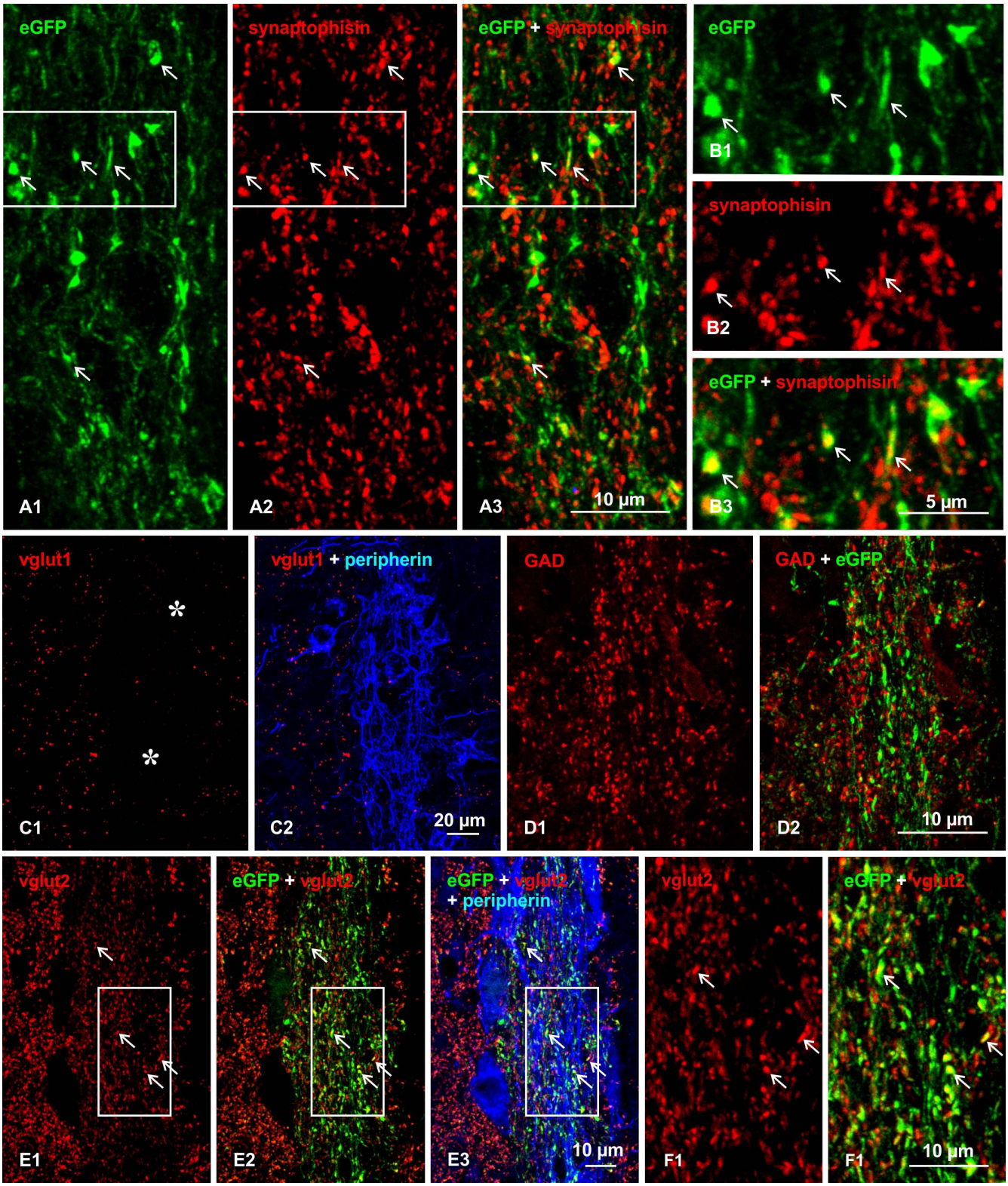
eGFP
synaptophisin
eGFP + synaptophisin
A1
A2
A3
10 μm
eGFP
B1
synaptophisin
B2
eGFP + synaptophisin
B3
5 μm
vglut1
vglut1 + peripherin
C1
C2
20 μm
GAD
GAD + eGFP
D1
D2
10 μm
vglut2
eGFP + vglut2
eGFP + vglut2 + peripherin
E1
E2
E3
10 μm
vglut2
eGFP + vglut2
F1
F1
10 μm

PART III: Manuscript 2

Examining the functional role of connexin36-containing gap junctions in sympathetic preganglionic neurons in responses to visceral afferent stimulation

A. Coleman[#], H. Tavakoli[#], J. Senecal, B. Lynn, K. Cowley, J.I. Nagy, K. Stecina*

 # These Authors have contributed equally to this study.

Department of Physiology and Pathophysiology, Max Rady College of Medicine, Rady Faculty of Health Sciences, University of Manitoba, Winnipeg, Canada

Running title: Function of connexin36 in sympathetic preganglionic neurons

No. of pages: 34
No. of figures: 7
No. of Tables: 3

Address for correspondence:
Dr. Katinka Stecina
Department of Physiology and Pathophysiology
Max Rady College of Medicine
Rady Faculty of Health Sciences
University of Manitoba
745 Bannatyne Ave, Winnipeg, Manitoba
Canada R3E 0J9
Email: Katinka.Stecina@umanitoba.ca
Tel. (204) 789-3767
Fax (204) 789-3761

Highlights

- Adult mice under isoflurane anaesthesia show response to colorectal distension (CRD)
- Respiratory rate changes after CRD in addition to blood pressure and heart rate
- Mice lacking connexin 36 protein have an attenuated blood pressure response to CRD
- Proposing a new *in vivo* method for dye-coupling-based estimation of gap junctional connectivity in adult sympathetic preganglionic cells

Abstract – The connexin36 (Cx36) protein is expressed in sympathetic preganglionic neurons (SPNs) and this protein is thought to enable electrical coupling. To uncover the functional role of Cx36 in SPNs we compared the responses to colorectal distension (CRD) and evaluated responses in wild type (wt) mice and in mice lacking Cx36 due to a global knock-out (Cx36ko) of this gene and also in spinal cord injured wt mice. The results showed that mean arterial blood pressure during CRD increased to 108±8% of baseline in wt mice (n=7) while in the Cx36ko mice (n=12) it did not change significantly but it showed a tendency to drop (to 97±2%). The heart rate did not show significant changes in either strains. This study also described, for the first time, respiratory rate changes in mice as part of the viscero-motor response to CRD. The increase to 109±2% of the baseline in wt mice was significant while the Cx36ko mice showed only a tendency for an increase. These results suggest a differential regulation of sympathetic activity associated with Cx36 expression in spinal intact mice. In wt mice with mid-thoracic complete spinal transection (n=2) we found that CRD stimulation also increased blood pressure when tested 6-8 days after injury. Furthermore, we used immunofluorescence labelling for Cx36 and SPNs in spinalized and intact mice as well as retrograde dye propagation in intact animals. Preliminary results showed that Cx36 expression near SPNs is detectable in mice 3 and 7 days after spinal cord injury. The retrograde dye experiments with intact mice provided proof-of-principle result that neurobiotin and tetramethylrhodamine dextran applied to nerves near the spinal cord can label neurons in adult mice given about 3 hours of survival after dye application. Overall, these experiments laid the foundations for new ways to examine the role of electrical coupling mediated via gap junctions formed by Cx36 protein in mature SPNs and related networks.

Keywords: gap junctions, electrical synapses, electrical coupling, autonomic dysreflexia, spinal cord injury model

Introduction

Autonomic nervous system (ANS), comprised of the sympathetic nervous system (SNS) and parasympathetic nervous system (PNS), is involved in regulating involuntary functions such as heartrate (HR), blood pressure (BP), digestion, fat metabolism, respiration and secretion by glands (Bankenahally and Krovvidi, 2016).

Sympathetic preganglionic neurons (SPNs), mostly located in the intermediolateral column (IML) of thoracic spinal cord segments are the last regulatory point of the central component of the SNS where sympathetic outflow can be controlled (Deuchars and Lall, 2015). Electrical coupling via Cx36-containing gap junctions have shown to be essential in synchronized neuronal activity in various other CNS areas such as thalamus, hippocampus and olfactory bulb (Christie et al., 2015; Fukuda and Kosaka, 2000; Landisman et al., 2002). In SPNs, however, the exact function of gap junctions is not yet clear.

Previous studies have provided electrophysiological (Logan et al., 1996a; Nolan., 1999) and anatomical (Lall et al., 2017; Logan et al., 1996b; Marina et al., 2008; Nolan et al., 1999) evidence for electrical coupling in SPNs via Cx36-containing gap junctions. Whole-cell recordings from 176/300 rat spinal cord neurons *in vitro* have revealed SPN spontaneous membrane oscillation which were synchronized in 23 paired recordings. It is noteworthy that the oscillations were abolished by tetrodotoxin application but not with intracellular lidocaine (Logan et al., 1996b). While the level of oscillations might have been influenced by the *in vitro* recordings, the data confirms at least some level of electrical coupling in groups of SPNs. This might indicate that not all SPNs need to be coupled to be functional. In fact, some groups of SPNs might need to be uncoupled for proper physiological responses.

Recent evidence suggests differential regulation of HR and BP in Cx36wt and Cx36ko mice with the latter having an attenuated response to noxious stimuli when examined in the "whole-heart brain stem" preparations (Lall et al., 2017). These differences noted by Lall and colleagues have been noted in animals with intact spinal cords. Preliminary data from recent experiments in our lab (Coleman et al., 2019) also showed some differences between the blood pressure responses of mice lacking the Cx36 protein globally (a knock-out mouse line, Cx36ko) and wild-type mice. Taken together these evidences lead us to hypothesize that mice lacking Cx36 have a reduced blood pressure response to noxious visceral stimuli *in vivo*. By expanding the number of animals tested in Coleman's thesis, we aimed to re-examine this hypothesis.

Abnormal regulation of BP and HR is also well known in people as well as rodents with spinal cord injury (SCI). Patients with SCI at or above the sixth thoracic segment experience rapid rise in BP, commonly followed by bradycardia in response to sensory stimulations in the periphery; a condition

referred to as autonomic dysreflexia (AD) (Hou and Rabchevsky, 2014; Lee and Joo, 2017). Whether changes in electrical coupling in SPNs contribute to AD is unclear. Upregulation of gap junctional coupling has been reported in axotomized motoneurons of adult rats (Chang et al., 2000). One study has also have claimed to detect a transient decrease in expression of Cx36 after SCI based on protein level detection by western blotting (Yates et al., 2008). To date, however, no studies have examined functional changes in autonomic responses along with anatomical data regarding Cx36 expression in spinal sympathetic neurons after SCI. Before testing functional changes in relation to Cx36 after SCI, it would be advantageous to map anatomical changes such as the distribution or the level of expression of Cx36 that follows SCI. In mice, no previous reports, to our knowledge, have examined the level of Cx36 in neurons following SCI, therefore this was one of the aims of this study.

Rodent models have been frequently used to study AD since the 1970s, but relatively few studies have investigated AD in mice. All studies to date have been performed in conscious mice and all previous experiments utilized colorectal distention (CRD) (Jacob et al., 2003; Jacob et al., 2001; Weaver and Brown, 2001a; Jarve et al., 2019; Ueno et al., 2016; Webb et al., 2006; Zhang et al., 2013) or cutaneous skin pinch (Jacob et al., 2003; Jacob et al., 2001a; Zhang et al., 2013) as the trigger stimulus to evoke AD. Only 3/5 papers, to our knowledge, have reported changes in HR and the degree of blood pressure and HR changes varied considerably in these studies. Other than our lab's preliminary data, no study, to our knowledge, has reported respiratory rate (RR) changes concurrently with cardiovascular changes during noxious stimulation in rodents. In mice, there are distinctively less established parameters of pressure and HR shifts constituting AD, albeit it is generally accepted that it can occur on a spontaneous basis as well as it can be induced by visceral (bowel) or somatic noxious (skin pinch) stimulation following SCI at mid-thoracic levels. Therefore, another aim in this study was to further characterize the HR, BP and RR changes in wild-type mice in response to colorectal distension after spinal cord injury when induced under isoflurane anesthesia.

Due to the limited evidence of the potential role of Cx36-containing gap junction in sympathetic activity, examining the sympathetic response to peripheral stimuli in Cx36wt and Cx36ko mice would be valuable for generating evidence for the functional role of Cx36 in adult mice. Furthermore, comparing the sympathetic response in mice with intact spinal cord to mice with injured spinal cord at or above T5-6 would provide further insights into the role of the Cx36 protein in AD and variations in its expression after SCI. Because there is no data regarding the level of Cx36 expression in SPNs, it would also be beneficial to evaluate the degree of coupling anatomically. Among neurons in other brain areas such as the inferior olive, electrical coupling by Cx36 has shown to be variable (Hoge et al., 2011).

This can be (and in the inferior olive it has been) assessed by applying dye onto individual neurons and observing other neighboring cells being labeled by the dye that is a small molecule so it can dissipate into cells that are coupled via gap junctions. Other studies have also used similar dyes for evaluating the degree of coupling in a larger scale. For example, Blivis and colleagues (Blivis et al., 2019) have employed retrograde dye application on spinal cord ventral roots to label neonatal motoneurons and interneurons which revealed the intersegmental dye coupling. Similar approaches can be used for SPNs in order to uncover the degree of electrical coupling and our aim in this study was to test the feasibility of dye-coupling, large-scale mapping of SPN connectivity. In summary, this study aimed to: 1) test responses to noxious stimuli in adult mice with an intact spinal cord and compare responses of Cx36ko and wild-type mice; 2) test responses to noxious stimuli in adult wild-type mice under isoflurane anesthesia after mid-thoracic SCI; 3) evaluate the degree of SPNs connectivity by dye-coupling in adult mice.

EXPERIMENTAL PROCEDURES

Animals

All experimental protocols and procedures used in this work complied with guidelines set by the Canadian Council on Animal Care and were approved by the Animal Care Committee at the University of Manitoba. Animals from two mouse colonies were used in the experiments: a B6;129S4 Gjd2tm1Paul-/-, the transgenic Cx36 knock-out (Cx36ko) strain and a B6;129S4 Gjd2twt, the wild-type (wt) strain. Overall, 44 mice (18 to 43 g) were used in these studies.

Spinal cord transection model

Six female and 10 male Cx36wt mice were used in spinalization and sham surgeries. Animals were given prophylactic antibiotics Clavamox (50mg/kg/day) in their drinking water at least one day before spinalization surgery alongside a soft (water enriched) diet.

The animal was anesthetized using 3% isoflurane (delivered in 95% oxygen) in a plastic box after which they were removed from the box, weighed on a digital scale and transferred to a mask to maintain anesthesia (typically 1.5-2.5% isoflurane as calibrated by from feedback based on vital signs). Respiratory rate (RR) was continuously monitored and the righting reflex (while in the box) and toe pinch (while on the heat pad) was also used to evaluate the depth of anesthesia. The eyes were treated with ophthalmic ointment to prevent dryness and the mouse was injected with non-steroidal anti-

inflammatory medication (2 mg/kg of Metacam/meloxicam) subcutaneously. Then, the surgical site on the back was shaved and cleaned with chlorhexidine and 70% alcohol. Afterwards, the mouse was transferred to another mask on a heated sterile surgical table. A thin layer of adhesive plastic (Clingwrap) was used to cover the animal except for the surgical field.

In order to block afferent fibers and reduce pain sensation, topical lidocaine gel (2%) was applied to the dorsal skin in the surgical field. A 1-2 cm longitudinal midline skin incision was made on the back over the low-thoracic and high-lumbar vertebral levels. Then, the third to fifth thoracic spinal cord segments were exposed following the dissection of ligaments, muscles and a minimal amount of dorsal parts of vertebral bones as well as the overlying dura mater. A small amount of lidocaine 2% was applied over the exposed spinal segments before the T4-T5 segment was completely transected with a 25G needle. The transection was verified by observing the mice behavior after the surgery.

Saline was used to wash the injury site and sterile surgical clips were used to close the incision. At the end of the surgery, the animal was removed from the mask, weighed on a digital scale. Then all mice received Buprenorphine (0.5 mg/kg) and 1 ml normal saline subcutaneously. For recovery, the animals were transferred to cages placed on a heated table until completely regaining consciousness and moving in the cage.

One or two animals were housed in standard caging with tissue paper covering the floor. The cages were placed partially on a heat pad in order to aid for the maintenance of optimal body temperature. The cages were enriched with food (Nutrigel and pallets) and Clavamox-enriched water at floor level. Animals were monitored for signs of infection, significant weight loss, intractable pain or discomfort (i.e. excessive grooming, aggression and decreased appetite) and body temperature every 8 hrs. In addition, bladder expression was performed on the mice and they were transferred to new, clean cages during each monitoring session. A second dose of Buprenorphine (0.05 mg/kg) was administered at about 24 hrs after the surgery and normal saline (1-2 ml subcutaneous) was administered typically every 8-16 hrs and in consultation with the Veterinary Services to aid hydration and bladder function recovery. The animals were perfused 3, or 6 - 8 days after the surgery. Aside from assessing the loss of bladder function, the loss of hindlimb function and the lack of tail movements and signs of spasticity, immunofluorescence microscopy was also used to confirm the complete spinalization.

Table 1 here

Arterial cannulation and cardiorespiratory monitoring for evaluating responses to visceral and somatic afferent stimulation

In vivo testing was performed on eight intact mice (6 Cx36ko, 2 wt) and four mice with spinal cord injury (4 wt) in these experiments. The animal was put in a plastic box and it was anesthetized with 3% isoflurane (delivered in room air, SomnoSuite®, Harward Apparatus, USA), after which the mouse was weighed on a digital scale. Then the mouse was transferred to a mask and a heat pad and anesthesia was maintained (1-2% isoflurane) based on feedback from monitoring the vital signs (PhysioSuite®). The animal was placed in a supine position, after which the ventral midline hair of its neck was clipped with scissors and lidocaine gel (2%) was applied topically to the same area. After verifying the lack of pedal reflexes, scissors were used to make an incision longitudinally in midline skin of the neck.

To expose the left or right carotid artery, the connective tissue and muscles around the trachea were dissected bluntly using non-toothed, fine forceps. Three fine threads were placed around the carotid artery to facilitate the cannulation, after it was identified based its pulsatile nature. To occlude and elongate the vessel, two threads were loosely tied on the opposite directions. Another thread was loosely tied close to the other lower thread to stabilize and secure the fiber optic probe after cannulation. A small cut was made in the carotid artery after which it was cannulated with the fiber optic probe. Then, the upper and lower threads secured also to the probe. After placing the fibre optic probe connected to a pressure monitor (Opsense, Pn-type probe, Canada) into one artery and the preparation stabilized as illustrated in Fig. 1, the pulsatile systolic blood pressure (SBP), pulsatile diastolic blood pressure (DBP), heart rate (HR) and respiratory rate (RR) were monitored continuously.

Figure 1 here

A balloon catheter made of latex (Foley catheter, Edwards Lifesciences) was inserted 1 to 2 cm into the colorectal region of the mouse body. The catheter was stabilized by being attached to the tail of the mouse and the mouse was left undisturbed for 10 to 15 minutes. Before inflating the balloon catheter, baseline data were recorded for 1 min. Then, the balloon was inflated with air to a diameter of 4 to 5 mm using a 1-3 mm Luer-lock syringe and the inflation was verified by visually inspecting the balloon before and after inserting it to the rectum. Colorectal distention (CRD) was maintained for 1 min after application and released completely afterwards. Recording continued for 1 to 2 min after the release of CRD application. At the end of each stimulation, the mice were left undisturbed to recover for 5 to 15 min. The cycle of baseline recording, distention application and recovery were repeated at least once for each animal. The catheter was removed only after all trials were completed.

Electrical stimulation of the tail and/or one hindlimb was performed using a pair of clip electrodes (copper played alligator clips). For tail stimulation, the cathode was attached to the base of the tail and the anode to the distal end of the tail. For foot stimulation, the cathode was placed above the ankle and the anode was clipped onto the 4th toe. This configuration stimulated branches of tibial nerve, including those innervating the digits and this evoked a visually detectable movement of the digits. Pulse parameters were initially set at a frequency of 1Hz, and pulse duration of 0.2 milliseconds. The minimal intensity required to evoke a visible tail or toe contraction was defined as the motor threshold (MTH). After identifying the MTH, the mice were left undisturbed for 1-5 minutes. Baseline cardiovascular parameters were recorded for one minute, after which electrical tail stimulation (ETS) was performed at varied intensities for 30-60 seconds. Recording continued for 2-5 minutes after the stimulus period. The mice were then left undisturbed for 3-10 minutes (a longer recovery time was given after high intensity stimulation, and a lower recovery time was given if there were no stimuli evoked changes in the measured parameters. Electrical stimulation was repeated in order to test: i) the effect of stimulation at different intensities and frequencies, and ii) changes evoked by repetitive stimuli in the same animal. This small movement elicited by low threshold currents (0.3 – 0.5 mA) suggested a localized spread of the electrical stimulus. Stimulus intensity was graded similar to methods used for tail stimulation. The results of the responses to electrical foot or tail stimulation are not reported here. Intra-tracheal epinephrine (1 mg/mL, Sigma) was injected in undiluted or in a 1:10 dilution with 0.9% saline in volumes ranging from 0.01 mL to 0.05 mL as a "pressor response" test in a subset of animals. The results after electrical stimulation and epinephrine injections are not addressed in the Results here.

Data collection and analysis

A custom software package designed by the Spinal Cord Research Centre (SCRC) at the University of Manitoba, Winnipeg, Canada, allowed digitizing (at 10 KHz, National Instruments DAQ) collecting and storing the data on a Linux personal computer. The fiber-optic sensory probe was calibrated by the manufacturer so that an output of 10 mV represented 1 mmHg BP. The probe was calibrated at the beginning of each experiment by entering the calibration parameters provided by the manufacturers. The sensor's output and the digitized recordings were checked for zero baseline before cannulating the carotid artery, ensuring that zero on the sensor was also at zero voltage after digitizing the signal. The BP, HR and RR were extracted from the waveforms by analyzing 15 second increments before, during and after stimulation. The baseline (control, or pre-CRD) measurements were the average of the 45 second period just prior to the stimulation. The analysis process is shown in Fig. 1D-G. The first step was to select each

heartbeat as a cycle by using a threshold crossing algorithm with visually guided manual corrections if needed, as shown in Fig. 1D. The systolic and diastolic pressure could be detected in each cycle as shown in Fig. 1E. The average systolic and diastolic pressure and the average difference was calculated as shown in Fig. 1F. The raw wave form collected from the fiber optic probe was filtered (digitally) at a cut off frequency ranging from 1-3 Hz for RR measurements as shown in Fig. 1G. These steps (E-G) were repeated in 3 periods just prior to stimulation, then in 4 periods during the 1 min CRD and in 3 periods after stimulation was stopped. The measured numbers from the original data files were further processed in an Excel. The peak and the mean values (BP, HR and RR) obtained during stimulation periods were used to calculate relative changes expressed as percentage of baseline (pre-CRD) values. Mean arterial pressure (MAP) was calculated by the data analysis software at the SCRC and/or Excel using the following formula: MAP = ((2*DBA)+SBP)/3. The heart rate and the respiratory rate expressed as "event per minute", were calculated using the formula: 60,000 [ms] / cycles [ms] (heart rate or respiratory, respectively, calculated for the 15s long periods). All data are reported as averages ± standard error of the means (SEM) unless noted otherwise.

The baseline (pre-CRD) measurements were compared between the two strains by using t-tests (two-tailed, homoscedastic) built into Excel separately in males and females. This was for the determination if there were any significant differences in the baseline points between the cohorts. Further statistical comparisons were done by using SigmaStat4.0 (Systat software, Inc., USA). The primary analysis (see Appendix 1) was to compare outcomes before and after CRD with a paired comparison between wild type and Cx36ko mice. The steps done in SigmaStat4.0 program consisted the followings: 1) the Shapiro-Wilk test was used to check for normality and if there was a normal distribution then paired t-test was used. If the data was not normally distributed (only in the case of the heart rate data from ko mice) then the Wilcoxon Signed Rank Test was used. A secondary analysis was done by using the one-way ANOVA test to compare the percent changes in the four groups (ko males and females and wt males and females) for each of the outcome measures (mean arterial blood pressure, heart rate and respiratory rate). The steps here were similar as above, first checked for normality and if there was a normal distribution then the Brown-Forsythe test was used as the Equal Variance Test. When passed, the difference between the group mean values were compared. If there was a greater difference than it would be expected by chance; pairwise multiple comparison procedures of the Tukey Test were applied. The power of performed test with alpha = 0.050 was also reported.

In vivo dye application on peripheral nerves of thoracic and lumbar regions

Two wt and six Cx36ko mice were used in these experiments (not listed in Table 1 but see Fig. 6). Mice were put in a plastic box and were anesthetized with 3% isoflurane delivered in room air and then weighed on a digital scale. Then, they were transferred onto a heat pad while anesthesia was being maintained with a mask with around 2% isoflurane. Oxygen saturation, heart HR and RR were monitored and recorded during the experiment. Dorsal midline hair of the back on the thoraco-lumbar segments were clipped and lidocaine was applied topically to the area. Then, scissors were used to make an incision longitudinally in midline skin. To expose the spinal cord, connective tissue and muscles were dissected until vertebral bones were reached. Then, vertebral bones covering T9 to T12 segments of spinal cord were removed alongside and the muscles were further dissected to expose a ventral root or a nerve connecting to the cord. Small (fabricated from PE8 cannula) containers were filled with neurobiotin (NB) or tetramethylrhodamine dextran (TMRD) and dissected ventral roots or nerves were dipped in these in order to separate the nerves from each other and contamination by more than one dye. Then the mice were left undisturbed for different length of time (3-5 hrs) followed by transcardial perfusion.

In some of the dye injection experiments, the mice were put in a supine position after exposure of targeted dorsal roots or nerves which was followed by tracheostomy. Then, the animals were transferred to a specialized frame, where they were connected to a ventilator. Temperature, HR, oxygen saturation and carbon dioxide production was continued to be monitored in the frame. The mice were paralyzed using pancuronium bromide to stop the movement originated from respiration and allow for a better placement of nerves/roots into the dye containers. These mice were also left undisturbed for a while after which they were allowed to recover 30 to 60 min and then perfused with the fixative. Supplementation of subcutaneous saline (0.05 mL/hr) was also given to improve survival and hydration.

Tissue preparation

Animals either after completing the *in vivo* experiment or at a set time point after SCI recovery surgery were deeply anesthetized with equithesin (3ml/kg) intraperitoneal injection and placed in supine position on a bed of ice. They were then perfused transcardially with 6 ml cold (4℃), prefixative solution containing sodium phosphate buffer (pH 7.4), 0.9% NaCl, 0.1% sodium nitrite and 1 unit/ml heparin. This was followed by cold 50 ml of fixative solution containing 0.16 mM sodium phosphate buffer (pH7.4), 0.2% picric acid and 4% formaldehyde (obtained from freshly depolymerized paraformaldehyde). Finally, the fixative was washed away with 20 ml of a solution containing 10% sucrose in 25 mM sodium phosphate buffer (pH 7.4). Spinal cords were then stored in cryoprotectant consisting of 25 mM sodium phosphate buffer (pH 7.4), 10% sucrose and 0.04% sodium azide until

sectioning. Tissues obtained and stored earlier were frozen with dry-ice, cut at a thickness of 15 to 16 μm using a cryostat, collected on gelatinized glass slides and stored in a freezer (-40℃) to be used at a later time.

Antibodies and immunofluorescence procedures

Immunofluorescence studies were conducted with streptavidin Alexa Fluor 488 conjugate antibody diluted 1:2000 (ThermoFisher, Rockford, Il, USA; formerly Life Technologies Corporation, and originally Invitrogen/Zymed Laboratories) to enhance visualization of neurobiotin dye. For evaluating potential changes in Cx36 expression in SCI mice, the monoclonal mouse anti-Cx36 antibody and chicken anti-peripherin antibody both diluted 1:600 (ThermoFisher, Rockford, Il, USA; formerly Life Technologies Corporation, and originally Invitrogen/Zymed Laboratories) were used as primary antibodies. Secondary antibodies used were Cy3-conjugated donkey anti-mouse antibody diluted 1:600 and AlexaFlour 488-conjugated donkey anti-chicken diluted 1:1000 (Jackson ImmunoResearch Laboratories, West Grove, PA, USA). Western blotting and/or immunohistochemical labelling validation of antibody specificity for target proteins was provided by the commercial supplier. The antibodies were diluted in 50 mM Tris-HCl, pH 7.4, containing 1.5% sodium chloride (TBS), 0.3% Triton X-100 (TBSTr) and 10% normal donkey serum.

The immunofluorescence labelling for neurobiotin dye was optimal with 4% formaldehyde fixative. Slide-mounted sections were removed from storage, air-dried at room temperature under a fan for 10 min, and then rehydrated in TBSTr for 20 min for three consecutive times. Sections were incubated with the antibody for 24 h at 4 °C. Then, the sections were washed for 20 min in TBSTr and 40 min (two consecutive 20 min) in Tris-HCL buffer. All sections were coversliped with the antifade medium Fluoromount-G (SouthernBiotech, Birmingham, AB, USA) and stored at -20 ºC prior to examination by fluorescence microscopy. For the SCI mice, 1% formaldehyde fixative was used to optimize Cx36 visualization. Slide-mounted sections from SCI mice were similarly dried and rehydrated. Sections were then incubated with the primary antibodies for 24 h at 4 °C. Then, they were washed for 60 min (3 consecutive 20 min) in TBSTr. These sections were then incubated with secondary antibodies for 90 min and washed for 20 min in TBSTr and 40 min (two consecutive 20 min) in Tris-HCL buffer before coversliping with the antifade medium Fluoromount-G (SouthernBiotech, Birmingham, AB, USA). Sections were stored at -20 °C prior to examination by fluorescence microscopy for several days.

Immunofluorescence was examined either on a wide-field Zeiss Imager Z2 microscope using ZEN image capture and analysis software (Carl Zeiss Canada, Toronto, Ontario, Canada). Data were collected

either as single scan or tiled images using 10x, 20x and 40x objective lens. Images were processed using Zeiss ZEN Blue software, and images were assembled using CorelDraw Graphics (Corel Corp., Canada) and Adobe Photoshop CS software (Adobe Systems, CA, USA).

RESULTS

In order to address the aims listed in the Introduction, we performed *in vivo* studies on mice and immunohistochemical analysis of spinal cord tissue. Taking advantage of the Cx36ko mouse line, we complemented preliminary data for comparing the heart rate (HR), blood pressure (BP) and respiratory rate (RR) changes in a total of wild-type (n=7) and Cx36ko (n=12) mice in response to colorectal distension. We also performed the same *in vivo* experiments on 4 mice out of our total 11 spinal cord injured ones (a full transection at mid-thoracic level). We harvested spinal cord tissue from injured (n=11) and sham-operated (n=3) animals to examine Cx36 levels above and below the injury and from adult mice subjected to dye backpropagation trials (n=4).

The drop in blood pressure as a typical response in Cx36ko mice after CRD differed from the increase of BP seen in all wild-type mice conformed to preliminary observations

Preliminary findings in our lab presented in the MSc thesis of A. Coleman (Coleman, 2019) showed that mice lacking the Cx36 protein usually exhibited a drop in blood pressure following CRD. This have been confirmed in the studies here. The added experiments, as illustrated in Fig. 2 show that the average mean arterial blood pressure during CRD was smaller than that prior to CRD in 5/7 Cx36ko mice while there was an increase in the mean arterial BP in the two wt mice as shown in panel Fig. 2B. The systolic blood pressure also showed a similar drop (not shown here) as the peak systolic BP during the 60 s CRD was smaller or equal to the pre-CRD levels in 5/7 mice. The changes in the HR are illustrated in Fig. 2C and D and the changes in the respiratory rate are shown in Fig. 2E and F. The heart and respiratory rate changes were more variable than the blood pressure changes in terms of individual responses. In most animals, the heart rate had a tendency for reduction while the respiratory rate had a tendency for increase after CRD.

Figure 2 here

Blood pressure, heart rate and respiratory changes could be compared now after the added experiments between higher sample size cohorts; in total 7 Cx36ko and 12 wt mice. Comparisons (as shows in Table 2) were made between the pre and post CRD outcome measures in all wt and in all Cx36ko mice grouped

(paired t-tests, see Appendix 1) and these are illustrated in Fig. 3. There was a significant increase from 96±4 to 105±4 mmHg in the wt mice (p=0.02, n=7). In the cx36ko mice, the blood pressure had a tendency to drop but the change from 111±8 to 107±8 mmHg was close to but not significant (n=12, p=0.059). The heart rate showed no significant change in either strain of mice. The respiratory rate significantly increased from 56±5 to 66±7 breath per minute in wt mice (p= 0.03). Respiration also had a tendency for increasing in the ko mice as it went from 52±3 to 56±2 breath per minute but this was not a significant increase.

Table 2 here

The blood pressure responses seemed to be similar in males (triangle symbols) and females (circle symbols) and comparisons of groups separated based on sex did not show differences in the baseline values (see Appendix 2 for more details on one-way ANOVA tests). The pre-CRD systolic blood pressure of the Cx36wt males (102±9 mmHg, n=2) was not different than that of the Cx36ko males (104±26 mmHg, n=5) and this was also the case for the females (94±11 mmHg, n=5 wt and 115±28, n=7 Cx36ko). No apparent differences were found in the heart rate of females before (wt: 568±57, ko:566±43) or after CRD (wt: 564±58, ko:560±49). The respiratory rate was also similar in males (wt: 61±12, ko: 52±13 breath per minute) and females (wt: 43±3, ko: 53±3).

Figure 3 here

Blood pressure, heart rate and respiratory rate changes found in spinal cord injured mice under isoflurane anesthesia

After transecting completely, the spinal cord at a mid-thoracic level (n=13, and n=3 with sham surgery) and allowing recovery for 6-8 days; we tested CRD responses in 4/13 mice. An increase in blood pressure after CRD was evident in 2/4 mice, as illustrated in Fig. 4. Both the systolic and the mean arterial pressure increased shortly (within 15-30 s) after initiating the CRD (Fig. 3A). These changes were similar to those observed in the intact wild-type mice. As in Fig. 4B, the heart rate increased also after CRD in the case of both mice. However, while one animal displayed a large increase, the other only modestly went above the baseline level. The respiratory rate also showed some change; however, these changes were small in comparison to what we observed in the intact mice. The other two animals tested after spinal cord injury did provide data (see more in Discussion).

Figure 4 here

Changes in Cx36 expression in SPNs at 3 and 7 days after mid-thoracic spinal cord injury in mice under isoflurane anesthesia

We collected spinal cord tissue from 11/13 mice with transection at mid-thoracic level and from all 3 sham operated mice. There were 2/16 mice with spinal transection that could not be used for data collection as these animals were lost during the recovery period likely due to some complications resulting from the surgery. After frozen sectioning the spinal tissue and applying immunohistochemical procedures, examples of horizontal spinal cord sections were obtained as shown in Fig. 5. The sections shown in Fig. 5.A-C were taken from a mouse 3 days after SCI and these images show similar amount of Cx36 puncta (red) to those observed in another mouse perfused 7 days after SCI. The Cx36 (red) could be detected in these preparations even after injury. Moreover, the identification of the peripherin positive (green) neurons in this part of the horizontal section (in the intermediolateral cell column) showed that Cx36 is there around the SPN neurons. These results demonstrate one example for each time point after SCI; and comparisons of sham operated, and SCI mice were planned but not completed (see Discussion).

Figure 5 here

Results from dye application to spinal roots or nerves in adult mice *in vivo*

We attempted to back-fill spinal neurons in 8 adult mice with dyes applied just outside the spinal canal onto sympathetic and/or muscle nerves. A schematic shown in Fig. 6A illustrates the basic principle followed here: two different dye - tetramethyl-rhodamine dextran (TMRD) or neurobiotin (NB) - application onto neighboring spinal roots or sympathetic nerves or mixed nerves in the vicinity of the vertebrae. We started first to test the time required for back-propagation when applied in an adult mouse under isoflurane anesthesia. Based on work done with TMRD in the neonatal rat preparation (Dr. Cowley's laboratory) we tested 3 hrs as the minimum and 5 hrs as the maximum survival times after dye application as shown in Fig. 6B. Overall, 3/8 animals provided no data as the animal was lost likely due to over-anesthesia and/or blood loss during the extensive laminectomy before dye application. One mouse survived only for an hour after dye application.

Figure 6 here

All other 4 animals survived for at least 3 hrs and these were perfused, and spinal tissue was examined in all but one. As illustrated in Fig. 6.C-F by the long horizontal sections spanning several spinal segments near the dye application region; the native fluorescence of the TMRD dye within the spinal gray (red signal) was evaluated first in serial horizontal sections (without any immunohistochemical processing). Sections close to each other (Fig. 6. C-D from experiment 3 and Fig. 6. E-F from experiment 4) were expected to show the TMRD signal in the levels where dyes were applied and in several "close by" sections. The white boxes mark the highest TMRD signal intensity deemed

upon examination. This helped to verify whether the red signal was not simply background random noise. If there was red signal in the same region in several neighboring sections, that was taken as a sign of positive results. Also, the location of the red signal in terms of being cytosolic vs. granular was also used to decide which tissue to process further.

The sections deemed TMRD positive were further processed for visualizing the NB. The optimization of this process also had to be done first and when we identified a series if incubation times that yielded positive results in tissue from at least three animals, we used that process for cross-comparisons of all TMRD positive sections. As illustrated in Fig. 7, distinct neurons expressed the TMRD and the NB; however, a few cells showing labelling for both could be identified (as marked by the arrows in Fig. 7). These results demonstrate the feasibility of the method and preliminary success but the quantification of NB and TMRD overlap and the comparison of such data in wt and Cx36ko mice was not completed (see Discussion).

Figure 7 here

DISCUSSION

This study tested responses to colorectal distension (CRD) in adult mice under isoflurane anaesthesia. The responses consisted of the classically described blood pressure and heart rate changes and additionally, we detected significant changes in the respiratory rate. The comparative analysis showed a clear difference in the responses of the two strains of mice tested here. While the wild-type mice exhibited a significant increase in blood pressure after CRD, there was a tendency for a decrease in blood pressure after CRD in mice lacking Cx36 protein. In absolute terms, the systolic blood pressure during CRD increased to 108±7% of baseline in wt males while in the Cx36ko males it was 97±3% and in the wt females, it increased to 109±8% of baseline while in the Cx36ko females it was 97±6%. This study also found significant respiratory rate increase in wild-type mice as part of the viscero-motor response to CRD. The respiratory rate during CRD increased in 16/19 mice, with most of the changes being greater than 10%.

Preliminary results were also obtained to verify that mice with severe spinal cord injury under isoflurane anaesthesia also display changes in blood pressure, heart rate and respiration when subjected to CRD and the Cx36 is present near SPN after injury. In addition, this work provided proof-of-principle results that assessing the population-level coupling of SPNs in adult mice by dye application to nerves is a feasible approach.

Significant changes in blood pressure and respiratory rate can be induced by CRD in anesthetized mice

In humans, colorectal distension results in a feeling of discomfort in the pelvic region and a feeling of abdominal fullness as well as pain in deep, visceral regions. This pain is typically referred to regions of the body matching sacral dermatomes. Noxious intestinal distention in animals has been well known to elicit reactions such as vasomotor, visceromotor, and respiratory responses see e.g. review by (Ness and Gebhart, 1990). The blood pressure could be reflexively regulated by somatic afferent input (Sato and Schmidt, 1987). Kimura and colleagues suggested that somatically induced cardiovascular reflex responses are a consequence of cardiovascular sympathetic responses and that these sympathetic responses have a strong segmental spinal reflex component plus a general supraspinal reflex component (Kimura et al., 1995). Often the term, "pressor" response is used to indicate a rise in blood pressure after sensory stimulation or drug administration. The term "depressor" response refers to reduced blood pressure in response to stimulation.

The vasomotor response includes a transient increase or decrease in arterial blood pressure, which is dependent on state and type of anesthesia (Ness and Gebhart, 1988a). When CRD was applied under different anesthetics and conscious states in rats, Ness and Gebhart described pressor responses when rats were anesthetized by halothane. Halothane gas anesthesia is the most similar method to the isoflurane anesthesia used here (Ness and Gebhart, 1988a). The pressor responses were different at 0.75% vs. 1.5% halothane levels in rats suggesting that the depth of anesthesia has a significant effect as shown in Fig. 1 by (Ness, 1999). The average response under 1.5% halothane anesthesia in rats was about 75% of the blood pressure response observed in awake rats to the same CRD stimulus (Ness, 1999).

There is much less information about the precise differences in the CRD-induced changes in mice than in rats. In conscious mice, blood pressure is regulated by visceral afferent inputs evoking viscero-visceral reflexes (Saleh et al., 1999). Most previous studies, however, examined CRD responses in spinalized mice where these reflexes are expected to be different than in spine intact mice. Table 3 summarizes the results of other studies on mice as well as our results in the context of currently available evidence on blood pressure and heart rate changes in absolute levels resulting from CRD. The result we obtained from intact mice in terms of blood pressure changes in the wt mice were in the same direction but about 50% of those found in awake mice with telemetric recordings (Zhang et al., 2013). The *in vitro*, working-heart-brainstem preparation using wt mice also found a similar pressor response in directionality to our results after chemical nociceptive stimulation (Lall et al., 2017). The heart rate changes found here, however, were much smaller (only about 10%) than other previously described changes in intact

(Zhang et al., 2013) or in spinalized (Jarve et al., 2019; Zhang et al., 2013) mice probably due to the use of isoflurane. Even our results from the spinalized mice were only about 50% of the changes seen in spinalized mice at times when peak dysreflexia occurs Jarve et al., 2019; Zhang et al., 2013).

Table 3 here

Underlying potential mechanisms of attenuated blood pressure increase and/or blood pressure drop in Cx36ko mice during CRD

The most striking findings in this study were those depicted in Fig. 3A showing that systolic blood pressure increased during CRD in only 2/12 Cx36ko mice (red symbols), while it has increased in all 6 wt mice (blue symbols). In animals, viscerally induced changes in BP can be elicited by electrically stimulating the vagus or splanchnic afferent nerves or by mechanically stimulating afferents from the mesentery or pelvic organs. For example, depressor responses can be evoked upon vagal stimulation (Mileva, 1976) or nociceptive splanchnic afferent stimulation (Lembeck and Donnerer, 1983) or bladder afferent stimulation (Ness et al., 2001) or bowel afferent stimulation (Ness and Gebhart, 1988b).

As mentioned in the Introduction, an attenuated pressor response was reported in another strain of mice lacking the Cx36 protein (Lall et al., 2017). That study attributed the differences to the disruption of the normal regulation of sympathetic outflow. However, our results not only found an attenuated pressor response but showed a tendency for a depressor response to occur in the Cx36ko mice. This observation could be the result of using *in vitro* vs. *in vivo* preparations in the previous and our study, respectively.

Other factors, however, may also explain the differences. Ness and Gebhart (Ness and Gebhart, 1988a) reported earlier that opposing BP responses occurred in rats after CRD depending on whether the animal was conscious or spinal intact. Lall and colleagues investigated the relationship between visceral CRD stimulation and its corresponding visceral responses, specifically, mean arterial blood pressure (MAP) and renal sympathetic nerve activity (RSNA), which is an index of vasoconstrictor activity. Reduced vasoconstriction was evident after CRD in the working-heart-brainstem preparation (Lall et al., 2017). Our results from these *in vivo* studies here, suggest that there may be a reduced vasoconstriction in the intact anesthetized state and possibly a small vasodilator response especially as the heart rate did not change significantly while the blood pressure had a tendency to drop rather than increase in the Cx36ko mice albeit without reaching a significant difference.

Based on early research (Lembeck and Skofitsch, 1982) the depressor response was thought to be originating from supraspinal centres, however, the later work of Gebhart and Ness debunked this concept

(Ness and Gebhart, 1988a,b). The later study showed support the assertion that the viscero- motor response to colorectal distension acts via a brainstem loop and it is abolished by most anaesthetics, but not by drugs blocking autonomic outflow. From other studies in rats, it seems that the picture is more complex. Firstly, there can be a fair amount of inter-individual variability in pressor vs. depressor responses in rat and mouse cohorts, especially in those after spinal cord injury see e.g. (Li et al., 2006)(Li et al., 2006). The inhibition of visceral sympathetic output occurs in response to noxious visceral afferent activation at lower segmental levels in anesthetized CNS-intact rats but this inhibition can be reversed by spinal transection (at C2) like done in the study by (Li et al., 2006). In other rat studies, neuroablation of thoracolumbar colonic afferents did not abolish behavioral, cardiovascular or visceromotor responses to colorectal distension see e.g. (Lembeck and Skofitsch, 1982) thus underscoring the importance of afferent input and ascending information for these responses. Secondly, supraspinal processing of visceral sensory information without a doubt occurs in the brainstem and that is necessary for the cardio-vascular and visceromotor responses. This is evidenced by the fact that spinalization, but not decerebration, abolished the responses to colorectal distension in rats. Such results have not been confirmed in mice, to our knowledge (see also Table 3). Therefore, drawing definite conclusions for the reason why our results differ in the two strains or why there is tendency for the BP to drop is not possible: either spinal or supraspinal sources could be involved in altering the sympathetic outflow.

In the existing literature about studies examining responses to CRD in rodents, several conditions have been identified when the response becomes a drop of the blood pressure. For example, blocking of angiotensin receptors (Jarve et al., 2019) and systemic estrogen administration have been found to reduce the severity of AD responses in mice. Estrogen, interestingly, was found to reduce responses to visceral but not to somatic afferent stimulation. Antagonizing metabotropic glutamate 5 receptors (mGluR5s) was also found to reduce BP responses to CRD in mice (Lindstorm et al., 2008). Interactions between Cx36 proteins and the above listed factors could all be contributing to the differences seen here.

Responses to CRD after spinal cord injury in mice

Urinary bladder or colon distension initiated a series of reflexes that caused hypertension and bradycardia as seen clinically as autonomic dysreflexia first described in rats by Krassioukov and Weaver (Krassioukov and Weaver, 1995)(Krassioukov and Weaver, 1995) and much later in mice (Jacob et al., 2001b); in both studies mice were in conscious awake state. Although autonomic dysreflexia was observed as early as 24 hrs after cord transection, within a few days, the dysreflexia became attenuated and by 30 days after SCI, autonomic dysreflexia increased and peaked. The observations from our study

are the first in the literature, to our knowledge, showing that mice express blood pressure and heart rate changes at 6-8 days after SCI. The 2/4 mice that underwent CRD testing after spinalization without a clear response to CRD had methodological problems. One mouse lost considerable amount of blood and the baseline mean arterial blood pressure at the start of CRD testing was around 50 mmHg; which was never that low in any of the 18 CRD experiments. The other animal from which AD data could not be extracted after testing had an artefact in the blood pressure recording which prevented us from quantifying the responses with certainty. More experiments will be necessary to quantify these changes under isoflurane anaesthesia; however, the clear changes in 2/4 animals are without a doubt confirm feasibility.

This is also the first study, to our knowledge, to provide evidence that there are respiratory responses to CRD in mice. The clinical ramifications of respiratory dysfunctions following SCI are severe (Inskip et al., 2012). The related issues involve pneumonia, atelectasis, bronchitis, reduced lung volumes and compliance, sleep apnea and respiratory insufficiency or dyspnoea, particularly during exercise. The incidence and severity of respiratory dysfunction increases with the level of SCI and respiratory complications are the leading cause of death in acute SCI. In chronic SCI, respiratory dysfunction also contributes significantly to mortality plus it is associated highly with reduced quality of life as summarized in the review by Inskip and colleagues (Inskip et al., 2012). A few studies have described respiratory changes in cats resulting from visceral afferent stimulation (Ness, 1999) however, no studies have followed up documenting respiratory changes after CRD in rodents, to our knowledge.

Preliminary data on dye application-based identification of coupled SPNs in adult mice

The dye application attempts were originally planned so that dye was to be placed on ventral roots neighboring thoracic segments with cut corresponding dorsal roots. This approach would have enabled the fastest travel time and lack of labelling in dorsal horn regions of afferent neurons and allowed for the improved visualization of labelling in the IML. These dyes are small molecules that penetrate coupled cells, thus allowing to visualize those neurons that are coupled between two neighboring segments. This approach could provide a better estimation of coupling in adult mice compared to earlier results from slice preparations where the vast majority of synaptic contacts of SPNs are missing due to the nature of the preparation (i.e. about 300-500 μm sections analyzed). This planned primary approach was not possible to achieve, due to the fragile and small roots. The positive attempts we had was by applying dye to lumbar ventral roots to test whether somatic motoneuron labelling was feasible; and these are the results shown in Fig. 7 based on the location of the labelled cells in the horizontal sections. We also tried

to apply dye on the sympathetic nerves before joining the chain ganglia. This would be limiting the number of labelled neurons in the thoracic grey and also severing only the dorsal roots in the appropriate segments may be possible if the dye is applied onto sympathetic nerves further from the column than ventral roots. The results from the dye application experiments provide proof-of-principle data for this method but our data are inconclusive in terms of identifying gap junctional coupling since our experiments had to stop before comparing Cx36ko and wt mice.

Methodological limitations

In the *in vivo* experimental series describing responses to CRD, a sex-based analysis by including sex as independent factor and using 2-way ANOVA (for sex and strain) was not performed due to the low sample sizes in the wild-type male group (n=2). Additional wt males would be necessary to test in order to obtain a more standard verification of how sex may influence the responses. Furthermore, the general age groups used here should be extended to examine also younger animals (like 20-30 days and 70-80 days old cohorts) in order to be certain that there are no compensations in the 60 days or older animals due to age in the knock-out mice.

A fiber optic probe was used to measure the BP after delivering the noxious stimulation. One important issue was the positioning of the probe, which could largely affect the results. In a sub-optimal position, the probe could show an attenuated BP response to CRD or fail to detect the number of heart beats. To solve this problem, the probe was zero-positioned just before insertion into the carotid artery and then, the recorded wave form was validated immediately afterwards. If an error was apparent, the probe was re-aligned. However, during the experiment if movements occurred (like chest movements resulting from the viscero-motor responses) the positioning could shift into a state when large artefacts border each heartbeat and differentiating the individual cycles is not possible. The plus side of using this probe is, however, the simultaneous observation of all three key parameters (blood pressure, heart rate and respiratory rate).

We tried to normalize the stimulus delivered by the catheter by checking its size before and after the insertion into rectum. The catheter was able to be inflated maximally (5 mm diameter) by applying sufficient air. The inflation was visually monitored as it was visible via the abdominal wall and skin elevation during CRD stimulation period. The data in which the catheter balloon burst was discarded. It is important to mention that it would be possible to use chemicals such as capsaicin or xylene to activate nociceptive afferents in the viscera. The chemical stimulation would activate a subtype of receptors different than those afferents that respond to mechanical stimulation, although, there is some overlap (as

Discussed later in part IV) so the chemical stimulation methods may have also been resulting in some variability.

Another limitation was keeping the mouse alive during the dye application surgeries. For all the dye injection experiments, the dye had to be applied on ventral roots or the whole nerve connecting to the spinal cord. It was extremely challenging and time consuming to dissect and isolate individual ventral roots after laminectomy. During this time, animals could lose a lot of blood due to the movement caused by respiration that sometimes resulted in unwanted incisions. To decrease the blood loss, we sometimes decided to apply the dye on the nerves instead of ventral roots because isolating them was easier. However, this approach increased the amount of time needed for the dye to back-fill the axons to label SPNs in the spinal cord. Alternatively, we tried paralyzing the mouse with Pancuronium bromide (a selective neuromuscular synapse blocking drug) after the laminectomy to stop respiration and transferring the animal to a specialized frame to keep the incision open and stable. Although this decreased the movement significantly it added other complexities to the procedure because the animal had to be connected to a ventilator and thus, undergo a tracheostomy. This made the set up more susceptible to fail in several stages including tracheostomy procedure, transferring the animal to the frame and oxygen delivery on the frame. So, there are advantages and disadvantages to both of these procedures for dye application, but we ended up choosing the second option and we had five additional mouse experiments planned in that configuration which could not be carried out due to the lab shut-down.

CONCLUSIONS

This work extends the body of facts about the responses of mice to visceral afferent stimulation. As shown in Table 3, the tendency for changes in the different preparations varies based on how the experiment is performed i.e. conscious animals or in different preparations as well as based on when responses are tested i.e. how many days post spinal cord injury. This study has provided evidence that in intact and in spinalized mice under isoflurane anesthesia, changes in heart rate and blood pressure can be detected, albeit these changes appeared smaller in absolute amplitude than changes reported in conscious mice. These main findings of this study confirm that there are baseline differences in cardiovascular control in mice lacking Cx 36 protein compared to wild-type mice (Lall et al., 2018). Confirming that these changes can be tested under isoflurane will allow the combination of SPN recordings from mice with functional tests.

These findings also lead us to the conclusion that after spinal cord injury, the comparison of the two mouse strains will not provide as clear evidence about the role of Cx36 as we hypothesized in the Introduction. The visceral afferent input from the colon has a different effect even in the intact state while the systemic NA-induced and the foot or tail electrical stimulation-induced responses, (Coleman 2019) evoked pressor responses in Cx36ko mice. Therefore, experiments comparing AD responses in Cx36ko and wt mice after spinal cord injury need to be differently designed in order to examine how Cx36 protein can contribute to AD.

The feasibility of quantifying the gap junctional connectivity based on dye application experiments has been described here. Using that approach in mice that underwent SCI would be a logical next step when further examining if gap junctional coupling in SPNs changes after spinal cord injury. The findings about significant respiratory changes present novel and functionally very relevant observations which also need to be followed-up in future studies.

Acknowledgements

This work was supported by grants from the Canadian Institutes of Health Research and the Canadian Natural Sciences and Engineering Research Council to K.S and J.I.N. These funding sources had no involvement in the design or any other facet of this report. We thank M. Setterbom for excellent technical assistance.

Conflict of interest

The authors have no conflict of interest to declare.

Author contributions

All of the authors contributed to design of the experiments, the collection and/or the analyses of the data and participated in writing the manuscript.

Data statement

The raw data will be provided upon request directed to the corresponding author.

Abbreviations

AD, autonomic dysreflexia; BP, blood pressure; ChAT, choline acetyltransferase; CNS, central nervous system; CRD, colorectal distension; Cx36, connexin36; HR, heart rate; IML, intermediolateral cell column; ko, knockout; RR, respiratory rate; RSNA, renal sympathetic nerve activity; SPN(s), sympathetic preganglionic neurons; TBS, 50 mM Tris-HCl containing 1.5% sodium chloride; TBST, 50 mM Tris-HCl containing 1.5% sodium chloride and 0.3% Triton X-100; TMRD, tetramethyl-rhodamine dextran; NB, neurobiotin; wt, wild-type.

REFERENCES CITED IN PART III

Bankenahally R, Krovvidi H (2016) Bankenahally R, Krovvidi H (2016) Autonomic nervous system: anatomy, physiology, and relevance in anaesthesia and critical care medicine. BJA Education 16:381-387

Blivis D, Falgairolle M, apos, Donovan MJ (2019) Dye-coupling between neonatal spinal motoneurons and interneurons revealed by prolonged back-filling of a ventral root with a low molecular weight tracer in the mouse. Scientific reports 9:3201-3209.

Chang Q, Pereda A, Pinter M, Balice-Gordon R (2000) Nerve Injury Induces Gap Junctional Coupling among Axotomized Adult Motor Neurons. J. Neurosci 20:674-684.

Christie JM, Bark C, Hormuzdi SG, Helbig I, Monyer H, Westbrook GL (2005) Connexin36 Mediates Spike Synchrony in Olfactory Bulb Glomeruli. Neuron 46:761-772.

Coleman A (2019) Connexin 36 containing gap junctions and the development of blood pressure changes during noxious stimulation in mice. Master of Science (M.Sc) Thesis University of Manitoba

Duchars SA, Lall VK (2015) Sympathetic preganglionic neurons: properties and inputs. Compr Physiol 5:829-869.

Fukuda T, Kosaka T (2000) Gap junctions linking the dendritic network of GABAergic interneurons in the hippocampus. J Neurosci 20:1519-1528.

Hoge GJ, Davidson KGV, Yasumura T, Castillo PE, Rash JE, Pereda AE (2011) The extent and strength of electrical coupling between inferior olivary neurons is heterogeneous. J Neurophysiol 105:1089-1101.

Hou S, Rabchevsky AG (2014) Autonomic consequences of spinal cord injury. Compr Physiol 4:1419-1453.

Inskip, JA, Ramer LM, Ramer MS, Krassioukov AV, Claydon VE (2012) Spectral Analyses of Cardiovascular Control in Rodents with Spinal Cord Injury. J Neurotraum 29:1638-1649.

Jacob JE, Gris P, Fehlings MG, Weaver LC, Brown A (2003) Autonomic dysreflexia after spinal cord transection or compression in 129Sv, C57BL, and Wallerian degeneration slow mutant mice. Exp Neurol 183:136-146

Jacob JE, Pniak A, Weaver LC, Brown A (2001a) Autonomic dysreflexia in a mouse model of spinal cord injury. Neuroscience 108:687-693.

Jacob JE, Pniak A, Weaver LC, Brown A (2001b) Autonomic dysreflexia in a mouse model of spinal cord injury. Neuroscience 108:687-693.

Jarve A, Todiras M, Lian X, Filippelli-Silva R, Qadri F, Martin RP, Bader M (2019) Distinct roles of angiotensin receptors in autonomic dysreflexia following high-level spinal cord injury in mice. Exp Neurol 311:173-181.

Kimura A, Ohsawa H, Sato A, Sato Y (1995) Somatocardiovascular reflexes in anesthetized rats with the central nervous system intact or acutely spinalized at the cervical level. Neurosci Res 22:297-305.

Krassioukov AV, Weaver LC (1995) Episodic hypertension due to autonomic dysreflexia in acute and chronic spinal cord-injured rats. Am J Physiol 268:2077-2083.

Lall VK, Bruce G, Voytenko L, Drinkhill M, Wellershaus K, Willecke K, Deuchars J, Deuchars SA (2017) Physiologic regulation of heart rate and blood pressure involves connexin 36-containing gap junctions. FASEB J 31:3966-3977.

Landisman CE, Long MA, Beierlein M, Deans M, Paul DL, Connors B (2002) Electrical synapses in the thalamic reticular nucleus. J Neurosci 22:1002-1009.

Lee ES, Joo MC (2017) Prevalence of Autonomic Dysreflexia in Patients with Spinal Cord Injury above T6. BioMed Res Int 2017.

Lembeck F, Donnerer J (1983) Reflex fall in blood pressure mediated by capsaicin-sensitive afferent fibers of the rat splanchnic nerve. Nebraska medical journal, 322:286-289.

Lembeck F, Skofitsch G (1982) Visceral pain reflex after pretreatment with capsaicin and morphine. Nebraska medical journal 321:116-122.

Li WM, Suzuki A, Cui KM (2006) Responses of blood pressure and renal sympathetic nerve activity to colorectal distension in anesthetized rats. J Physiol Sci 56:153-156.

Lindstrom E, Brusberg M, Hughes PA, Martin CM, Brierley SM, Phillis BD, Blackshaw LA (2008) Involvement of metabotropic glutamate 5 receptor in visceral pain. Pain 137:295-305.

Logan SD, Pickering AE, Gibson IC, Nolan MF, Spanswick D (1996a) Electrotonic coupling between rat sympathetic preganglionic neurones in vitro. J Physiol 495 (Pt 2):491.

Logan SD, Spanswick D, Pickering AE, Gibson IC, Nolan MF, Cammack C (1996b) Gap junction coupling and the regulation of excitability in sympathetic preganglionic neurons. J Auton Nerv Syst 58:202-206.

Logan SD, Spanswick D, Pickering AE, Gibson IC, Nolan, MF, Cammack C (1996) Gap junction coupling and the regulation of excitability in sympathetic preganglionic neurons. J Auton Nerv Syst 58:202-206.

Marina N, Becker DL, Gilbey MP (2008) Immunohistochemical detection of connexin36 in sympathetic preganglionic and somatic motoneurons in the adult rat. Auton Neurosci 139:15-23.

Mileva S (1976) On the mechanism of the depressor reaction upon afferent vagal stimulation in cats. II. Role of the beta-adrenergic structures for the development of the depressor reaction. Acta Physiol Pharmacol Bulg 2:30-38.

Ness TJ (1999) Models of Visceral Nociception. *ILAR J 40*:119-128.

Ness TJ, Gebhart GF (1988a) Colorectal distension as a noxious visceral stimulus: physiologic and pharmacologic characterization of pseudaffective reflexes in the rat. Brain Res 450:153-169.

Ness TJ, Gebhart GF (1988b) Colorectal distension as a noxious visceral stimulus: physiologic and pharmacologic characterization of pseudaffective reflexes in the rat. Brain Res 450:153-169.

Ness TJ, Gebhart GF (1990) Visceral pain: a review of experimental studies. Pain 41:167-234.

Ness TJ, Lewis-Sides A, Castroman P (2001) Characterization of pressor and visceromotor reflex responses to bladder distention in rats: sources of variability and effect of analgesics. J Urol 165:968-974.

Nolan MF, Logan SD, Spanswick D (1999) Electrophysiological properties of electrical synapses between rat sympathetic preganglionic neurones in vitro. J Physiol 519:753-764

Saleh TM, Connell BJ, Allen GV (1999) Visceral afferent activation-induced changes in sympathetic nerve activity and baroreflex sensitivity. Am J Physiol 276(6 Pt 2):R1780-1791.

Sato A, Schmidt R F (1987) The modulation of visceral functions by somatic afferent activity. Jpn J Physiol 37:1-17.

Ueno M, Ueno-Nakamura Y, Niehaus J, Popovich PG, Yoshida Y (2016) Silencing spinal interneurons inhibits immune suppressive autonomic reflexes caused by spinal cord injury. Nat Neurosci.

Webb AA, Chan CB, Brown A, Saleh TM (2006) Estrogen reduces the severity of autonomic dysfunction in spinal cord-injured male mice. Behav Brain Res 171:338-349.

Yates C, Charlesworth A, Allen SR, Reese NB, Skinner RD, Garcia-Rill E (2008) The onset of hyperreflexia in the rat following complete spinal cord transection. Spinal Cord 46:798.

Zhang Y, Guan Z, Reader B, Shawler T, Mandrekar-Colucci S, Huang K, Popovich PG (2013) Autonomic Dysreflexia Causes Chronic Immune Suppression after Spinal Cord Injury. J Neurosci 33:12970-12981.

Figure legends

Figure 1. Schematics of *in vivo* testing and data analysis steps when using a fibre optic probe for blood pressure measurements

A. Diagram of isoflurane (ISO) anesthetized mouse on oxygen when testing colorectal stimulation (CRD) with Folyl catheter that used a balloon maximally inflating to 5 mm. The foot or tail stimulation was done electrically. **B**. Blood pressure recordings (2 min) when using a fibre optic probe inserted into the carotid artery on one side. C. Components of the blood pressure recordings (5s) that were used to quantify systolic and diastolic pressure and the heart and respiratory rates. D. A threshold crossing method (with manual corrections if needed) was used to identify each heartbeat cycle. **E**. The peak (systolic) and nadir (diastolic) pressure was measured for each cycle. **F**. The change from peak to nadir for each cycle and the average cycle lengths for a 15 s period was calculated. **G**. The fibre optic recording was digitally filtered (3 Hz cutoff, low-pass) and a threshold-crossing algorithm was used to select cycles indicating each breath and the average cycle length in a 15 s period.

Figure 2. Results from mice with intact spinal cords to colorectal distension

Data from supplemented experiments broken down by age and sex showing mean arterial blood pressure (MAP, mmHg) before (pre) and during colorectal distension (CRD) in **Cx36** knock-out (ko) mice (**A**) and in wild-type (wt) mice (**B**). Heart rate (beats per minute) in Cx36 knock-out (ko) mice (**C**) and in wild-type (wt) mice (**D**). Respiratory rate (breaths per minute) in Cx36 knock-out (ko) mice (**E**) and in wild-type (wt) mice (**F**). Averages were from 3x15s long recordings before CRD and 4x15s periods during CRD

Figure 3. Comparison of responses to CRD in the two strains

Relative size of systolic blood pressure (**A**), heart rate (**B**), and respiratory rate (**C**) expressed as percent of values measured before colorectal distension (pre-CRD, averaged from 3x15s long recordings) and during colorectal distension (CRD, averaged from 4x15s periods) in Cx36 knock-out (ko) mice (blue symbols) and in wild-type (wt) mice (red symbols). Data show original and supplemented experiments for all males (triangles) and females (circles). The grouped absolute means (with standard error of the mean) for all wild-type (wt) and Cx36 knock-out (Cx36ko) mice are shown for mean blood pressure (**D**), for heart rate (**E**) and for respiratory rate (**F**).

Figure 4. Responses of anesthetized mice with injured spinal cords to colorectal distension

Absolute values of blood pressure (**A**), heart rate (**B**) and respiratory rate (**C**) changes induced by colorectal distension in wild-type mice (n=2 males) under isoflurane anesthesia 6 days (SCI-M2) and 7 days (SCI-M2) after spinal cord injury consisting of a complete mid-thoracic transection. Each data point represents an average value from a15s periods before (pre-CRD) or after CRD (seconds after CRD indicated on the x-axis).

Figure 5. Expression of Cx36 in spinal neurons after spinal cord transection

Double immunofluorescence labeling of Cx36 and SPNs in adult mice three (**A-C**) and seven (**D-F**) days after spinal cord injury selected from tissue below the injury level (mid-thoracic) with 20x magnification. (**A, D**) Images of SPNs in horizontal view labeled with peripherin. (**B, E**) Images of Cx36 puncta in the same field labeled with anti-Cx36 antibody. (**C, F**) Overlaid images of Cx36 puncta and SPNs in the same field.

Figure 6. Dye back-propagation to spinal cells of adult mice

(A) Schematic image of the orientation of the dye containers near the vertebral columns applied for several hours in isoflurane anesthetized mice. (**B**) All experiments listing the sex (M=male) and the weight (W, grams, g) of each animal in which tetramethyl-rhodamine dextran (TMRD) or neurobiotin (NB) was application onto neighbouring spinal roots (R, dorsal, D or ventral, V) or sympathetic nerves (SN) dissected before reaching the ganglion chain or mixed nerves (N) in the vicinity of the vertebral column on route to the intercostal muscles. (**C-F**) Images stitched together showing a long horizontal section of several spinal segments with the native fluorescent TMRD signal (red) from experiment 3 (**C-D**) and from experiment 4 (**E-F**).

Figure 7. Double-labelling of TMRD and NB in spinal cells of adult mice.

Triple immunofluorescence labeling of neurons in adult mice from experiment 4 with 20x magnification. (**A**) Image of cells in horizontal view labeled with TMRD (red). (**B**) Image of cells in the same field labeled with anti-neurobiotin antibody (NB, green). (**C**) Overlay images of labeling with TMRD, neurobiotin and DAPI (blue) in the same field. The arrows indicate cells deemed positive for red TMRD and NB and DAPI (yellow signal).

Table 1. Characteristics of the mice used

The experiments performed that were previously done in lab (indicated by *) and later added to test responses to colorectal distension (CRD) showing the age (days), the strain (wild-type, wt or Cx36 knock-out, ko), the weight (in grams) and the sex (M:male, F:female) of each animal. The column labelled spinal cord indicated if intact or spinal injured state was examined. The N/A in the CRD field indicates that that animal was used only for tissue analysis and no CRD testing was performed.

Table 2. Comparison of changes before and after CRD in the two strains

The means (±standard error of the mean) for the key outcome measures used here: the mean arterial blood pressure (MAP), the heart rate (HR) and the respiratory rate (RR) are shown when data from wild type (wt, n=7) and Cx36 knock-out (Cx36ko, n=12) mice were grouped. Stars indicate significant differences in values between the before (pre) and the after colorectal distension (CRD) conditions.

Table 3. Blood pressure and heart rate changes in mice

The publication (paper) the mouse strain used, the stimulus applied (CRD: colorectal distension, chem.: chemical stimulation) and the state of the animal during testing (.C: conscious, T: telemetry, A.: anesthetized, Is.: isoflurane, WHBP: working heart-brainstem preparation) listed when testing intact and/or injured mice at specific times (days) after spinal cord injury (SCI post inj.). The "+" and the "–" refer to increases or decreases, respectively with means of mmHg or beats per minute (bpm) values shown and the number of animals tested (in parenthesis). The star indicates Cx36 knock-out mice as the strain tested.

Figure 1.

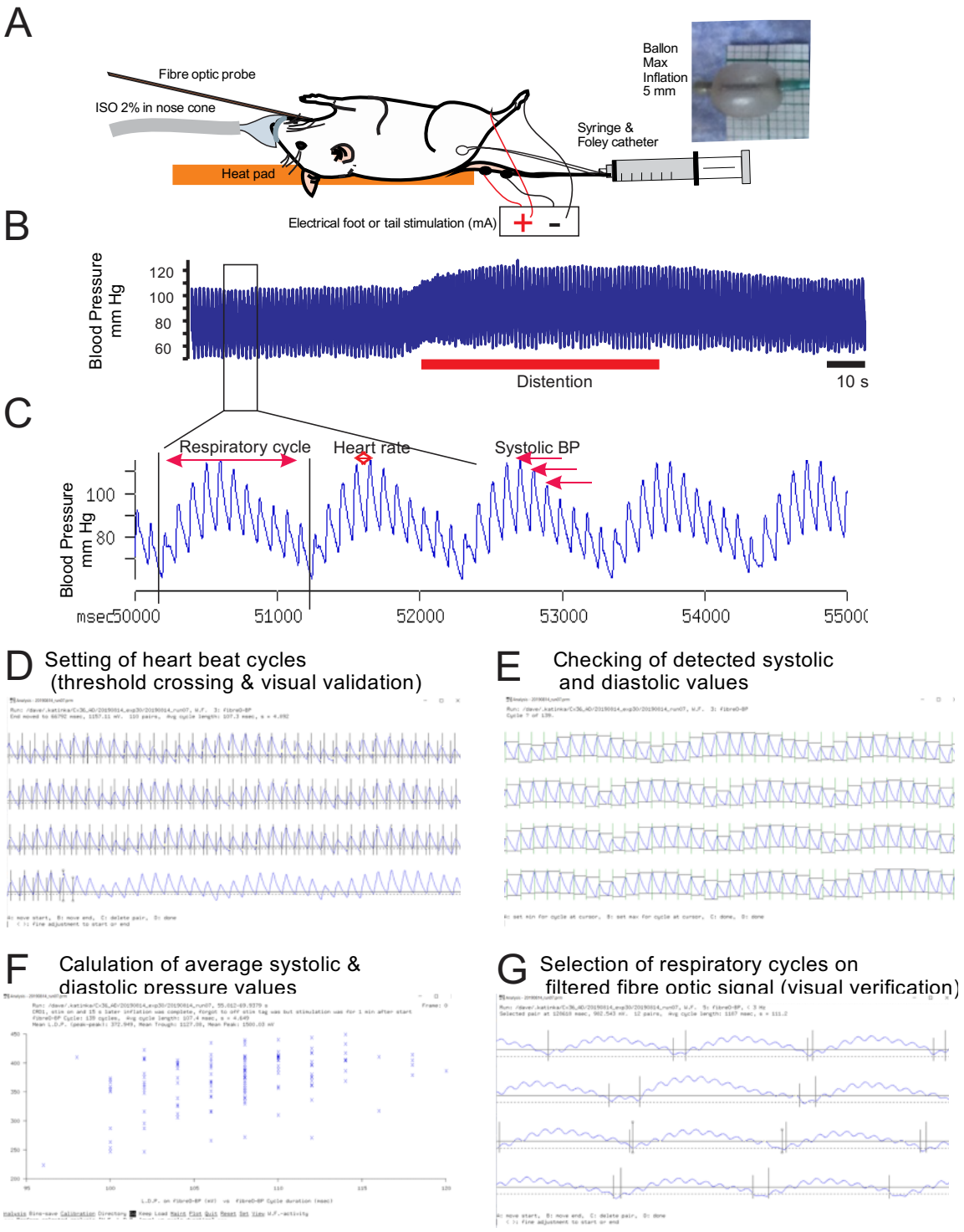
A
Fibre optic probe
ISO 2% in nose cone
Heat pad
Ballon
Max
Inflation
5 mm
Syringe &
Foley catheter
Electrical foot or tail stimulation (mA)
+
-
B
Blood Pressure
mm Hg
120
100
80
60
Distention
10 s
C
Respiratory cycle
Heart rate
Systolic BP
Blood Pressure
mm Hg
100
80
msec
50000
51000
52000
53000
54000
55000
D
Setting of heart beat cycles
(threshold crossing & visual validation)
E
Checking of detected systolic
and diastolic values
F
Calulation of average systolic &
diastolic pressure values
G
Selection of respiratory cycles on
filtered fibre optic signal (visual verification)

Figure 2.

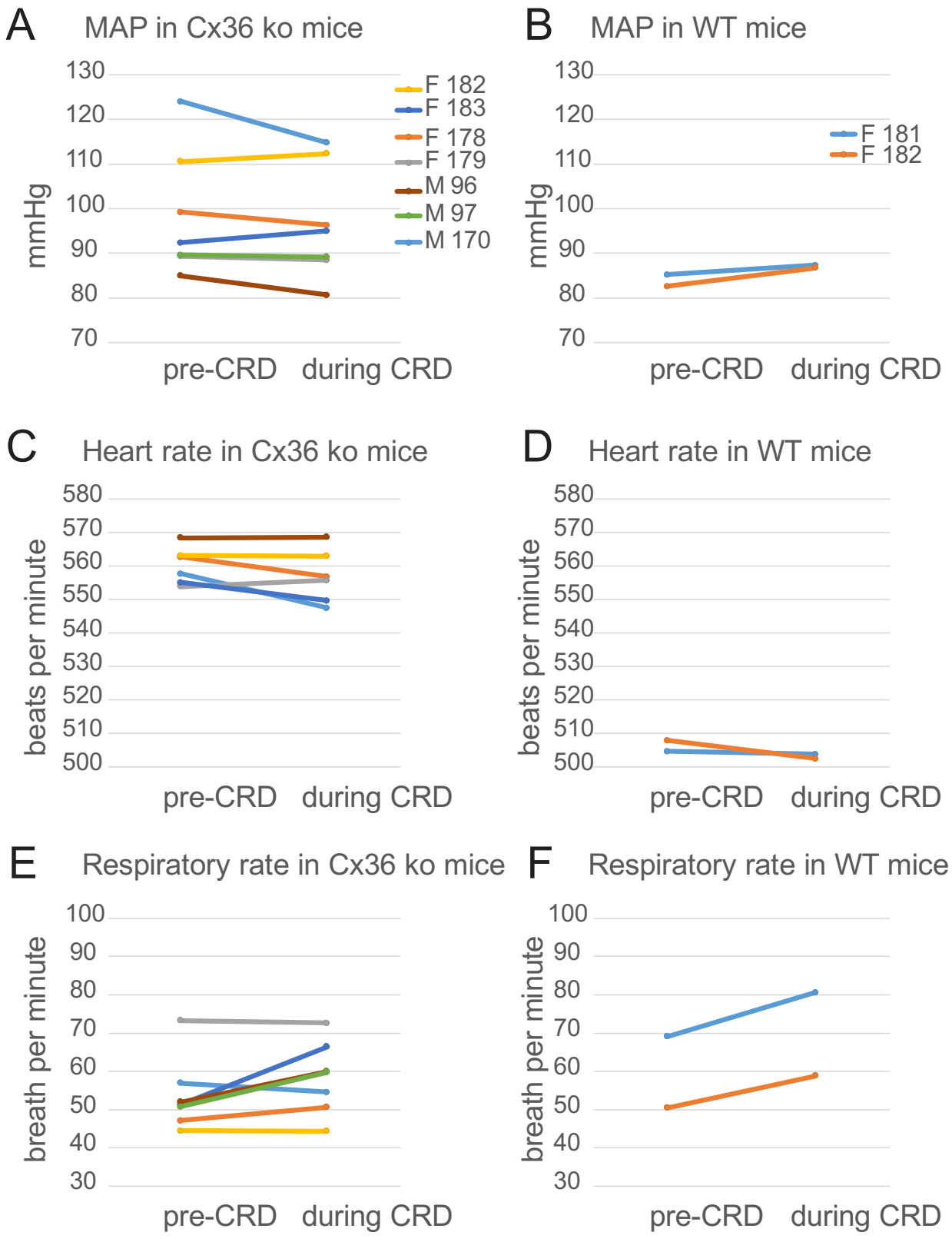
A
MAP in Cx36 ko mice
mmHg
130
120
110
100
90
80
70
F 182
F 183
F 178
F 179
M 96
M 97
M 170
pre-CRD
during CRD
B
MAP in WT mice
mmHg
F 181
F 182
pre-CRD
during CRD
C
Heart rate in Cx36 ko mice
beats per minute
580
570
560
550
540
530
520
510
500
pre-CRD
during CRD
D
Heart rate in WT mice
beats per minute
pre-CRD
during CRD
E
Respiratory rate in Cx36 ko mice
breath per minute
100
90
80
70
60
50
40
30
pre-CRD
during CRD
F
Respiratory rate in WT mice
breath per minute
pre-CRD
during CRD

Figure 3.

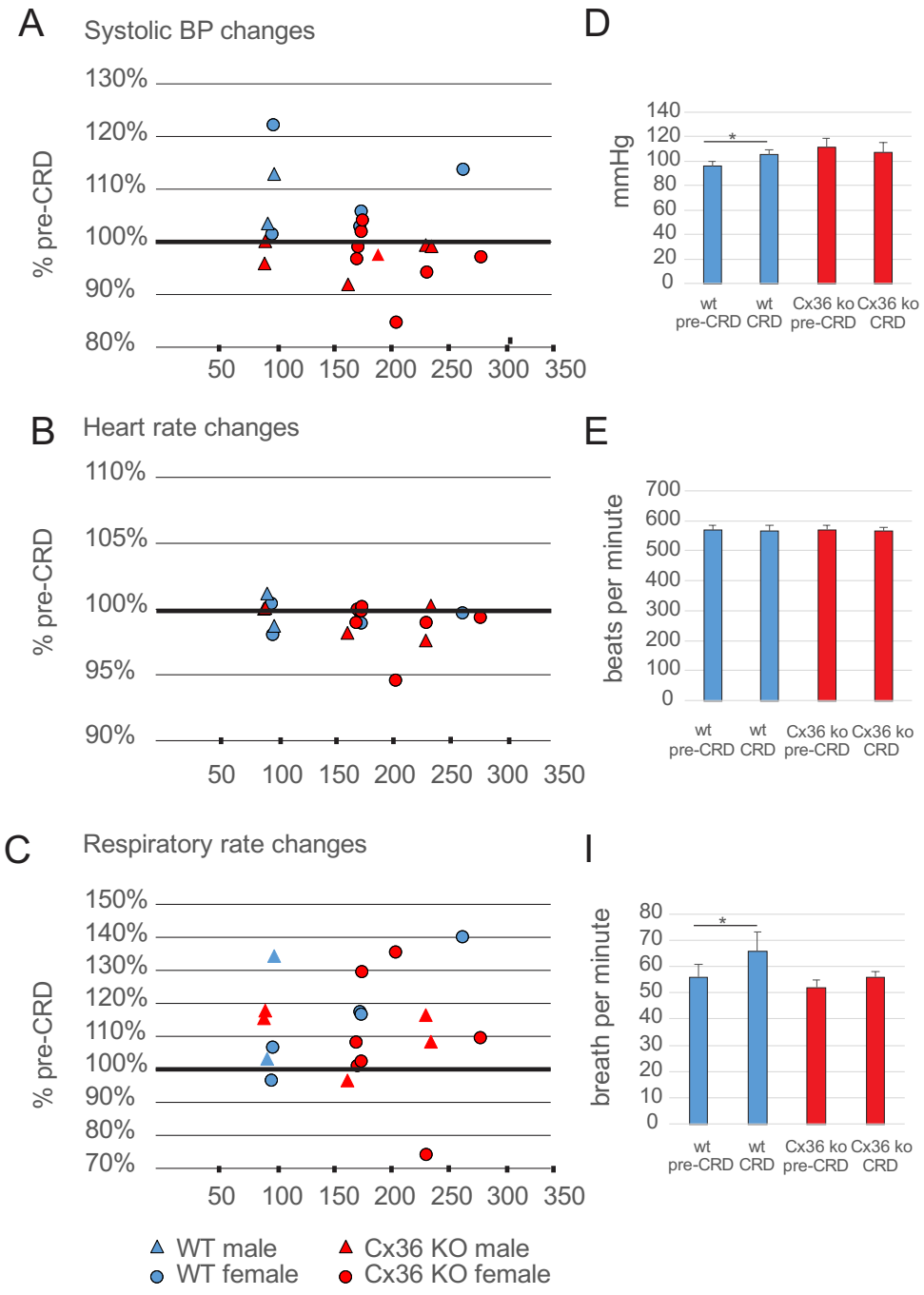
A
Systolic BP changes
% pre-CRD
130%
120%
110%
100%
90%
80%
50 100 150 200 250 300 350
D
mmHg
140
120
100
80
60
40
20
0
*
wt pre-CRD
wt CRD
Cx36 ko pre-CRD
Cx36 ko CRD
B
Heart rate changes
% pre-CRD
110%
105%
100%
95%
90%
50 100 150 200 250 300 350
E
beats per minute
700
600
500
400
300
200
100
0
wt pre-CRD
wt CRD
Cx36 ko pre-CRD
Cx36 ko CRD
C
Respiratory rate changes
% pre-CRD
150%
140%
130%
120%
110%
100%
90%
80%
70%
50 100 150 200 250 300 350
WT male
WT female
Cx36 KO male
Cx36 KO female
I
breath per minute
80
70
60
50
40
30
20
10
0
*
wt pre-CRD
wt CRD
Cx36 ko pre-CRD
Cx36 ko CRD

Figure 4.

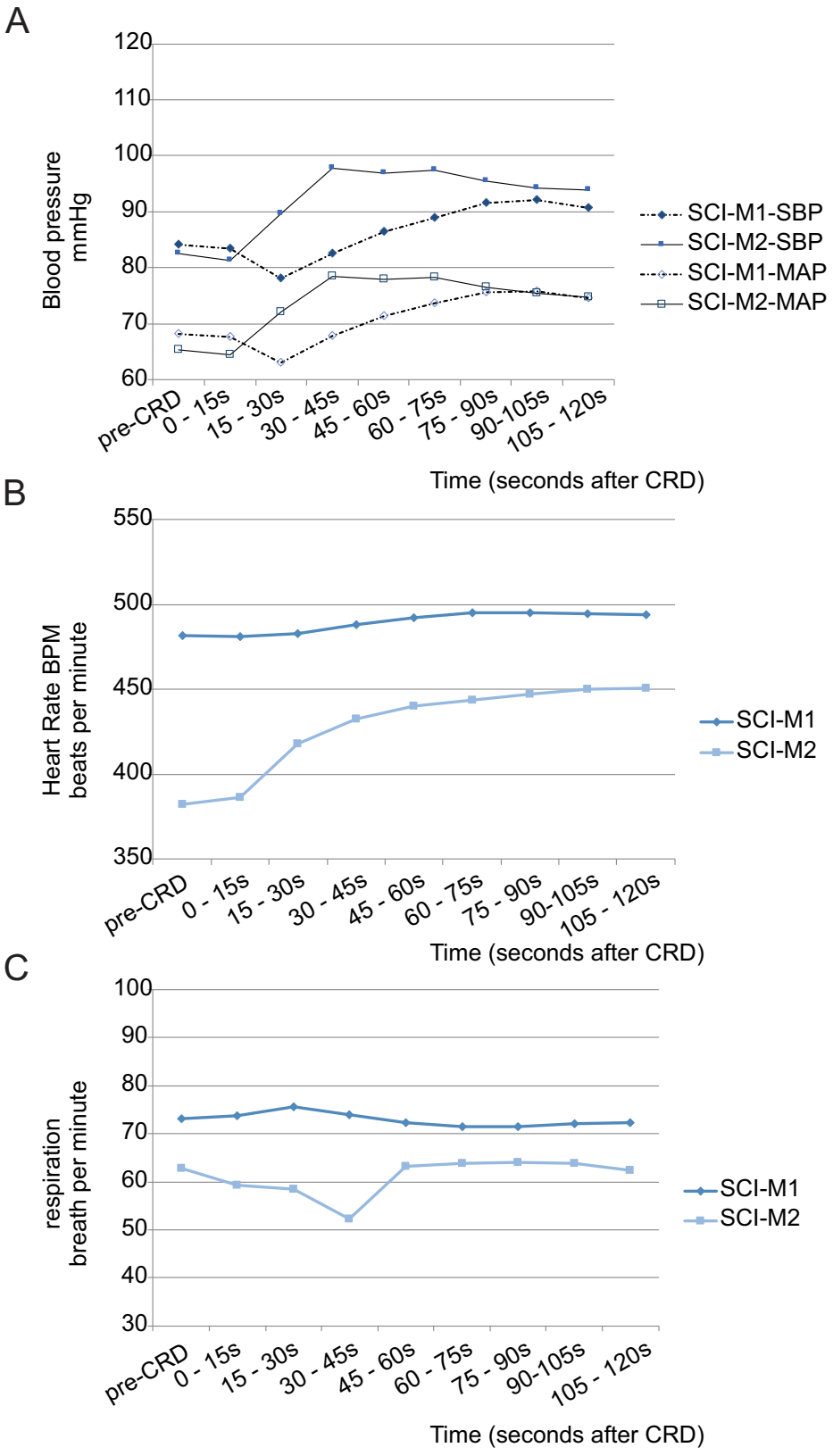
A
120
110
100
90
80
70
60
Blood pressure mmHg
pre-CRD
0 - 15s
15 - 30s
30 - 45s
45 - 60s
60 - 75s
75 - 90s
90-105s
105 - 120s
Time (seconds after CRD)
SCI-M1-SBP
SCI-M2-SBP
SCI-M1-MAP
SCI-M2-MAP
B
550
500
450
400
350
Heart Rate BPM beats per minute
pre-CRD
0 - 15s
15 - 30s
30 - 45s
45 - 60s
60 - 75s
75 - 90s
90-105s
105 - 120s
Time (seconds after CRD)
SCI-M1
SCI-M2
C
100
90
80
70
60
50
40
30
respiration breath per minute
pre-CRD
0 - 15s
15 - 30s
30 - 45s
45 - 60s
60 - 75s
75 - 90s
90-105s
105 - 120s
Time (seconds after CRD)
SCI-M1
SCI-M2

Figure 5.

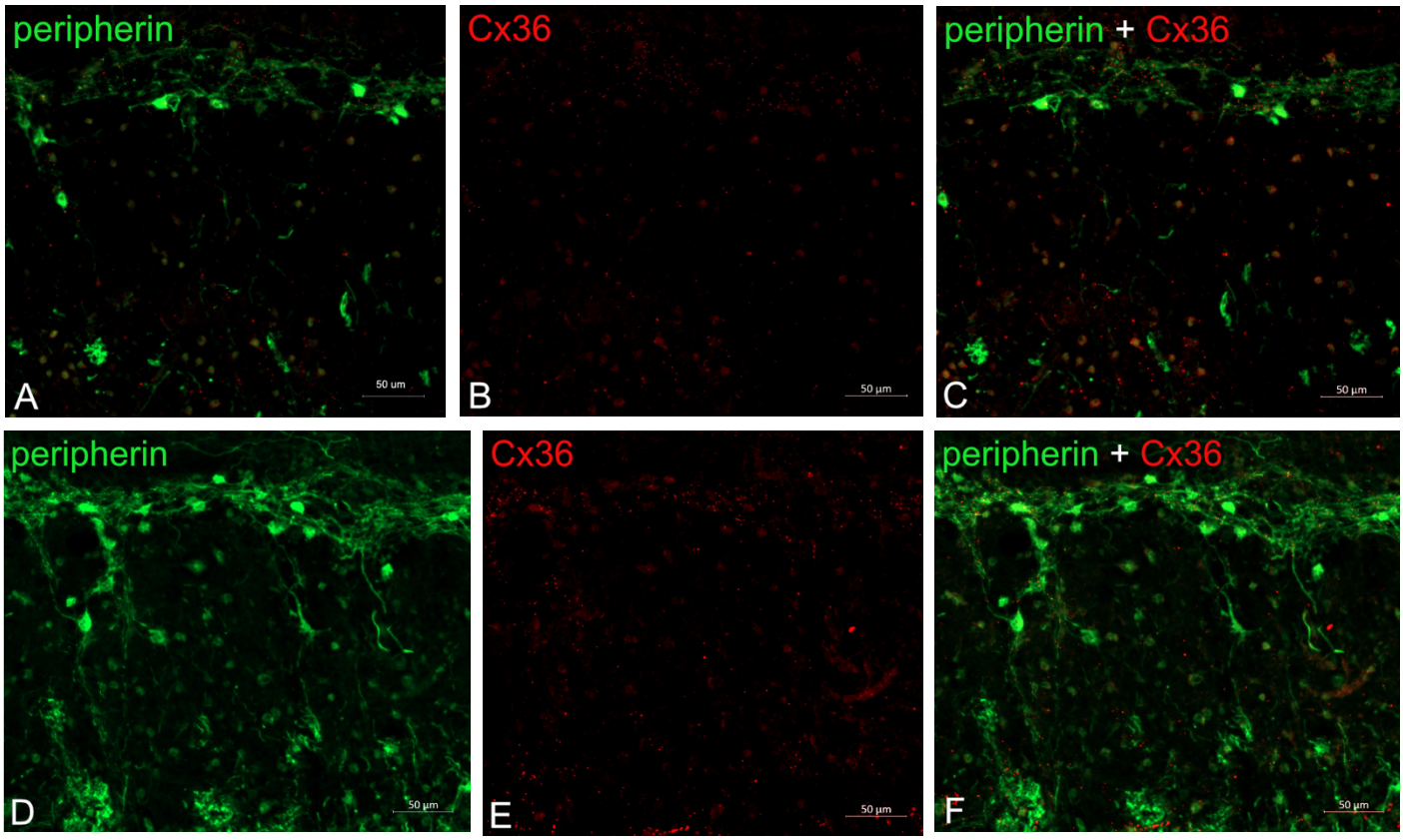

Figure 6.

A

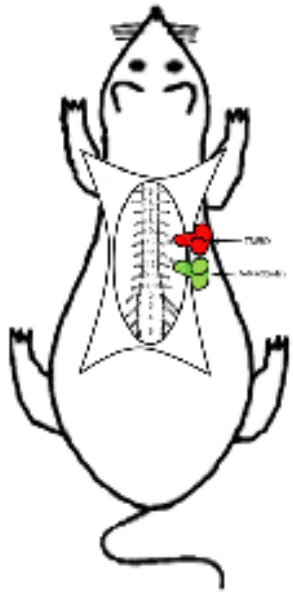

B

Exp-ko	Sex	W (g)	NB	TMRD	T (h)
Exp 1	M	22	na	na	0
Exp 2	M	22	T13-SN	T12-SN	4
Exp 3	M	41	T11-N, T13N	T12-N	3
Exp 4	M	43	R T11-N	L L5-N, R T10-SN, RT12 SN	3.5
Exp 5	M	27	L T13-VR, L L4-VDR	L L1-DVR	1
Exp 6	M	25	na	na	0
Exp-wt	**Sex**	**W (g)**	**NB**	**TMRD**	**Time**
Exp 7	M	32	na	na	0
Exp 8	M	27	T12-N	T11-N	3.5

C D E F

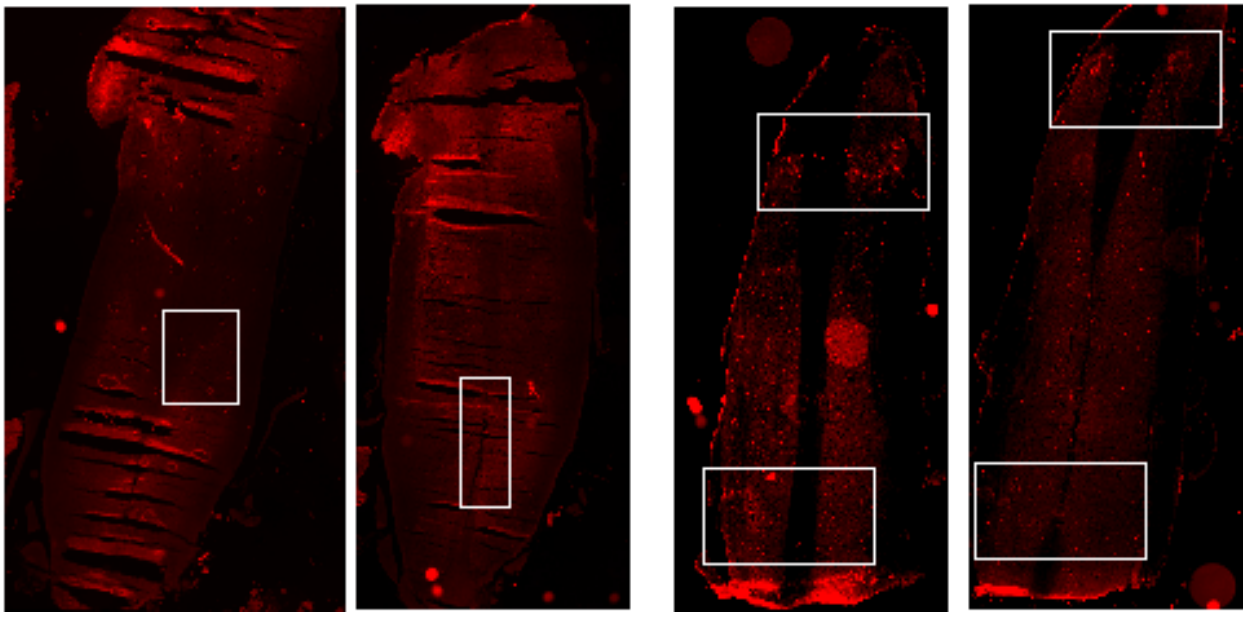

Figure 7.

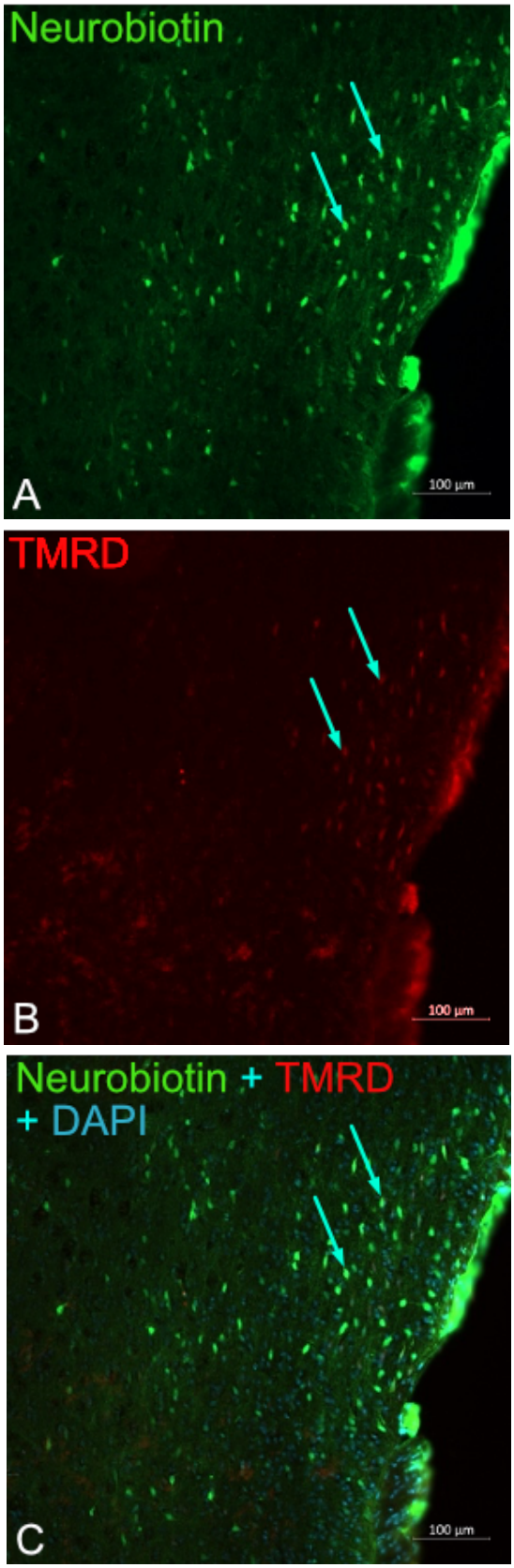
Neurobiotin
A
100 µm
TMRD
B
100 µm
Neurobiotin + TMRD
+ DAPI
C
100 µm

Table 1.

AD exp number	Age groups	Age (days)	Mouse strain	Sex	Weight (g)	Spinal cord	Days post SCI	CRD testing
37	95-105 days	96	Cx36ko	M	28.8	intact	N/A	tested
38		97	Cx36ko	M	26.6	intact	N/A	tested
20*		98	Cx36wt	M	31.1	intact	N/A	tested
21*		99	Cx36wt	M	32.5	intact	N/A	tested
23*		103	Cx36wt	F	26.1	intact	N/A	tested
24*		104	Cx36wt	F	29.8	intact	N/A	tested
25*		105	Cx36wt	M	30.2	intact	N/A	tested
30	170-185 days	170	Cx36ko	M	-	intact	N/A	tested
31		178	Cx36ko	F	32.6	intact	N/A	tested
32		179	Cx36ko	F	32.6	intact	N/A	tested
33		182	Cx36ko	F	32	intact	N/A	tested
34		183	Cx36ko	F	22	intact	N/A	tested
35		181	Cx36wt	F	32	intact	N/A	tested
36		182	Cx36wt	F	32.5	intact	N/A	tested
13*	210-300 days	213	Cx36ko	F	28	intact	N/A	tested
6*		239	Cx36ko	M	37.2	intact	N/A	tested
15*		240	Cx36ko	F	21	intact	N/A	tested
16*		244	Cx36ko	M	34.4	intact	N/A	tested
12*		298	Cx36ko	F	32.6	intact	N/A	tested
11*		272	Cx36wt	F	33.6	intact	N/A	tested
SCI exp number		**Age (days)**	**Mouse strain**	**Sex**	**Weight (g)**	**Spinal cord**	**Days post SCI**	**CRD testing**
5		127	Cx36wt	M	32.9	injured	3	N/A
6		127	Cx36wt	M	29.6	injured	3	N/A
11		73	Cx36wt	M	20	injured	3	N/A
14		69	Cx36wt	M	21.3	injured	3	N/A
10		132	Cx36wt	F	19.8	injured	4	N/A
9		136	Cx36wt	F	23.7	injured	8	N/A
16		65	Cx36wt	F	19.8	injured	7	N/A
18		79	Cx36wt	M	23.9	injured	7	N/A
19		80	Cx36wt	F	19.6	injured	7	N/A
13		69	Cx36wt	M	20.9	sham	7	N/A
20		80	Cx36wt	F	21.5	sham	7	N/A
17		79	Cx36wt	M	24.6	sham	7	tested
7		132	Cx36wt	M	32	injured	8	tested
12		69	Cx36wt	M	21.6	injured	7	tested
8		131	Cx36wt	M	26.4	injured	6	tested
15		68	Cx36wt	F	20	injured	N/A	N/A

Table 2.

Mean ±SEM	wt pre	wt CRD	Cx36ko pre	Cx36ko CRD
MAP (mmHg)	96±4	105±4*	111±8	107±8
HR (bpm)	568±18	565±18	570±13	565±14
RR (brpm)	56±5	66±7*	52±3	56±2

Table 3.

Paper	Stimulus & State	Mouse strain	Intact BP mmHg	Intact HR bpm	SCI post inj. days	SCI BP	SCI HR
Jacob *et. al.* 2001	CRD C.	129Sv	-----	-----	14 days	+37(6)	-----
Webb *et. al.* 2006	CRD C.	C57BL/6	-----	-----	14 days	+32(8)	-----
Zhang *et. al. 2*013	CRD C.T.	C57BL/6	+20(6)	+50(6)	14 days	+20(6)	+60(6)
Lall *et. al.* 2017	Chem. WHBP	C57BL/6*	Up	down	-----	-----	-----
Lall *et. al.* 2017	Chem. WHBP	C57BL/6	Up	down	-----	-----	-----
Jarve et. al. 2019	CRD C.	C57BL/6	-----	-----	30 days	+18(8)	-60(8)
This study	CRD A.Is.	B6,129S4*	-4(7)	-5(7)	-----	------	------
This study	CRD A.Is.	B6,129S4	+9(12	-3(12)	6-8 days	+11(2)	+14(2)

Appendices

Appendix 1

Paired t-test: Monday, June 08, 2020, 5:44:40 PM

Data source: Data 1 in all WT KO AD data 20200608 stats.SNB

Normality Test (Shapiro-Wilk): Passed (P = 0.314)

Treatment Name	N	Missing	Mean	Std Dev	SEM
all KO pre BP	12	0	110.521	26.530	7.659
all KO CRD BP	12	0	107.433	26.525	7.657
Difference	12	0	3.088	5.085	1.468

t = 2.104 with 11 degrees of freedom.

95 percent two-tailed confidence interval for difference of means: -0.143 to 6.319

Two-tailed P-value = 0.0592

The change that occurred with the treatment is not great enough to exclude the possibility that the difference is due to chance (P = 0.059)

One-tailed P-value = 0.0296

The sample mean of treatment all KO pre BP exceeds the sample mean of treatment all WT CRD BP by an amount that is greater than would be expected by chance, rejecting the hypothesis that the population mean of treatment all WT CRD BP is greater than or equal to the population mean of treatment all KO pre BP. (P = 0.059)

Power of performed two-tailed test with alpha = 0.050: 0.484

Power of performed one-tailed test with alpha = 0.050: 0.628

Paired t-test: Monday, June 08, 2020, 5:41:00 PM

Data source: Data 1 in all WT KO AD data 20200608 stats.SNB

Normality Test (Shapiro-Wilk): Passed (P = 0.401)

Treatment Name	N	Missing	Mean	Std Dev	SEM
all Wt pre BP	7	0	96.487	10.168	3.843
all WT CRD BP	7	0	104.923	10.844	4.099
Difference	7	0	-8.436	6.646	2.512

t = -3.358 with 6 degrees of freedom.

95 percent two-tailed confidence interval for difference of means: -14.582 to -2.289

Two-tailed P-value = 0.0153

The change that occurred with the treatment is greater than would be expected by chance; there is a statistically significant change (P = 0.015)

One-tailed P-value = 0.00763

The sample mean of treatment all WT CRD BP exceeds the sample mean of treatment all Wt pre BP by an amount that is greater than would be expected by chance, rejecting the hypothesis that the population mean of treatment all Wt pre BP is greater than or equal to the population mean of treatment all WT CRD BP. (P = 0.015)

Power of performed two-tailed test with alpha = 0.050: 0.798

Power of performed one-tailed test with alpha = 0.050: 0.904

Paired t-test: Monday, June 08, 2020, 5:48:34 PM

Data source: Data 1 in all WT KO AD data 20200608 stats.SNB

Normality Test (Shapiro-Wilk): Failed (P < 0.050)

Test execution ended by user request, Signed Rank Test begun

Wilcoxon Signed Rank Test Monday, June 08, 2020, 5:48:34 PM

Data source: Data 1 in all WT KO AD data 20200608 stats.SNB

Group	N	Missing	Median	25%	75%
all KO pre HR	12	0	560.149	547.785	597.842
all KO CRD HR	12	0	556.500	540.091	593.097

W= -43.000 T+ = 11.500 T-= -54.500
Z-Statistic (based on positive ranks) = -1.913
P(est.)= 0.062 P(exact)= 0.054

The change that occurred with the treatment is not great enough to exclude the possibility that it is due to chance (P = 0.054).

Paired t-test: Monday, June 08, 2020, 5:47:44 PM

Data source: Data 1 in all WT KO AD data 20200608 stats.SNB

Normality Test (Shapiro-Wilk): Passed (P = 0.995)

Treatment Name	N	Missing	Mean	Std Dev	SEM
all WT pre HR	7	0	567.555	47.125	17.812
all WT CRD HR	7	0	565.000	48.211	18.222
Difference	7	0	2.555	6.166	2.331

t = 1.096 with 6 degrees of freedom.

95 percent two-tailed confidence interval for difference of means: -3.148 to 8.257

Two-tailed P-value = 0.315

The change that occurred with the treatment is not great enough to exclude the possibility that the difference is due to chance (P = 0.315)

One-tailed P-value = 0.158

The sample mean of treatment all WT pre HR does not exceed the sample mean of the treatment all WT CRD HR by an amount great enough to exclude the possibility that the difference is due to random sampling variability. The hypothesis that the population mean of treatment all WT CRD HR is greater than or equal to the population mean of treatment all WT pre HR cannot be rejected. (P = 0.315)

Power of performed two-tailed test with alpha = 0.050: 0.153

The power of the performed test (0.153) is below the desired power of 0.800.
Less than desired power indicates you are less likely to detect a difference when one actually exists.
Negative results should be interpreted cautiously.

Power of performed one-tailed test with alpha = 0.050: 0.251

The power of the performed test (0.251) is below the desired power of 0.800.
Less than desired power indicates you are less likely to detect a difference when one actually exists.
Negative results should be interpreted cautiously.

Paired t-test: Monday, June 08, 2020, 5:56:55 PM

Data source: Data 1 in all WT KO AD data 20200608 stats.SNB

Normality Test (Shapiro-Wilk): Passed (P = 0.102)

Treatment Name	N	Missing	Mean	Std Dev	SEM
all KO pre RR	12	0	52.422	10.125	2.923
all KO CRD RR	12	0	56.439	8.569	2.474
Difference	12	0	-4.018	8.419	2.430

t = -1.653 with 11 degrees of freedom.

95 percent two-tailed confidence interval for difference of means: -9.367 to 1.331

Two-tailed P-value = 0.127

The change that occurred with the treatment is not great enough to exclude the possibility that the difference is due to chance (P = 0.127)

One-tailed P-value = 0.0633

The sample mean of treatment all KO CRD RR does not exceed the sample mean of the treatment all KO pre RR by an amount great enough to exclude the possibility that the difference is due to random sampling variability. The hypothesis that the population mean of treatment all KO pre RR is greater than or equal to the population mean of treatment all KO CRD RR cannot be rejected. (P = 0.127)

Power of performed two-tailed test with alpha = 0.050: 0.327

The power of the performed test (0.327) is below the desired power of 0.800.
Less than desired power indicates you are less likely to detect a difference when one actually exists.
Negative results should be interpreted cautiously.

Power of performed one-tailed test with alpha = 0.050: 0.463

The power of the performed test (0.463) is below the desired power of 0.800.
Less than desired power indicates you are less likely to detect a difference when one actually exists.
Negative results should be interpreted cautiously.

Paired t-test: Monday, June 08, 2020, 5:56:08 PM

Data source: Data 1 in all WT KO AD data 20200608 stats.SNB

Normality Test (Shapiro-Wilk): Passed (P = 0.826)

Treatment Name	N	Missing	Mean	Std Dev	SEM
all WT pre RR	7	0	56.139	13.214	4.994
all WT CRD RR	7	0	65.603	18.500	6.992
Difference	7	0	-9.464	9.318	3.522

t = -2.687 with 6 degrees of freedom.

95 percent two-tailed confidence interval for difference of means: -18.082 to -0.846

Two-tailed P-value = 0.0362

The change that occurred with the treatment is greater than would be expected by chance; there is a statistically significant change (P = 0.036)

One-tailed P-value = 0.0181

The sample mean of treatment all WT CRD RR exceeds the sample mean of treatment all WT pre RR by an amount that is greater than would be expected by chance, rejecting the hypothesis that the population mean of treatment all WT pre RR is greater than or equal to the population mean of treatment all WT CRD RR. (P = 0.036)

Power of performed two-tailed test with alpha = 0.050: 0.614

Power of performed one-tailed test with alpha = 0.050: 0.766

Appendix 2

One Way Repeated Measures Analysis of Variance Tuesday, June 09, 2020, 2:23:08 PM

Normality Test (Shapiro-Wilk): Passed (P = 0.985)

Equal Variance Test (Brown-Forsythe): Passed (P = 0.378)

Treatment Name	N	Missing	Mean	Std Dev	SEM
pre-WTM	2	0	102.408	8.851	6.259
CRD-WTM	2	0	110.563	2.775	1.963
pre-KOM	5	0	104.140	26.238	11.734
CRD-KOM	5	0	100.770	21.881	9.786
pre-WTF	5	0	94.119	10.534	4.711
CRD-WTF	5	0	102.667	12.337	5.517
pre-KOF	7	0	115.079	27.808	10.510
CRD-KOF	7	0	112.192	30.120	11.384

Source of Variation	DF	SS	MS	F	P
Between Subjects	6	11183.666	1863.944		
Between Treatments	7	927.980	132.569	0.676	0.691
Residual	24	4706.777	196.116		
Total	37	17718.465	478.877		

The differences in the mean values among the treatment groups are not great enough to exclude the possibility that the difference is due to random sampling variability; there is not a statistically significant difference (P = 0.691).

Power of performed test with alpha = 0.050: --

Expected Mean Squares:
Approximate DF Residual = 24.000
Expected MS(Subj) = var(res) + 5.000 var(Subj)
Expected MS(Treatment) = var(res) + var(Treatment)
Expected MS(Residual) = var(res)

One Way Analysis of Variance Tuesday, May 19, 2020, 9:24:13 AM

Data source: Data 1 in all AD data 20200519 Hossein thesis.SNB

Normality Test (Shapiro-Wilk): Passed (P = 0.478)

Equal Variance Test (Brown-Forsythe): Passed (P = 0.684)

Group Name	N	Missing	Mean	Std Dev	SEM
pre-WTM	2	0	566.594	9.009	6.370
CRD-WTM	2	0	566.431	18.994	13.431
pre-KOM	5	0	574.511	50.843	22.737
CRD-KOM	5	0	570.355	54.466	24.358
pre-WTF	5	0	567.939	57.535	25.730
CRD-WTF	5	0	564.428	58.265	26.057
pre-KOF	7	0	566.745	43.018	16.259
CRD-KOF	7	0	560.605	49.002	18.521

Source of Variation	DF	SS	MS	F	P
Between Groups	7	663.350	94.764	0.0379	1.000
Residual	30	74979.082	2499.303		
Total	37	75642.432			

The differences in the mean values among the treatment groups are not great enough to exclude the possibility that the difference is due to random sampling variability; there is not a statistically significant difference (P = 1.000).

Power of performed test with alpha = 0.050: --

One Way Analysis of Variance Tuesday, May 19, 2020, 11:33:24 AM

Normality Test (Shapiro-Wilk): Passed (P = 0.816)

Equal Variance Test (Brown-Forsythe): Passed (P = 0.383)

Group Name	N	Missing	Mean	Std Dev	SEM
pre-WTM	2	0	43.372	2.302	1.628
CRD-WTM	2	0	51.700	12.304	8.700
pre-KOM	5	0	52.837	3.312	1.481
CRD-KOM	5	0	58.472	4.572	2.045
pre-WTF	5	0	61.245	12.104	5.413
CRD-WTF	5	0	71.164	18.445	8.249
pre-KOF	7	0	52.125	13.431	5.076
CRD-KOF	7	0	54.988	10.713	4.049

Source of Variation	DF	SS	MS	F	P
Between Groups	7	1811.501	258.786	1.940	0.098
Residual	30	4002.104	133.403		
Total	37	5813.605			

The differences in the mean values among the treatment groups are not great enough to exclude the possibility that the difference is due to random sampling variability; there is not a statistically significant difference (P = 0.098).

Power of performed test with alpha = 0.050: 0.333

The power of the performed test (0.333) is below the desired power of 0.800.
Less than desired power indicates you are less likely to detect a difference when one actually exists.
Negative results should be interpreted cautiously.

Part IV: Conclusion and future directions

4.1. Electrical coupling via Cx36 is widespread in SPNs

In this study, we have documented the expression of Cx36 in SPNs along the thoracic segments of spinal cord in the IML, lateral funiculus, intercalatus and central autonomic area. Cx36 puncta signifying electrical coupling, were clearly apparent as early as 10 to 12 postnatal days as well as in mature rats and mice. Our results also raise the possibility of SPN innervation by groups of glutamatergic and GABAergic neurons that appear to be electrically coupled with Cx36-containing gap junctions.

4.2. Organization of SPN electrical coupling

We confirmed and documented the expression of Cx36-containing gap junctions in SPNs that can function as electrical synapses. Earlier electrophysiological studies that provided evidence for SPN electrical coupling with paired whole cell recordings, reported spikelets only in a fraction (26%) of these neurons (Logan et al., 1996a). On the other hand, anatomical studies using CFP as a reporter for Cx36 has shown that the majority (94%) of SPNs, at least in the IML, express Cx36 (Lall et al., 2017). A similar phenomenon has been observed in a number of other CNS areas such as mesencephalic trigeminal nucleus (MesV) where many neurons express Cx36 but do not allow neurobiotin dye transfer from that neuron to the neighboring cells (Curti et al., 2012). This discrepancy might be artifactual, stemming from the *in vitro* environment of those electrophysiological studies. It is also reasonable to associate this difference with change in Cx36-containing gap junction as they can be up or downregulated depending on supraspinal and intraspinal innervation that secrete a variety of neurotransmitters. Serotonin originating from raphe nucleus, noradrenalin from paraventricular nucleus of the hypothalamus and A5 pontine region as well as acetylcholine released from local interneurons are among the neurotransmitters that affect SPNs (Llewellyn-Smith, 2009a; Deuchars and Lall, 2015). These neurotransmitters have shown to

have an uncoupling effect in brain areas such as somatosensory cortex (Rörig and Sutor, 1996) and hippocampus (Velazquez et al., 1997; Zsiros and Maccaferri, 2008). Consequently, they are expected to have a similar impact on SPN gap junctional coupling. Cx36 phosphorylation via molecules such as PKA, PKC and cAMP can also affect electrical coupling in SPNs as it does in some other CNS areas such as retina of the eye (Li et al., 2013). Furthermore, electrical coupling can be affected by pH level and Magnesium ion concentration. In an alkaline environment conductance increases as the Mg concentration increases and vice versa. However, in an acidic environment conductance increases regardless of Mg concentration (Rimkute et al., 2018). This might be another method of gap junction control in SPNs.

Distribution of gap junctions can be studied utilizing neuronal dye tracing. This method has been employed in a few studies about SPN gap junctional coupling with very limited success. Biocytin that is the dye used in these studies does not show extensive labeling of SPNs (Logan et al., 1996a; Logan et al., 1996b). Similarly, dye tracing attempts in studies involving Cx36-containing gap junctions in other CNS areas have been unsuccessful. For instance, injecting neurobiotin and biocytin in individual inhibitory interneurons of cerebral cortex has not resulted in dye transfer to the coupled cells in some cases (Gibson et al., 1999; Galarreta and Hestrin, 2001). To improve the dye transfer including neurobiotin across Cx36-containing gap junctions, dye application could be attempted in a low pH environment or a high pH environment with a high concentration of Mg ion (Račkauskas et al., 2010; Rimkute et al., 2018). If dye coupling was satisfying in such state, the result could be used to determine the organization of SPN electrical coupling in more detail. The experiments taking advantage of dye labelling via sympathetic nerves described in part III of the thesis will provide a new way of quantifying cluster analysis and address the question about what percentage of the population is coupled in the adult state.

4.3. Blood pressure change in response to noxious stimulation in intact and SCI mice

When we investigated the sympathetic response to colorectal distension (CRD) in intact and SCI mice, our results showed Cx36 expression could be involved in differential regulation of sympathetic activity. In our study, Cx36 wt mice had an increased BP and Cx36 ko mice had a decreased BP after CRD application compared to the baseline (pre-CRD) pressure. CRD stimulation in mice with mid-thoracic spinal injury had an increase in BP similar to the results from intact wild types.

4.4. Potential central pathways disrupting blood pressure regulation in Cx36ko animals

Our data shows difference in BP regulation between Cx36 wt and Cx36ko mice. The transgenic knockout mouse model used in our study has the Cx36 gene globally removed. This means that the observed difference could be the result of Cx36 absence in some other areas of the nervous system, such as neural pathways involved in pain processing. Studies suggest that Cx36 expression is widespread in spinal cord laminae of mammals (Lemieux et al., 2010). Cx36 is found in spinal cord of adult mice and has a regulatory role in presynaptic inhibition involving sensory fibers and presynaptic inhibitory interneurons (Bautista et al., 2012). Cx36 is also observed in axon terminals of primary afferent neurons of rats (Bautista et al., 2014a). Recent evidence further confirms that Cx36-containing gap junctions form electrical synapses between small peripheral sensory fibers (Nagy et al., 2018b). In our study, we also raised the possibility of inhibitory and/or excitatory neuron populations coupled by Cx36 innervating SPNs. The potential input from these neurons could also affect SPN activity. This might be another pathway disrupted in Cx36 null mice. making it difficult to interpret the cause of differential BP responses in Cx36wt and Cx36ko mice.

4.5. Colorectal afferents and CRD activated neurons in mice

Colorectal distension (CRD) results in the mechanical stimulation of visceral afferents and has been widely studied in attempts to further understand the physiology and pathophysiology of viscero-sensory responses (references listed in Ness and Gebhart 1990). Data from numerous experiments

suggest that graded CRD stimulation produces strength-dependent responses in behaviour as well as in the BP in rats. The complexity of afferents in the colon is vast and it is not possible to review all aspects in relation to my work (for a recent review see e.g.; (Brierley et al., 2018)) however some basic principles of afferent types, responses to distension and potential linkage to Cx36 proteins will be addressed here.

Afferents in the colon responding to CRD include mesenteric afferents that show distension-evoked firing responses and these have distension-response thresholds in the noxious range. Therefore, mesenteric afferents likely contribute to signalling mechanically induced pain. Mesenteric afferents are specific to the splanchnic innervation and these fibres comprise about 50% of all mechanosensitive afferents innervating the colon (Brierley et al., 2018). Differences in afferent responses to intralaminar pressure in wildtype and Cx36ko mice can be expected based on previous work from the Nagy lab. In Cx36-deficient mice (same ko strain as used in this study) electrical stimulation of the smooth muscle *in vitro* induced a biphasic contraction-relaxation response as in the wild-type mice, but the first relaxation period was significantly reduced (Nagy et al., 2014). Furthermore, the early component was followed by a significantly increased contractile response at the cessation of the electrical stimulus. Gap junctions between inhibitory nitrergic enteric neurons have been proposed in rodents, and these altered responses observed *in vitro* could have implications when mechanical stimulation is presented *in vivo*, as it has been done in our study. Shorter relaxation and occasionally the reversal of relaxation to contractions immediately after stimulation and increased overall contractility *in vitro* could be giving a basis for assuming that there may be altered afferent responses in the Cx36ko mice. The increased overall contractility, however, would results in increased reflexes based on the graded nature of the responses seen in rodents after CRD. This, however, does not fit with the actual observations on depressed responses in the Cx36ko mice.

Neurons excited by abdominal stimulation, such as CRD, have been identified by extracellular recordings of action potentials in the dorsal gray matter of the spinal cord and most neurons firing after CRD received input from somatic receptive fields as well as responded to changes in intraluminar pressure (Kozlowski et al 2000). Neurons within the lumbosacral Rexed laminae I, II, V, VI, VII and X have been found to be active during CRD correlating with the termination sites of pelvic afferents (Kozlowski, 2000; Kozlowski et al., 2000). In mice, recent retrograde tracing studies identified unique populations of afferent neurons and central projections within the spinal cord dorsal horn activated during colorectal distension (Brierley et al., 2018). There were major differences in terms of how many activated cells could be found in various spinal cord regions within the distribution pattern of colonic afferents. In the lumbosacral L-S1 regions the non-noxious *in vivo* colorectal distension evoked significant neuronal activation (pERK-immunoreactivity) but this was not the case for thoraco-lumbar regions examined. This is not to say that IML cells are not activated, but it is to recognize that thoracic segmental IML activity is influenced by spinal processing of colonic mechanosensation which appears to be occurring mostly in the lumbo-sacral regions.

4.6. Limitations of the study

A major limitation of this study was that the transgenic mouse model available to us did not express Cx36 anywhere in the animal's body. As a consequence, the differences observed in blood pressure regulation could very well be the result of Cx36-containing gap junctions' absence in other areas of nervous system and not in SPNs as discussed earlier. This issue could potentially be overcome by developing a transgenic mouse that does not express Cx36 specifically in SPNs. This could involve use of Cx36 floxed-CFP mice mated with ChAT-cre mice to get Cx36ko exclusively in cholinergic cells including SPNs. Using this method, we can be more certain that the potential difference in sympathetic activity is associated with the role of Cx36 only in SPNs.

One goal of the present study was to reveal the gap junctional organization between SPNs. Thus, it could be valuable to show Cx36 puncta along with the dye labeling. One issue regarding this co-labeling was the different optimal fixation strengths. Cx36 antibodies needed 1% formaldehyde fixation and both TMRD and NB dyes worked with 4% formaldehyde fixative. Furthermore, we used streptavidin Alexa 488 to enhance the NB visualization with a protocol that did not match with that of secondary antibodies used to visualize Cx36. This issue could be alleviated by first showing Cx36 puncta on SPNs labeled using a marker that gave adequate results with 1-4% formaldehyde fixative (e.g., peripherin), and then showing SPNs labeled with the same marker along with the dyes.

In terms of the functional studies, this project was hinging on many new methods first used in the lab. The use of the fiber optic blood pressure monitor provided both advantages and disadvantages (as discusses in part III) however, by the end of the last series the success rate of the experiments was much higher than earlier series (c.f. Coleman 2019). The *in vivo* experiments required for the dye-loading seemed conceptually feasible, however, the major obstacle faced there was the blood loss of the animals during the extensive laminectomy to access the roots and/or the nerves close to the spinal column. The small size of the sympathetic nerves and the fragile nature of this preparation required us to try various ways to apply the dye to have an improved success rate. Almost each experiment thus far has been with a slightly different approach for how to expose and label the nerves, but the main outcome is that now we have a method in the frame that may result in consistent success.

4.7. Future directions

To further investigate the level of electrical coupling between SPNs a number of electrophysiological and anatomical methods can be useful. To better understand the organization of electrical coupling, an appropriate SPN marker such as peripherin can be utilized along with dye

application. This could enhance our knowledge not only about electrical coupling in SPNs in general, but also about the role of Cx36 in intersegmental signal transmission between SPNs that span more than a segment in the spinal cord.

The data obtained from SCI animals did not show a significant difference in Cx36 expression compared with that of intact ones. However, for a conclusive argument to be made, more investigation along with Cx36 quantification is needed. Considering the highly modulated nature of gap junctions (O'Donnell and Grace, 1996; Rörig and Sutor, 1996; Velazquez et al., 1997; Zsiros and Maccaferri, 2008; Goodenough and Paul, 2009; Račkauskas et al., 2010; Li et al., 2013; Rimkute et al., 2018), one can imagine that it is not the expression of Cx36-containing gap junctions that is affected after the injury but it is their permeability status. In other words, even if the expression does not change, channels might open or close after the injury which might be possible to visualize utilizing dye tracing methods. Becausee it would be more challenging to dissect individual ventral roots of an already spinalized mouse, dye injections into individual SPNs is suggested. The dye should be injected into SPNs above and below the injury level and compared to an intact mouse to be able to obtain interpretable results.

To study the role of Cx36 in BP regulation electrophysiologically, BP change resulted from sympathetic response to afferent stimulation (CRD application) can be evaluated utilizing the type of transgenic mouse that lacks Cx36 specifically in cholinergique cells including SPNs. Another way to reveal the role of electrical coupling in sympathetic activity is to apply gap junctional blockers onto the Cx36wt mouse spinal cord and compare the results to the Cx36ko. A similar study can be conducted using SCI mice and gap junction blockers. In addittion, level of signal transmittion through gap junctions between spinal cord segments can be inverstigated using ventral root stimulations with recording from a neughboring ventral root in Cx36ko and Cx36wt with/without gap junction blockers.

Our data suggests excitatory and inhibitory input to SPNs from other coupled neurons in the spinal cord. Other studies also reported Cx36 expression in spinal cord neurons other than SPNs such as presynaptic inhibitory interneurons (Bautista et al., 2012) and primary afferent neurons (Bautista et al., 2014a). It is known that normal BP regulation is disrupted in mice with SCI. As discussed in lenghth earlier, the disruption might be due to a change in electrical coupling in SPNs. Alternatively, the BP disregulation can be due to change in Cx36-containing gap junction in the other coupled neurons of spinal cord. In order to clarify this issue, Cx36 labeling can be done in future studies on spinalized mice lacking Cx36 specifically in SPNs above and below the injury level.

Reciprocal and non-reciprocal sympathetic reflexes are another important issue to be studied in the future. SPNs involved in sympathetic reflexes, innervate many organs and can cause physiologically opposite affects upon activation (Jänig, 1996; Morrison, 2001). Logically, it can be infered that SPNs involved in inducing conflicting end results in the body should not be coupled for an appropriate response. If this is the case, it is valuable to know which SPN groups are coupled to each other. Methods such as pseudorabies retrograde transynaptic transport and dye coupling might be useful to clearly uncover the detailed organization of electrical coupling among SPNs. In additiion to the selective coupling, it would be intersting to know if this type of coupling is static or subject to change based on physiological variations.

5. References cited in PART I and PART IV

Allen KJ, Lesli SW (2020) StatPearls. In.

Alcamí P, Pereda AE (2019) Beyond plasticity: the dynamic impact of electrical synapses on neural circuits. Nat Rev Neurosci 20:253-271.

Allen K, Fuchs EC, Jaschonek H, Bannerman DM, Monyer H (2011) Gap junctions between interneurons are required for normal spatial coding in the hippocampus and short-term spatial memory. The Journal of neuroscience : the official journal of the Society for Neuroscience 31:6542.

Anderson CR, Edwards SL, Furness JB, Bredt DS, Snyder SH (1993) The distribution of nitric oxide synthase-containing autonomic preganglionic terminals in the rat. Brain Research 614:78-85.

Appel NM, Elde RP (1988) The intermediolateral cell column of the thoracic spinal cord is comprised of target-specific subnuclei: evidence from retrograde transport studies and immunohistochemistry. J Neurosci 8:1767-1775.

Barber RP, Phelps PE, Houser CR, Crawford GD, Salvaterra PM, Vaughn JE (1984) The morphology and distribution of neurons containing choline acetyltransferase in the adult rat spinal cord: An immunocytochemical study. Journal of Comparative Neurology 229:329-346.

Bautista W, McCrea DA, Nagy JI (2014a) Connexin36 identified at morphologically mixed chemical/electrical synapses on trigeminal motoneurons and at primary afferent terminals on spinal cord neurons in adult mouse and rat. Neuroscience 263:159-180.

Bautista W, Nagy JI, Dai Y, McCrea DA (2012) Requirement of neuronal connexin36 in pathways mediating presynaptic inhibition of primary afferents in functionally mature mouse spinal cord. Journal of Physiology 590:3821-3839.

Bautista W, Rash JE, Vanderpool KG, Yasumura T, Nagy JI (2014b) Re-evaluation of connexins associated with motoneurons in rodent spinal cord, sexually dimorphic motor nuclei and trigeminal motor nucleus. Eur J Neurosci 39:757-770.

Bennett MV (1997) Gap junctions as electrical synapses. J Neurocytol 26:349-366.

Bittman K, Becker DL, Cicirata F, Parnavelas JG (2002) Connexin expression in homotypic and heterotypic cell coupling in the developing cerebral cortex. J Comp Neurol 443:201-212.

Blakley BW, Garcia CEA, Da Sliva SR, Florêncio VMB, Nagy JI (2015) Elevated auditory brainstem response thresholds in mice with Connexin36 gene ablation. Acta Oto-Laryngologica 135:814-818.

Blankenship AG, Hamby AM, Firl A, Vyas S, Maxeiner S, Willecke K, Feller MB (2011) The role of neuronal connexins 36 and 45 in shaping spontaneous firing patterns in the developing retina. J Neurosci 31:9998-10008.

Blatow M, Rozov A, Katona I, Hormuzdi SG, Meyer AH, Whittington MA, Caputi A, Monyer H (2003) A Novel Network of Multipolar Bursting Interneurons Generates Theta Frequency Oscillations in Neocortex. Neuron 38:805-817.

Blenkinsop TA, Lang EJ (2006) Block of inferior olive gap junctional coupling decreases Purkinje cell complex spike synchrony and rhythmicity. The Journal of neuroscience : the official journal of the Society for Neuroscience 26:1739-1748.

Bou-Flores C, Berger AJ (2001) Gap junctions and inhibitory synapses modulate inspiratory motoneuron synchronization. Journal of Neurophysiology 85:1543-1551.

Brierley SM, Hibberd TJ, Spencer NJ (2018) Spinal Afferent Innervation of the Colon and Rectum. Front Cell Neurosci 12:467.

Bruzzone R, Dermietzel R (2006) Structure and function of gap junctions in the developing brain. Cell and Tissue Research 326:239-248.

Buhl D, Harris K, Hormuzdi S, Monyer H, Buzsaki G (2003) Selective Impairment of Hippocampal Gamma Oscillations in Connexin-36 Knock-Out Mouse In Vivo. Journal of Neuroscience 23:1013-1018.

Chang Q, Gonzalez M, Pinter M, Balice-Gordon R (1999) Gap Junctional Coupling and Patterns of Connexin Expression among Neonatal Rat Lumbar Spinal Motor Neurons. Journal of Neuroscience 19:10813-10828.
Chang Q, Pereda A, Pinter M, Balice-Gordon R (2000) Nerve Injury Induces Gap Junctional Coupling among Axotomized Adult Motor Neurons. Journal of Neuroscience 20:674-684.
Chopra AS, Miyatani M, Craven BC (2018) Cardiovascular disease risk in individuals with chronic spinal cord injury: Prevalence of untreated risk factors and poor adherence to treatment guidelines. The Journal of Spinal Cord Medicine 41:2-9.
Christie JM, Bark C, Hormuzdi SG, Helbig I, Monyer H, Westbrook GL (2005) Connexin36 Mediates Spike Synchrony in Olfactory Bulb Glomeruli. Neuron 46:761-772.
Coleman A (2019) Connexin 36 containing gap junctions and the development of blood pressure changes during noxious stimulation in mice.
Connors BW (2009) Electrical signaling with neuronal gap junctions: Humana Press Inc.
Curti S, Hoge G, Nagy JI, Pereda AE (2012) Synergy between electrical coupling and membrane properties promotes strong synchronization of neurons of the mesencephalic trigeminal nucleus. J Neurosci 32:4341-4359.
Dale H (1935) Pharmacology and Nerve-endings (Walter Ernest Dixon Memorial Lecture): (Section of Therapeutics and Pharmacology). Proc R Soc Med 28:319-332.
De Gruijl JR, Hoogland TM, De Zeeuw CI (2014) Behavioral correlates of complex spike synchrony in cerebellar microzones. The Journal of neuroscience : the official journal of the Society for Neuroscience 34:8937-8947.
Dembowsky K, Czachurski J, Seller H (1985) Morphology of sympathetic preganglionic neurons in the thoracic spinal cord of the cat: An intracellular horseradish peroxidase study. Journal of Comparative Neurology 238:453-465.
Deuchars SA, Lall VK (2015) Sympathetic preganglionic neurons: properties and inputs. Compr Physiol 5:829-869.
Diamond LM, Cribbet MR (2013) Links between adolescent sympathetic and parasympathetic nervous system functioning and interpersonal behavior over time. International Journal of Psychophysiology 88:339-348.
Dimitris GP, Anatoly AB, Xiao-Hui Z, Hans-Peter K, John PW (2004) Fundamental role of inferior olive connexin 36 in muscle coherence during tremor. Proceedings of the National Academy of Sciences of the United States of America 101:7164.
Eccles J (1976) From electrical to chemical transmission in the central nervous system. Notes Rec R Soc Lond 30:219-230.
Eldahan KC, Rabchevsky AG (2018) Autonomic dysreflexia after spinal cord injury: Systemic pathophysiology and methods of management. Autonomic Neuroscience: Basic and Clinical 209:59-70.
Evans WH (2015) Cell communication across gap junctions: a historical perspective and current developments. Biochem Soc Trans 43:450-459.
Fatt P (1950) The electromotive action of acetylcholine at the motor end‐plate. The Journal of Physiology 111:408-422.
Feldberg W (1950) The role of acetylcholine in the central nervous system. British medical bulletin 6:312-321.
Fukuda T, Kosaka T (2000) Gap junctions linking the dendritic network of GABAergic interneurons in the hippocampus. The Journal of neuroscience : the official journal of the Society for Neuroscience 20:1519-1528.
Fukuda T, Kosaka T, Singer W, Galuske RAW (2006) Gap junctions among dendrites of cortical GABAergic neurons establish a dense and widespread intercolumnar network. The Journal of neuroscience : the official journal of the Society for Neuroscience 26:3434-3443.

Galarreta M, Hestrin S (2001) Electrical synapses between GABA-releasing interneurons. Nat Rev Neurosci 2:425-433.
Gibson JR, Beierlein M, Connors BW (1999) Two networks of electrically coupled inhibitory neurons in neocortex. Nature 402:75-79.
Goodenough DA, Paul DL (2009) Gap junctions. Cold Spring Harb Perspect Biol 1:a002576.
Haas JS, Zavala B, Landisman CE (2011) Activity-dependent long-term depression of electrical synapses. Science (New York, NY) 334:389.
Hestrin S, Galarreta M (2005) Electrical synapses define networks of neocortical GABAergic neurons. Trends in Neurosciences 28:304-309.
Hinrichs JM, Llewellyn‐Smith IJ (2009) Variability in the occurrence of nitric oxide synthase immunoreactivity in different populations of rat sympathetic preganglionic neurons. Journal of Comparative Neurology 514:492-506.
Hoge GJ, Davidson KGV, Yasumura T, Castillo PE, Rash JE, Pereda AE (2011) The extent and strength of electrical coupling between inferior olivary neurons is heterogeneous. Journal of neurophysiology 105:1089-1101.
Hormuzdi SG, Pais I, Lebeau FEN, Towers SK, Rozov A, Buhl EH, Whittington MA, Monyer H (2001) Impaired Electrical Signaling Disrupts Gamma Frequency Oscillations in Connexin 36-Deficient Mice. Neuron 31:487-495.
Hosoya Y, Okado N, Kohno K, Sugiura Y (1991) Coincidence of “ladder-like patterns” in distributions of monoaminergic terminals and sympathetic preganglionic neurons in the rat spinal cord. Experimental Brain Research 86:224-228.
Hou S, Rabchevsky AG (2014) Autonomic consequences of spinal cord injury. Compr Physiol 4:1419-1453.
Hu Z, Shi W, Riquelme M, Shi Q, Biswas S, Lo W-K, White T, Gu S, Jiang J (2017) Connexin 50 Functions as an Adhesive Molecule and Promotes Lens Cell Differentiation. Sci Rep 7:5298-5298.
Hussain DMU (2014) Connexins: The Gap Junction Proteins, 1st ed. 2014. Edition. New Delhi: Springer India.
Jänig W (1996) Spinal cord reflex organization of sympathetic systems. Prog Brain Res 107:43-77.
Kandel ER (2013) Principles of neural science, 5th ed.. Edition. New York: New York : McGraw-Hill Medical.
Katz B (1969) The release of neural transmitter substances.
Kozlowski CM (2000) The 5-HT3 receptor antagonist alosetron inhibits the colorectal distention induced depressor response and spinal c-fos expression in the anaesthetised rat. Gut 46:474-480.
Kozlowski CM, Bountra C, Grundy D (2000) The effect of fentanyl, DNQX and MK‐801 on dorsal horn neurones responsive to colorectal distension in the anaesthetized rat. Neurogastroenterology & Motility 12:239-247.
Krassioukov AV, Weaver LC (1995) Episodic hypertension due to autonomic dysreflexia in acute and chronic spinal cord-injured rats. American Journal of Physiology 268:2077-2083.
Kreuzberg MM, Deuchars J, Weiss E, Schober A, Sonntag S, Wellershaus K, Draguhn A, Willecke K (2008) Expression of connexin30.2 in interneurons of the central nervous system in the mouse. Molecular and Cellular Neuroscience 37:119-134.
Kuo DC, Yamasaki DS, Krauthamer GM (1980) Segmental organization of sympathetic preganglionic neurons of the splanchnic nerve as revealed by retrograde transport of horseradish peroxidase. Neurosci Lett 17:11-16.
Lall VK, Bruce G, Voytenko L, Drinkhill M, Wellershaus K, Willecke K, Deuchars J, Deuchars SA (2017) Physiologic regulation of heart rate and blood pressure involves connexin 36-containing gap junctions. FASEB J 31:3966-3977.
Landisman CE, Long MA, Beierlein M, Deans M, Paul DL, Connors B (2002) Electrical synapses in the thalamic reticular nucleus. Journal Of Neuroscience 22:1002-1009.
Lee ES, Joo MC (2017) Prevalence of Autonomic Dysreflexia in Patients with Spinal Cord Injury above T6. BioMed Research International 2017.

Lee S-C, Cruikshank SJ, Connors BW (2010) Electrical and chemical synapses between relay neurons in developing thalamus. The Journal of physiology 588:2403.
Lemieux M, Cabana T, Pflieger J-F (2010) Distribution of the Neuronal Gap Junction Protein Connexin36 in the Spinal Cord Enlargements of Developing and Adult Opossums, Monodelphis domestica. Brain, Behavior and Evolution 75:23-32.
Leznik E, Llinás R (2005) Role of gap junctions in synchronized neuronal oscillations in the inferior olive. Journal of neurophysiology 94:2447-2456.
Li H, Zhang Z, Blackburn MR, Wang SW, Ribelayga CP, O'Brien J (2013) Adenosine and dopamine receptors coregulate photoreceptor coupling via gap junction phosphorylation in mouse retina. The Journal of neuroscience : the official journal of the Society for Neuroscience 33:3135-3150.
Li WM, Suzuki A, Cui KM (2006) Responses of blood pressure and renal sympathetic nerve activity to colorectal distension in anesthetized rats. J Physiol Sci 56:153-156.
Llewellyn-Smith IJ (2009a) Anatomy of synaptic circuits controlling the activity of sympathetic preganglionic neurons. Journal of Chemical Neuroanatomy 38:231-239.
Llewellyn-Smith IJ (2009b) Anatomy of synaptic circuits controlling the activity of sympathetic preganglionic neurons. J Chem Neuroanat 38:231-239.
Loewi O (1956) On the intraneural state of acetylcholine. Experientia 12:331-333.
Logan SD, Pickering AE, Gibson IC, Nolan MF, Spanswick D (1996a) Electrotonic coupling between rat sympathetic preganglionic neurones in vitro. The Journal of physiology 495 (Pt 2):491.
Logan SD, Spanswick D, Pickering AE, Gibson IC, Nolan MF, Cammack C (1996b) Gap junction coupling and the regulation of excitability in sympathetic preganglionic neurons. Journal of the Autonomic Nervous System 58:202-206.
Long MA, Landisman CE, Connors BW (2004) Small clusters of electrically coupled neurons generate synchronous rhythms in the thalamic reticular nucleus. The Journal of neuroscience : the official journal of the Society for Neuroscience 24:341-349.
Long MA, Jutras MJ, Connors BW, Burwell RD (2005) Electrical synapses coordinate activity in the suprachiasmatic nucleus. Nature neuroscience 8:61-66.
Ma Y, Hioki H, Konno M, Pan S, Nakamura H, Nakamura KC, Furuta T, Li J-l, Kaneko T (2011) Expression of Gap Junction Protein Connexin36 in Multiple Subtypes of GABAergic Neurons in Adult Rat Somatosensory Cortex. Cerebral Cortex 21:2639-2649.
Maeda S, Tsukihara T (2011) Structure of the gap junction channel and its implications for its biological functions. Cellular and Molecular Life Sciences 68:1115-1129.
Maier N, Güldenagel M, Söhl G, Siegmund H, Willecke K, Draguhn A (2002) Reduction of high‐frequency network oscillations (ripples) and pathological network discharges in hippocampal slices from connexin 36‐deficient mice. Journal of Physiology 541:521-528.
Marina N, Becker DL, Gilbey MP (2008) Immunohistochemical detection of connexin36 in sympathetic preganglionic and somatic motoneurons in the adult rat. Auton Neurosci 139:15-23.
Martin GM, David PO (2012) Central nervous system control of metabolism. Nature 491:357.
Martinez DA, Hayrapetyan PV, Moreno CA, Beyer CE (2002) Connexin43 and Connexin45 Form Heteromeric Gap Junction Channels in Which Individual Components Determine Permeability and Regulation. Circulation Research: Journal of the American Heart Association 90:1100-1107.
Morrison SF (2001) Differential control of sympathetic outflow. American journal of physiology Regulatory, integrative and comparative physiology 281:R683-R698.
Nagy JI, Rash JE (2017) Cx36, Cx43 and Cx45 in mouse and rat cerebellar cortex: species-specific expression, compensation in Cx36 null mice and co-localization in neurons vs. glia. The European journal of neuroscience 46:1790-1804.
Nagy JI, Dudek FE, Rash JE (2004) Update on connexins and gap junctions in neurons and glia in the mammalian nervous system. Brain Research Reviews 47:191-215.

Nagy JI, Urena-Ramirez V, Ghia J-E (2014) Functional alterations in gut contractility after connexin36 ablation and evidence for gap junctions forming electrical synapses between nitrergic enteric neurons. FEBS Letters 588:1480-1490.
Nagy JI, Pereda AE, Rash JE (2018a) Electrical synapses in mammalian CNS: Past eras, present focus and future directions. Biochim Biophys Acta Biomembr 1860:102-123.
Nagy JI, Lynn BD, Senecal JMM, Stecina K (2018b) Connexin36 Expression in Primary Afferent Neurons in Relation to the Axon Reflex and Modality Coding of Somatic Sensation. Neuroscience 383:216-234.
Nolan MF, Logan SD, Spanswick D (1999) Electrophysiological properties of electrical synapses between rat sympathetic preganglionic neurones in vitro. J Physiol 519 Pt 3:753-764.
Noonan VK, Fingas M, Farry A, Baxter D, Singh A, Fehlings MG, Dvorak MF (2012) Incidence and prevalence of spinal cord injury in Canada: a national perspective. Neuroepidemiology 38:219-226.
O'Donnell P, Grace AA (1996) Cortical afferents modulate striatal gap junction permeability via nitric oxide. Neuroscience 76:1-5.
Pablo Huidobro-Toro J, Verónica Donoso M (2004) Sympathetic co-transmission: the coordinated action of ATP and noradrenaline and their modulation by neuropeptide Y in human vascular neuroeffector junctions. European Journal of Pharmacology 500:27-35.
Penn AA, Wong RO, Shatz CJ (1994) Neuronal coupling in the developing mammalian retina. J Neurosci 14:3805-3815.
Peracchia C (2019) Gap junction structure and chemical regulation : direct calmodulin role in cell-to-cell channel gating. London, United Kingdom: Academic Press, an imprint of Elsevier.
Pereda AE (2014) Electrical synapses and their functional interactions with chemical synapses. Nat Rev Neurosci 15:250-263.
Pereda AE, Curti S, Hoge G, Cachope R, Flores CE, Rash JE (2013) Gap junction-mediated electrical transmission: Regulatory mechanisms and plasticity. BBA - Biomembranes 1828:134-146.
Petras JM, Cummings JF (1972) Autonomic neurons in the spinal cord of the rhesus monkey: A correlation of the findings of cytoarchitectonics and sympathectomy with fiber degeneration following dorsal rhizotomy. Journal of Comparative Neurology 146:189-218.
Placantonakis DG, Bukovsky AA, Aicher SA, Kiem HP, Welsh JP (2006) Continuous electrical oscillations emerge from a coupled network: A study of the inferior olive using lentiviral knockdown of connexin36. Journal of Neuroscience 26:5008-5016.
Pyner S, Coote JH (1994) A comparison between the adult rat and neonate rat of the architecture of sympathetic preganglionic neurones projecting to the superior cervical ganglion, stellate ganglion and adrenal medulla. Journal of the Autonomic Nervous System 48:153-166.
Pyner S, Coote JH (1995) Arrangement of dendrites and morphological characteristics of sympathetic preganglionic neurones projecting to the superior cervical ganglion and adrenal medulla in adult cat. Journal of the Autonomic Nervous System 52:35-41.
Pérez De Sevilla MÜLler L, Dedek K, Janssen-Bienhold U, Meyer A, Kreuzberg MM, Lorenz S, Willecke K, Weiler R (2010) Expression and modulation of connexin30.2, a novel gap junction protein in the mouse retina. Visual Neuroscience 27:91-101.
Rabchevsky AG (2006) Segmental organization of spinal reflexes mediating autonomic dysreflexia after spinal cord injury. Prog Brain Res 152:265-274.
Rash J, Kamasawa N, Davidson K, Yasumura T, Pereda A, Nagy J (2012) Connexin Composition in Apposed Gap Junction Hemiplaques Revealed by Matched Double-Replica Freeze-Fracture Replica Immunogold Labeling. The Journal of Membrane Biology 245:333-344.
Rash J, Davidson K, Kamasawa N, Yasumura T, Kamasawa M, Zhang C, Michaels R, Restrepo D, Ottersen O, Olson C, Nagy J (2005) Ultrastructural localization of connexins (Cx36, Cx43, Cx45), glutamate receptors and aquaporin-4 in rodent olfactory mucosa, olfactory nerve and olfactory bulb. Journal of Neurocytology 34:307-341.

Rash JE, Olson CO, Pouliot WA, Davidson KGV, Yasumura T, Furman CS, Royer S, Kamasawa N, Nagy JI, Dudek FE (2007) Connexin36 vs. connexin32, “miniature” neuronal gap junctions, and limited electrotonic coupling in rodent suprachiasmatic nucleus. Neuroscience 149:350-371.
Račkauskas M, Neverauskas V, Skeberdis VA (2010) Diversity and properties of connexin gap junction channels. Medicina 46:1-12.
Rekling JC, Shao XM, Feldman JL (2000) Electrical coupling and excitatory synaptic transmission between rhythmogenic respiratory neurons in the preBötzinger complex. The Journal of neuroscience : the official journal of the Society for Neuroscience 20:RC113-RC113.
Rimkute L, Kraujalis T, Snipas M, Palacios-Prado N, Jotautis V, Skeberdis VA, Bukauskas FF (2018) Modulation of Connexin-36 Gap Junction Channels by Intracellular pH and Magnesium Ions.(Report). Frontiers in Physiology 9.
Rubin E, Purves D (1980) Segmental organization of sympathetic preganglionic neurons in the mammalian spinal cord. J Comp Neurol 192:163-174.
Rörig B, Sutor B (1996) Serotonin Regulates Gap Junction Coupling in the Developing Rat Somatosensory Cortex. European Journal of Neuroscience 8:1685-1695.
Sasaki K, Bower JM, Llinás R (1989) Multiple Purkinje Cell Recording in Rodent Cerebellar Cortex. European Journal of Neuroscience 1:572-586.
Savic G, Devivo MJ, Frankel HL, Jamous MA, Soni BM, Charlifue S (2017) Causes of death after traumatic spinal cord injury—a 70-year British study. Spinal Cord 55.
Solomon IC (2003) Connexin36 distribution in putative CO 2-chemosensitive brainstem regions in rat. Respiratory Physiology & Neurobiology 139:1-20.
Solomon IC, Chon KH, Rodriguez MN (2003) Blockade of brain stem gap junctions increases phrenic burst frequency and reduces phrenic burst synchronization in adult rat. Journal of neurophysiology 89:135-149.
Stewart AB, Béla V (2009) The diverse functional roles and regulation of neuronal gap junctions in the retina. Nature Reviews Neuroscience 10:495.
Takeuchi H, Kawanokuchi J, Mizuno T, Suzumura A (2014) Expression profile of connexins in the central nervous system. Clinical and Experimental Neuroimmunology 5:385-387.
Traub RD, Whittington MA, Gutiérrez R, Draguhn A (2018) Electrical coupling between hippocampal neurons: contrasting roles of principal cell gap junctions and interneuron gap junctions. Cell Tissue Res 373:671-691.
Tresch MC, Kiehn O (2000) Motor coordination without action potentials in the mammalian spinal cord. Nat Neurosci 3:593-599.
Uhlenberg B, Schuelke M, Rüschendorf F, Ruf N, Kaindl AM, Henneke M, Thiele H, Stoltenburg-Didinger G, Aksu F, Topaloğlu H, Nürnberg P, Hübner C, Weschke B, Gärtner J (2004) Mutations in the gene encoding gap junction protein alpha 12 (connexin 46.6) cause Pelizaeus-Merzbacher-like disease. Am J Hum Genet 75:251-260.
Uhlhaas PJ, Roux F, Rodriguez E, Rotarska-Jagiela A, Singer W (2010) Neural synchrony and the development of cortical networks. Trends Cogn Sci 14:72-80.
Velazquez JLP, Han D, Carlen PL (1997) Neurotransmitter Modulation of Gap Junctional Communication in the Rat Hippocampus. European Journal of Neuroscience 9:2522-2531.
Vinay L, Brocard F, Pflieger JF, Simeoni-Alias J, Clarac F (2000) Perinatal development of lumbar motoneurons and their inputs in the rat. Brain Res Bull 53:635-647.
Wan D, Krassioukov AV (2014) Life-threatening outcomes associated with autonomic dysreflexia: A clinical review. In, pp 2-10: Taylor & Francis.
Wang MH, Chen N, Wang JH (2014) The coupling features of electrical synapses modulate neuronal synchrony in hypothalamic superachiasmatic nucleus. Brain Res 1550:9-17.
Winterhager E (2005) Gap Junctions in Development and Disease: Berlin, Heidelberg : Springer Berlin Heidelberg.

Yates C, Charlesworth A, Allen SR, Reese NB, Skinner RD, Garcia-Rill E (2008) The onset of hyperreflexia in the rat following complete spinal cord transection. Spinal Cord 46:798.
Yeager M, Nicholson BJ (1996) Structure of gap junction intercellular channels. Current Opinion in Structural Biology 6:183-192.
Zolnik TA, Connors BW (2016) Electrical synapses and the development of inhibitory circuits in the thalamus. Journal of Physiology 594:2579-2592.
Zsiros V, Maccaferri G (2008) Noradrenergic modulation of electrical coupling in GABAergic networks of the hippocampus. The Journal of neuroscience : the official journal of the Society for Neuroscience 28:1804.